ANGELO MOLINARO

New insights into creatine transporter deficiency

Identification of neuropathological and metabolic targets for treatment

– 81 –

PREMIO TESI DI DOTTORATO

Commissione giudicatrice, anno 2019

Vincenzo Varano, *Presidente della Commissione*

Tito Arecchi, *Area Scientifica*
Aldo Bompani, *Area delle Scienze Sociali*
Mario Caciagli, *Area delle Scienze Sociali*
Franco Cambi, *Area Umanistica*
Giancarlo Garfagnini, *Area Umanistica*
Roberto Genesio, *Area Tecnologica*
Flavio Moroni, *Area Biomedica*
Adolfo Pazzagli, *Area Biomedica*
Giuliano Pinto, *Area Umanistica*
Vincenzo Schettino, *Area Scientifica*
Maria Chiara Torricelli, *Area Tecnologica*
Luca Uzielli, *Area Tecnologica*
Graziella Vescovini, *Area Umanistica*

Angelo Molinaro

New insights into creatine transporter deficiency

Identification of neuropathological and metabolic targets for treatment

Graphic design: Alberto Pizarro Fernández, Lettera Meccanica SRLs

***

Published by Firenze University Press

This book is printed on acid-free paper
Printed in Italy

Ai miei genitori

Table of contents

Historical perspective

In 1832 the French philosopher and scientist Michel Eugene Chevreul successfully extracted creatine from meat (the muscles of mammalians) and named it "creatine" from the Greek word κρέας (kreas), meaning "meat". After Chevreul's discovery, Justus von Liebig, a German chemist, in 1847 demonstrated that creatine concentration was higher in wild animals compared to domestic ones and he concluded that creatine concentration in muscular tissue was dependent upon the level of activity.

In 1912, researchers at Harvard University showed that ingestion of creatine could rise muscular creatine content and later studies demonstrated that creatine supplementation induced nitrogen retention suggesting increasing protein content in muscle. This effect was reversible with the withdrawal of creatine (Haffernan, 2015).

In 1923 the content of creatine in human body was measured in about 100 grams, 95% of which stored in muscle tissue. In the light of all these findings, Alfred Chanutin, in 1926, for the first time studied the effect of creatine in humans. He administered 10 g of creatine a day for a week and found increased creatine content in muscles, proposing that creatine have anabolic effects (Chanutin, 1926).

In 1990s the use of creatine as anabolic agent to increase athletes' performance began and currently creatine is one of the most popular supplements in sport (Balsom, Söderlund and Ekblom, 1994).

In 1994, in a patient with extrapyramidal movement disorder and low creatinine concentration in serum and urine, by using proton magnetic resonance spectroscopy, a generalized depletion of creatine in the brain was described for the first time (Stöckler et al., 1994). When the Authors tried to treat the patient with arginine (a creatine precursor), they found that the metabolite guanidine acetate increased in the brain, not paralleled by an increase in creatine, indicating that the defect was in the second of the two enzymes responsible for creatine synthesis (see below).

In 2001 another patient presenting with developmental delay and hypotonia was found to have low brain creatine content: but in this case serum and urine creatine levels were increased (Salomons et al., 2001). Genetic analysis revealed a nonsense mutation in gene coding for creatine transporter and low uptake of creatine in fibroblasts coming from the patient. This was the first description of the clinical syndrome due to genetic defects of the creatine transporter.

Physiology of creatine and its transporter

Creatine biochemistry

Creatine (Cr) is a nitrogenous organic acid found in vertebrates having many physiologic functions, some of which have only recently been being investigated. The best-studied role of Cr is its function as transient intracellular storage of high-energy phosphate bonds, used to regenerate adenosine triphosphate (ATP) starting from adenosine diphosphate (ADP) and from the phosphorylated form of Cr (phosphocreatine, PCr) in the following reversible enzymatic reaction (Figure 1) catalyzed by the enzyme Cr kinase (CK):

$$\text{Phosphocreatine} + \text{ADP} \leftrightarrow \text{creatine} + \text{ATP}.$$

Consistently with this energetic role, tissues with high metabolic rates have a large pool of PCr in order to regenerate ATP fast during intense use.

The so called "creatine cycle" also acts as transport system for phosphate bonds between sites of production (mitochondria, glycolysis) and sites of consumption inside the cell. The mitochondrial form of CK phosphorylates Cr to PCr reducing the ATP/ADP ratio to a level that allow ATP synthase to continue working. On the other side of the mitochondrial membranes, in the cytoplasm, PCr is used at sites of high metabolic requirements to restore ATP starting from ADP. The Cr produced in the last reaction diffuses back to mitochondria completing the Cr cycle. According to this view, the transport of high-energy phosphates from production to consumption sites is ensured mainly by means of PCr-Cr cycle. Cr and PCr are molecules smaller and less negatively charged compared to ATP or ADP; these properties could allow reaching higher concentrations and then a more efficient flux of high-energy phosphates in cells strongly relying upon Cr cycle (Wyss and Kaddurah-Daouk, 2000).

The major share of Cr (and PCr) in human body is found in muscle, up to 30 mM. The brain, as expected by its high metabolic rate, contains a concentration of Cr of about 10 mM (Wyss and Kaddurah-Daouk, 2000).

Many other functions of Cr have been described or hypothesized. It is an osmolyte and has anti-oxidant and anti-apoptotic effects (Andres et al., 2008). The release of Cr into the synaptic cleft was observed and a putative role as neuromodulator or even as true neurotransmitter has been envisaged (Almeida et al., 2006). Cr is now widely used as nutritional supplement, and its use in different neurological or psychiatric dis-

orders like mitochondrial encephalopathy, stroke, traumatic neurological injury, neurodegenerative and muscular disorders has been tested (Andres et al., 2008; Evangeliou et al., 2009).

Creatine supply

There are two ways by which normal levels of Cr can be achieved and maintained in tissues in physiological conditions: (I) endogenous synthesis and (II) exogenous intake by food. Both contribute to the amount of this metabolite in normal tissues.

The synthesis of Cr is a two-step reaction which requires the amino acids arginine (Arg) and glycine (Gly) as initial reagents. The enzyme L-arginine:glycine amidinotransferase (AGAT) transfers the amidino group of Arg to Gly in order to produce L-ornithine and guanidinoacetic acid (GAA). In the second step the enzyme S-adenosyl-L-methionine:N-guanidinoacetate methyltransferase methylates the amidino group of GAA to produce Cr (Figure 2).

During evolution AGAT and GAMT have probably evolved with lamprey and they are not detected in invertebrates whereas they are present in most, but not all, vertebrates. Nevertheless, some invertebrates contain significant amount of Cr, of its phosphorylated metabolite and of CK, suggesting mechanisms for the uptake of Cr from environment or not yet detectable synthesis enzymes. Notably, from an evolutionary point of view, in invertebrates lacking Cr the same function of energy storage is held, in an analogous reaction to the Cr cycle, by Arg, that is one of the precursors of Cr.

Despite the seeming simplicity of the Cr cycle, the biochemical picture is complicated by the fact that many tissues seem to lack one of the enzymes involved in the synthesis of Cr or its precursors.

Mammalian kidney expresses high levels of AGAT but usually low levels of GAMT. Liver, on the contrary, contains high amounts of GAMT and low levels of AGAT in most species. However, monkey and human also have high amounts of AGAT in liver, whereas common laboratory mammals such as rats and mice seem to be devoid of AGAT activity in this tissue (Wyss and Kaddurah-Daouk, 2000). This pattern of biosynthetic enzyme expression could relate to some differences noticeable in phenotype between humans and mice affected by Cr metabolism disorders. Based on these findings, the following outline about Cr synthesis in mammals has been proposed: the kidney would be the main site of GAA production; this metabolite is then transported through blood to liver where it is methylated to Cr. Finally, Cr is again transported by blood to all tissues where it is taken up.

In contrast, other findings described a reduction of Cr synthesis in models with nephrectomy (Levillain, Marescau and Deyn, 1995), suggesting that, notwithstanding the possible expression of both enzymes in human liver, kidney could nevertheless be required for Cr synthesis. Therefore, the biochemical pathways of Cr metabolism and the exchange of Cr and its metabolites among many tissues or cell types seem more complex. Furthermore, differences in mammal species make findings in one species difficult to apply to other ones, and particularly to human.

Finally, Cr and PCr are non-enzymatically converted into creatinine, which diffuses out of the cells and is excreted by the kidneys into the urine. By this catabolic pathway about 1.7% of the total Cr pool of the body is lost every day and needs to be replaced (Wyss and Kaddurah-Daouk, 2000).

Creatine transporter

Cr can be taken up by ingested food and about one-half of the daily required Cr amount is provided by this way (Brosnan and Brosnan, 2007). For this purpose, a Cr transporter (CrT) exists that is responsible for a saturable Na^+- and Cl^--dependent uptake into cells against a large concentration gradient.

The CrT is encoded by the SLC6A8 gene that in human is located on Xq28. It is made up of 13 exons, with a predicted protein of 635 amino acids and a molecular mass of 70.5 kDa (Guimbal and Kilimann, 1993). It is a member of the SLC6 family of Na^+- and Cl^-- dependent plasma membrane transporters for neurotransmitters which encompasses transporters for GABA, norepinephrine, dopamine, serotonin, glycine, taurine, proline, and betaine (Kristensen et al., 2011). Like the other members of the SLC6 family, the CrT consists of 12 transmembrane domains, containing sites for N-glycosylation and several sites for phosphorylation.

In humans, CrT is expressed predominantly in muscle, kidney and heart, and also in many other tissues including brain (Iyer et al., 1996). This pattern of expression reflects the high levels of Cr in muscle and heart and the important role of kidney in Cr reuptake from urine (Guimbal and Kilimann, 1993).

The CrT is expressed in kidney in the apical membrane (the brush border) whereas little or no expression is identifiable in the basolateral membrane (García-Delgado et al., 2001). That is, the Cr is transported from the tubular lumen into the cell and this mechanism requires that a different and still unknown Cr transporter must be expressed on the basolateral membrane domain in order for Cr to exit the cell into the bloodstream. A very similar pattern of expression is observed also in small intestine where Cr introduced with food is absorbed (Nash et al., 1994).

Creatine transporter expression in brain

CrT is expressed in many structures of the brain, particularly in the olfactory bulb, cerebellum, hippocampus, cortex and several brainstem nuclei (Braissant et al., 2008). Regarding the cell types, CrT expression is found in both neurons and glial cells. However, the CrT presence in glial cells is still debated. In some studies, CrT is expressed in oligodendrocytes but not in astrocytes (Braissant et al., 2005), whereas other Authors found expression also in astrocytes (Carducci et al., 2012). The differences observed could be explained by differences in materials and methods used.

According to in vitro studies of rat hippocampal neurons, CrT is mainly expressed in dendrites and in some axon terminals (Dodd et al., 2010); this localization can be explained by the high energy requirements for re-establishing the ion electrochemical

gradients disrupted during neuronal signaling but also for its envisaged role as neuro-transmitter. Evidence was found of the presence of CrT in synaptosomal membrane, which would precisely be the expected place where CrT should be found if Cr were secreted as neurotransmitter/neuromodulator (Peral, Vázquez-Carretero and Ilundain, 2010).

A recent transcriptional analysis led to discovery that CrT is highly expressed in fast-spiking neurons parvalbumin-positive (PV+) inhibitory interneurons (Saunders et al., 2018). This observation well fits the hypothesis that higher Cr concentration can be required in fast-spiking neurons in order to meet the high energy needs of this cell type.

Creatine uptake regulation

The uptake of Cr is strictly regulated by many factors, first of which is Cr itself that decreases its own uptake (Loike et al., 1988). This control mechanism is important to avoid accumulation of high concentration of Cr and subsequent ATP depletion.

Among the other important factors, AMP activated protein kinase (AMPK), which is involved in regulating energy homeostasis by downregulating energy consuming pathways in favor of energy generating processes, inhibits CrT activity and expression in the apical membrane of kidney proximal tubule cells, possibly indirectly via inhibition of mTOR (Li et al., 2010), exemplifying the complex signaling network responsible for Cr regulation, aimed at matching Cr concentration to current cell energy requirements.

Creatine transporter deficiency

Etiology

Thanks to proton magnetic-resonance spectroscopy (1H-MRS) it is possible to measure concentration of Cr, and other metabolites, in the brain. This technique allowed discovering Cr deficiency conditions as definite disorders of Cr metabolism. Three cerebral Cr deficiency syndromes (CCDS) have so far been described, all of them characterized by severe intellectual disability.

GAMT-deficiency was the first CCDS to be described in 1994 (Stöckler et al., 1994), followed by the discovery of the other two conditions, AGAT and CrT deficiency (CTD, also named CCDS1) (Item et al., 2001; van de Kamp, Mancini and Salomons, 2014). The two enzymatic disorders (AGAT and GAMT-deficiency) impair Cr synthesis and are inherited in an autosomal recessive manner. The defect of the transporter impairs Cr uptake by the cell and it is an X-linked disease. It was estimated that CrT deficiency can be the etiology of about 2% of the cases of intellectual disability in males (van de Kamp, Mancini, and Salomons 2014).

Clinical features

The clinical picture of patients affected by Cr deficiency syndromes is dominated, in all the three genetic disorders, by intellectual disability, seizures and autistic-like behavior. Patients with GAMT defects can also show aggressive and self-injurious behaviors (Mercimek-Mahmutoglu et al., 2006).

More specifically, CCDS1 is characterized by intellectual disability with sever speech delay which involves virtually the totality of patients; behavioral abnormalities and seizures are common. Moreover, the intellectual disability seems progressive (van de Kamp et al. 2013). Some patients have autistic-like features, others show hyperactivity. The motor system is less impaired: a delay in acquisition of independent walking can be observed, as well as subtle extrapyramidal alterations in some patients, but a clear muscle weakness has only rarely been described in human (van de Kamp et al. 2013).

MRS reveals the most characteristic feature of CrT deficiency: the severe depletion of Cr in the brain. Cr content in human muscle seems preserved in CrT defects whereas it is reduced in defects involving the two biosynthetic enzymes (deGrauw et al., 2003; Edvardson et al., 2010).

Laboratory findings help clinicians to diagnose CrT disorders. The defect of CrT is characterized by an increased urine Cr/creatinine ratio, probably due to the impair in renal reabsorption of Cr. Cr plasma levels are normal while Cr in cerebro-spinal fluid (CSF) are normal or increased, similar to what happens in some other defects of neurotransmitter transporters, like serotonin transporter (van de Kamp et al. 2013).

Moreover, some patients affected by CrT defects show biochemical markers peculiar to mitochondrial encephalopathies (increased plasma lactate, urinary 3-methylglutaconic, tricarboxylic acid cycle intermediates and secondary decreases of variable respiratory chain complexes) (Hathaway et al., 2010). These findings are not surprising if the energetic role of Cr in cell and mitochondrial metabolism is considered.

Genetic and inheritance

Many different types of genetic mutations affecting the SLC6A8 gene have been described: missense and nonsense mutations, splice error mutations (intronic or synonymous variants with aberrant splicing), a translation initiation site mutation and multi-exon deletions (LOVD database (http://www.LOVD.nl/SLC6A8)). In some cases, a missense mutation can result in a residual transporter function which in turn can, in some cases, be associated to a mild phenotype (Betsalel et al., 2012). Most of the genetic alterations observed are concentrated in the transmembrane domains 7 and 8 of the protein (van de Kamp et al. 2015).

Because the SLC6A8 gene is located on chromosome X, the disorder is an X-linked condition. About one third of the cases are due to de novo mutations (van de Kamp et al. 2013). The disorder mainly affects male patients, but female patients can show a mild symptomatic phenotype (van de Kamp et al. 2011). In these cases, diagnosis can be difficult because of the clinical pictures and a higher frequency of normal biochemical markers. Female phenotype variability is higher than observed in male, due to the random inactivation of X chromosome.

Pathophysiology

As described, a biosynthetic pathway exists for Cr synthesis; nevertheless, the defect of the transporter gives rise to a severe disorder. This seems to suggest that the biosynthetic pathway alone is not sufficient to provide the necessary amount of Cr or, as discussed above, not every tissue may be able to carry out the whole synthetic reaction. These tissues would rely upon the CrT in order to exchange Cr or its metabolites.

On the other side, the observation that some tissues seem spared in CrT defects, like muscle in human patients, probably means that in these tissues the enzymatic pathway is fully expressed and working, and it is able to ensure the provision of Cr content in absence of any exogenous source. It is probable, therefore, that in most tissues both mechanisms, uptake and synthesis, are active and required to maintain normal Cr concentration.

Notwithstanding the expression of AGAT, GAMT and CrT is described in neurons and glial cells, uptake of Cr in brain from blood seems limited (Perasso et al., 2003), as also indicated by the fact that in Cr synthesis defects the restoration of Cr levels in brain by exogenous supplementation is a process which proceeds very slowly and requires high Cr doses (Stöckler, Hanefeld, and Frahm 1996; Leuzzi et al. 2000). Moreover, some studies in cultured astrocytes measured low expression levels of CrT in brain, but literature about this issue is conflicting. If CrT expression were low in brain, as the above studies would suggest, it would be difficult to explain how CrT deficiency leads to a severe impairment of brain Cr content and to a severe disorder. In order to reconcile these contrasting observations, different theories have been advanced.

The neuron-glial relationship hypothesis is based upon the preferential expression of GAMT in oligodendrocytes (Tachikawa et al., 2004) and predicts that Cr is mainly produced in glial cells and then transferred to neurons by means of the CrT. However, expression of both biosynthetic enzymes was described in neuron and glial cultures in some studies (Carducci et al. 2012; Braissant et al. 2001), challenging this hypothesis.

The dissociation hypothesis states that AGAT and GAMT are expressed in many different brain cell types but rarely co-expressed in the same cells and, thus, the intermediate metabolite GAA must be transported by means of the CrT from one cell to another. However, this would lead to high levels of toxic metabolite GAA in CrT defects (as observed in defects of GAMT) that are not observed (van de Kamp et al. 2012).

The observation that, in CrT defects, Cr concentration is normal or even high in CSF, could be consistent with the hypothesis that a mechanism of Cr reuptake is lacking in this disorder (van de Kamp et al. 2013). CrT is member of a family of neurotransmitter transporters responsible for the reuptake of serotonin and dopamine, and defects of these transporters cause a biochemical phenotype similar to what observed in CrT defects (low intracellular metabolite concentration and high extracellular concentration). In vitro data show that hippocampal neurons release about 35% of their Cr content in 1-2 hours (Dodd et al., 2010). These observations, and further data regarding the restricted synthesis capability of Cr in neurons and glia (Carducci et al., 2012) suggest that one fundamental mechanism of Cr provision in brain cells is the reuptake, making the CrT a pivotal device in Cr metabolism and leading to the reuptake failure hypothesis as mechanism of Cr deficiency in CCDS1.

It is well possible that the biochemical picture is more complex and most of the mechanisms described could be implicated in the pathophysiology.

The defects of Cr synthesis can be treated with variable success. Supplementation of Cr with ornithine, accompanied by arginine restriction in GAMT defects, proved useful in both AGAT and GAMT-defects, with at least partial restoration of cerebral Cr content and improvement of the clinical picture. In some cases, when the therapy started very early, an almost normal development was observed (Edvardson et al., 2010; Ndika et al., 2012; Nouioua et al., 2013).

On the contrary, the defects of Cr transporter cannot be successfully treated by Cr supplementation, as proven by many studies (Bizzi et al., 2002; Anselm et al., 2006;

Póo-Argüelles et al., 2006). Arginine supplementation can increase, in vitro, the synthesis of Cr (Leuzzi et al. 2008) but showed only mild improved in some patients (Chilosi et al. 2008; Chilosi et al. 2012; Mercimek-Mahmutoglu et al. 2010).

A way to bypass the blood brain barrier (BBB) could exploit lipophilic derivatives of Cr. Many molecules were tested (creatine-benzyl-ester, phosphocreatine-Mg-complex acetate, creatine-ethyl-ester, dodecyl-creatine-ester) and some of them led to an increase in Cr levels in mouse or human brain cells cultures (Lunardi et al., 2006; Perasso et al., 2009; Fons et al., 2010). These compounds tend to be degraded very early and no effect was found when tested in patients (Fons et al., 2010).

Cyclocreatine (cycloCr) is a Cr analog less polar than Cr itself, which showed some improvement in mouse models and uptake in cell cultures after blocking the Cr transporter (Kurosawa et al., 2012; Enrico et al., 2013). The kinetics of the phosphorylation of cycloCr is different compared to Cr and this could limit its usefulness (Walker, 1979). Further studies are thus necessary to assess the efficacy of this derivative.

CCDS1 is therefore a disorder for which an effective treatment is still missing. The etiology of the disease, the lack of a transporter, could represent an obstacle difficult to circumvent with simple replacement therapy and, therefore, more sophisticated approaches could probably be required.

Mouse models of CCDS1

In our laboratory two different mouse lines are available to study CCDS1 patho-physiology and test putative treatment strategies. The first model is a ubiquitous model carrying a loss-of-function deletion of exons 5 – 7 in the Slc68a gene. The second model is a conditional knock-out (KO) in which the expression of the CrT is impaired only in cells derived by neuronal precursors (i.e. neurons and glia) by crossing a floxed CrT line with a line expressing Cre-recombinase under the promoter of the Nestin gene (see Meterials and Methods).

Other lines are available in other laboratories. One is a ubiquitous KO model generated by deletion of exons 2 – 4 in the Slc6a8 gene. Two other lines are conditional KO: one using a Ca^{2+}/calmodulin-dependent protein kinase II (CaMKII) promoter to drive Cre-recombinase expression in order to achieve a CrT deletion only in postnatal forebrain excitatory neurons; another model has been created by crossing floxed Slc6a8 mice with Nestin-cre mice (Udobi et al., 2018), similarly to our conditional model.

The following sections will report preliminary findings drawn by the ubiquitous KO model present in our facility (Baroncelli et al., 2014) because it is the same adopted for the present work. These findings were the state of knowledge about the characterization of this model from which the present study started. Where differences have been found between the current model and the other ones, appropriate comments and interpretations will be provided. The detailed description of the experiments from which these findings are drawn can be found in the Material and Methods section.

Creatine concentrations and body weight

KO mice had a reduced Cr concentration in the brain, in both cortex and hippo-campus, and in muscle, heart and kidney compared to wild-type (WT) littermates.

The general appearance of KO mice was normal except for reduced body growth: at post-natal day (P) 60 the weight of KO was lower than WT.

Behavioral tests

To test general locomotor activity and anxiety-related behavior the open field arena was used. Both WT and KO mice spent more time in peripheral regions avoiding the center. No difference was found in the amount of time spent in periphery, in motion speed and in total distance walked between the two genotypes.

Declarative memory was assessed by using object recognition test (ORT) which evaluates the capacity of recognizing a familiar object from a novel one. Both experimental groups explored the objects for the same amount of time during the sample phase, whereas during the test phase at 24 h, WT showed higher preference for the novel object compared to KO.

Spatial working memory was evaluated by measuring the rate of spontaneous alternation in the Y maze. Both groups explored all the three arms of the maze without any difference in the total number of entries and any bias for one of the arms, indicating that general exploratory behavior was preserved in KO. The alternation rate was at chance level for KO, compared to the high alternation observed in the WT, showing a specific mnestic alteration.

The Morris water maze (MWM) was used to assess spatial learning and memory. Lower swimming speed was detected in KO, and the performance was thus expressed in terms of distance swum to find the hidden platform. During the training phase, the distance covered to locate the platform was longer in KO compared to WT in the last three days. In order to evaluate the strength of learning and to discriminate between spatial and non-spatial strategies to find the platform, on the last day the platform was removed and the time spent in the quadrant where the platform had previously been located was measured. WT mice spent more time in the target quadrant whereas KO showed no significant preference.

General locomotor activity can also be assessed in a non-aversive environment (compared to the open filed arena which has an aversive component) simply measuring home-cage locomotor activity. In this context KO showed decreased activity during night period compared to WT. The day-time activity was normal.

The KO model used seems to recapitulate well the genetic and neurochemical features of patients affected by CCDS1. A remarkable difference compared to human is the finding of reduced Cr levels in KO mice muscle which is not observed in patients. This finding is not an idiosyncrasy of the specific model because it is shared by the other ubiquitous model (Russell et al., 2014), indicating that it is an intrinsic difference between mouse and human physiology. Consistent with muscle Cr impairment, motor performances were impaired in KO mice, as described above.

Because of the differences found in motor and muscle performances between mice and patients, another model of CrT defect is described in literature in which the CrT has been knocked-out only in forebrain excitatory neurons. Despite the fact that this model shows alterations consistent with those observed in patients and without muscle involvement, this conditional model has an intrinsic strong limitation and cannot precisely recapitulate the pathophysiology of the brain involvement in CrT defect: CrT expression in inhibitory interneurons is preserved in this conditional model but, as already cited before, it is very high in at least a subclass of this cell type (namely, fast-spiking PV+ interneurons) in physiological conditions, meaning that CrT must

hold an important role in PV+ neurons physiology. Sparing CrT expression in inhibitory neurons can thus lead to a huge bias in the results and conclusions obtained from this model.

To preserve muscular function, in order to recapitulate patients' phenotype, conditional models in which the CrT is selectively disrupted selectively in all CNS cells, neurons and glia, can be very useful to dissect the many pathogen etic events of CCDS1.

Aim of the study

CCDS1 is a severe disorder with no effective treatment currently available and with high negative impact on life quality and expectancy of patients, as well as their families' life quality. Social impacts are great too, due to the requirement for long health assistance, with huge economic burden.

Valid therapeutic options can only come from a deep understanding of etiology and pathophysiology of this disorder. The little knowledge about the mechanisms and the effects of Cr deficiency on neural circuits stems, to some extent, from the paucity of studies on animal models. Two germline murine models of CCDS1 and one model of GAMT deficiency were available when the current project started and they were analyzed only in some behavioral domains and at neurochemical level, while studies on AGAT deficient mice were limited to metabolic effects of Cr deficiency (Choe et al., 2013). Learning and memory deficits, impaired motor activity and Cr depletion in the brain and muscles have been reported in GAMT and CrT models in the adult age (Torremans et al., 2005; Skelton et al., 2011; Baroncelli et al., 2014). However, little is known about the presence of autistic-like behavioral features and the onset and progression of the phenotype.

Furthermore, a growing number of studies showed that extraneural dysfunctions could underlie behavioral deficits in other mouse models of neurodevelopmental disorders (Depino, 2013; Sherwin, Dinan and Cryan, 2018). However, no thorough assessment exists about this aspect in Cr deficiency disorders, causing a limited understanding of the relative contributions of periphery in CCDS1 pathophysiology.

In order to fill these gaps and to dissect the molecular mechanisms of the pathophysiology of CrT defects, we took advantages of two different transgenic mouse lines, a ubiquitous one in which CrT is defective in all body cells, and a conditional one in which CrT expression is only impaired in cells derived from neuronal and glial precursors, i.e. only in CNS cells. The latter model allowed us to recapitulate better the phenotype observed in human patients in which muscle involvement is only a rare finding or at a limited extent, and it also proved invaluable in discriminating between neural and extraneural contributions to the pathophysiology of CCDS1.

Materials and methods

Animals

As CrT deficiency is an X-linked pathology, male mice were selected for this study. $CrT^{-/y}$ and $CrT^{+/y}$ mice on a C57BL/6 J background were generated as described previously (Baroncelli et al., 2014). Animals were maintained at 22 °C under a 12-h light–dark cycle (average illumination levels of 1.2 cd/m2). Food (4RF25 GLP Certificate, Mucedola) and water were available ad libitum. To target CrT deletion to neuronal and glial cells of the central nervous system we used a mouse (Tronche et al., 1999) expressing Cre-recombinase under the Nestin promoter (Nestin:Cre). CrT+/fl females were crossed with Nestin:Cre male mice to generate a mouse line carrying the floxed CrT and Nestin:Cre alleles. Mice with three genotypes were used as experimental animals: mice carrying the brain specific deletion of CrT (Nestin:Cre-$CrT^{-/y}$, nes-$CrT^{-/y}$), mice expressing the floxed allele but not Cre-recombinase (CrTfl/y), and mice expressing Cre-recombinase but not carrying the floxed allele (Nestin:Cre-$CrT^{+/y}$, nes-$CrT^{+/y}$). These genotypes were obtained in the same litters. Since CrTfl/y mice did not display any difference in Cr levels with respect to nes-$CrT^{+/y}$ animals, we performed behavioral and anatomical investigation only in the other two experimental groups. All experiments were carried out in accordance with the European Communities Council Directive of 24 November 1986 (86/609/EEC) and were approved by the Italian Ministry of Health (authorization number 259/2016-PR).

Detection of SLC6A8 mutations by PCR

Genomic DNA was isolated from mouse tail using a kit, and the protocol suggested by the manufacturer (DNeasy Blood & Tissue Kit, Qiagen, USA). DNA was amplified for CrT mutant and wild-type alleles using a standard polymerase chain reaction (PCR) protocol with the following primers: F:AGGTTTCCTCAGGTTATAGAGA; R:CCCTAGGTGTATCTAACATC; R1: TCGTGGTATCGTTATGCGCC. Primers for Cre recombinase expression were: F: AACGCACTGATTTCGACC; R: CAACACCATTTTTTCTGACCC. For PCR amplification, we used 300 ng of DNA in a 25 µl reaction volume containing 0.2mM of each dNTP, 2 µM of F primer, 1 µM of R primer, 1 µM of R1 primer and 0.5 U/µl Red Taq DNA polymerase (Sigma-Aldrich, Italy).

The PCR conditions were as follows: 94 °C for 4 min followed by 37 cycles at 94 °C for 30 s, 58 °C for 30 s, 72 °C for 40 s and a final extension at 72 °C for 7 min. Amplicons were separated using 2% agarose gel and visualized under UV light after staining with Green Gel Plus (Fisher Molecular Biology, Rome, Italy). Amplicon sizes were: WT allele = 462 bp; mutant allele = 371 bp; Cre allele = 310 bp.

Behavioral testing

The testing order for behavioral assessment performed in the same animals consisted of: open field (1 day duration), ORT at 1h (1 day), ORT at 24h (3 days), Y maze (1 day), MWM with hidden platform (7 days), rotarod (1 day), three chamber social test (1 day) and self-grooming (1 day). The mice were tested on one task at a time with the next behavioral test starting at least 1 day after the completion of the previous one. While open field, ORT, Y maze, rotarod and self-grooming were longitudinally administered to the same animals, MWM was performed in separate groups of animals at the different ages tested. Y maze has been also used to test cognitive functions in juvenile animals (P28).

Social behavior has been tested only in 6-month old animals. In order to reduce the circadian effects, behavioral tests were performed during the same time interval each day (2:00 PM – 6:00 PM; light phase). All behavioral tests were conducted in blind with respect to the genotype of animals. Animals not performing the task required were excluded from the analysis. Mice were weighed at the end of experiments.

Open field and object recognition test (ORT)

The apparatus consisted of a square arena (60 x 60 x 30 cm) constructed in polyvinyl chloride with black walls and a white floor. The mice received one session of 10-min duration in the empty arena to habituate them to the apparatus and test room. Animal position was continuously recorded by a video tracking system (Noldus Ethovision XT). In the recording software an area corresponding to the center of the arena (a central square 30 x 30 cm), and a peripheral region (corresponding to the remaining portion of the arena) were defined. The total movement of the animal and the time spent in the center or in the periphery area were automatically computed. Mouse activity during this habituation session was analyzed for evaluating the behavior in the open field arena. The ORT consisted of two phases: sample and testing phase. During the sample phase, two identical objects were placed in diagonally opposite corners of the arena, approximately 6 cm from the walls, and mice were allowed 10 min to explore the objects, then they were returned to their cage. The objects to be discriminated were made of plastic, metal, or glass material and were too heavy to be displaced by the mice. The testing phase was performed either 1h or 24h after the sample phase. One of the two familiar objects was replaced with a new one, while the other object was replaced by an identical copy. The objects were placed in the same locations as the previous ones. The mice were allowed to explore objects for 5 min. To avoid possible preferences for one of two objects, the choice of the new and old object and the

position of the new one were randomized among animals. The amount of time spent exploring each object (nose sniffing and head orientation within < 1.0 cm) was recorded and evaluated by the experimenter blind to the mouse genotype. Arena and objects were cleaned with 10% ethanol between trials to stop the build-up of olfactory cues. Mice exploring the two objects for less than 10 s during the sample phase were excluded from testing. A discrimination index was computed as DI = (T new – T old)/(T new + T old), where T new is the time spent exploring the new object, and T old is the time spent exploring the old one (Baroncelli et al., 2014).

Y maze spontaneous alternation

We used a Y-shaped maze with three symmetrical grey solid plastic arms at a 120-degree angle (26 cm length, 10 cm width and 15 cm height). Mice were placed in the center of the maze and allowed to freely explore the maze for 8 minutes. The apparatus was cleaned with 10% ethanol between trials to avoid the build-up of odor traces. All sessions were video-recorded (Noldus Ethovision XT) for offline blind analysis. The arm entry was defined as all four limbs within the arm. A triad was defined as a set of three arm entries, when each entry was to a different arm of the maze. The number of arm entries and the number of triads were recorded in order to calculate the alternation percentage, generated by dividing the number of triads by the number of possible alternations and then multiplying by 100 (Baroncelli et al., 2014).

Morris water maze

Mice were trained for four trials per day and for a total of 7 days (Baroncelli et al., 2014) in a circular water tank, made from grey polypropylene (diameter: 120 cm; height: 40 cm), filled to a depth of 25 cm with water (23 °C) rendered opaque by the addition of a non-toxic white paint. Four positions around the edge of the tank were arbitrarily designated North (N), South (S), East (E) and West (W), which provided four alternative start positions and also defined the division of the tank into four quadrants, i.e. NE, SE, SW and NW. A square clear Perspex escape platform (11 x 11 cm) was submerged 0.5 cm below the water surface and placed at the midpoint of one of the four quadrants. The hidden platform remained in the same quadrant during training, while the starting positions (N, S, E or W) were randomized across trials. The pool was situated in a room containing extra-maze cues that provide specific visual reference points for locating the submerged platform. Mice were allowed up to 60 s to locate the escape platform, and their swimming paths were automatically recorded by the Noldus Ethovision system. If the mouse failed to reach the platform within 60 s, the trial was terminated and the mouse was guided onto the platform for 15 s. On the last trial of the last training day, mice received a probe trial, during which the escape platform was removed from the tank and the swimming paths were recorded over 60 s while mice searched for the missing platform. The swimming paths were recorded and analyzed with the Noldus Ethovision system.

Rotarod and grip strength

Motor coordination and abilities were assessed using the rotarod test as described by Lonetti and colleagues (Lonetti et al., 2010). Animals were placed on a drum with increasing rotation speed from 4 to 40 rpm. The time spent on the drum was recorded by an automated unit, which stops as the mouse fall. Motor abilities were assessed by conducting the test for four consecutive times with an interval of 5 min in the same day. In the grip strength test a peak amplifier automatically measures the peak pull-force achieved by animals' forelimbs.

Three-chamber social test

The three-chamber paradigm test has been successfully employed to study sociability and preference for social novelty in several mutant mouse lines. 'Sociability' is defined as a propensity to spend time with a conspecific, as compared to time spent alone in an identical but empty chamber; 'preference for social novelty' is defined as propensity to spend time with a new mouse rather than with a familiar mouse (Moy et al., 2004). We adapted the protocol reported by Kaidanovich-Beilin and colleagues (Kaidanovich-Beilin et al., 2011). The apparatus consisted in a rectangular, three-chamber box made from clear Plexiglas (72 cm wide x 50 cm length x 33 high). Each chamber is 24 x 50 cm and the dividing walls are made from clear Plexiglas, with an open middle section, which allows free access to each chamber. Two identical, wire cup-like containers with removable lids were placed inside the apparatus, one in each side chamber. Each container was made of metal wires allowing for air exchange between the interior and exterior of the cup but small enough to prevent direct physical interactions between the inside animal and the subject mouse. Two classes of mouse were used in this experiment, one acting as a control, naïve animal, while the other is the test subject. The control mouse was a mouse of the same background, age, gender and weight, without any prior contact with the subject mouse. Two control mice were required per experiment, one used for session I (Stranger 1) and another for session II (Stranger 2). The same control mice were used between trials. Control mice were gradually habituated to wire-cup housing in the three-chamber box for 4 days (30 min per day) before the starting of test session. After 10 min of habituation in the arena with empty wire cups of the subject mouse, we placed Stranger 1 inside one of the wire cups. The subject mice were allowed to explore each of the three chambers for 10 min (session I). Animal position was continuously recorded by a video tracking system (Noldus Ethovision XT). The amount of time spent exploring each wire cup was recorded and evaluated by the experimenter blind to the mouse genotype. A discrimination index was computed as DI = (Tsoc – Tobj) / (Tsoc + Tobj), where Tsoc is the time spent exploring the cup housing the Stranger 1, and Tobj is the time spent exploring the other cup. In session II we placed Stranger 2 inside the wire cup in the opposite side chamber. Duration of session II was 10 min and we calculated the same DI described above, differentiating the exploration time of the subject mouse between Stranger 1 and Stranger 2. The placement of Stranger 1 and Stranger 2 in the left or

right side of the box was randomized between trials. Arena and wire cups were cleaned with 10% ethanol between trials to prevent olfactory cue bias.

Self-grooming

Mice were scored for spontaneous grooming behaviors as described earlier (McFarlane et al., 2008). Each mouse was placed individually into a clean, empty, standard mouse cage (27 cm length x 20 cm wide x 15 cm high) without bedding. Animal behaviors were videotaped for 20 min. After a 10-min habituation period in the test cage, each mouse was scored with a stopwatch for 10 min for cumulative time spent grooming all body regions.

Biochemical analysis

For Cr and GAA assay, mouse tissues, immediately frozen on dry ice and stored at -80°C until the analysis, were homogenized in 0.7 ml PBS buffer (Sigma-Aldrich, Italy) at 4°C using an ultrasonic disruptor (Microson Heat System, NY, USA) for brain or a glass manual homogenizer (VWR, Italy) for kidney, heart and muscle. After centrifugation (600 x g for 10 min at 4°C) an aliquot of the homogenate (50 ml) was assayed for protein content and the supernatant used for Cr assay as previously described (Alessandrì et al., 2005). Briefly, 50 ml of saturated sodium hydrogen carbonate and 50 ml of a mixture containing 2-phenylbutyric acid (I.S.) in toluene (6.09 mmol/l; Sigma-Aldrich, Italy) were added to 200 ml of homogenate or to 100 ml of serum and urine, respectively. After adding 1ml of toluene and 50 ml of hexafluoro-2,4-pentanedione (Sigma-Aldrich, Italy) to form bistrifluoromethyl-pyrimidine derivatives, the mixture was stirred overnight at 80°C. The organic layer was centrifuged, dried under nitrogen and 2 ml of the residue derivatized at room temperature with 100 ml of BSTFA+TMCS (Sigma-Aldrich, Italy) injected into the Gas Chromatography/Mass Spectrometry (GC/MS) instrument. GC analyses were performed using an Agilent 6890N GC equipped with an HP5MS capillary column (0.25 mm x 30 m, film thickness 0.25 mm) and an Agilent mass spectrometer 5973N (Agilent Technologies, Italy). The mass spectrometer was set in EI-single ion monitoring mode (SIM). The ions with m/z of 192 for I.S., 258 for Cr and 225 for GAA were used for calculation of the metabolites, using standard curves ranging 5–90 mmol/l and 0.30–6 mmol/l for Cr and GAA, respectively. Data were processed by the G1701DA MSD ChemStation software. All the aqueous solutions were prepared using ultrapure water produced by a Millipore system.

Immunohistochemistry

Mice were perfused transcardially with 4% paraformaldehyde in phosphate buffer. Brains were post-fixed and impregnated with 30% sucrose in phosphate buffered saline (PBS). Coronal brain sections (40 mm thick) were cut on a freezing mi-

crotome and collected in PBS before being processed for immunohistochemistry. After a blocking step, free-floating slices were incubated O/N at 4°C in a solution of primary antibody (NeuN, Millipore, 1:500; Ki67, Abcam, 1:400; DCX, Abcam, 1:200; vGlut1, Synaptic System, 1:500; vGAT, Synaptic System, 1:1,000; Iba-1, Wako, 1:400) and antigen-antibody interaction was revealed with suitable Alexa Fluor-conjugated secondary antibodies (1:400, Invitrogen). Immunostaining for Ki67 involved an additional treatment with sodium citrate for antigen retrieval. Sections were then counterstained with Hoechst dye (1:500, Sigma), mounted on microscope slides and coverslipped using Vectashield mounting medium for fluorescence (Vector Laboratories Inc.).

Image analysis

NeuN and Iba1: to quantify the density of neuronal and microglial cells in the cerebral cortex we used the StereoInvestigator software (MicroBrightField) equipped with motorized X–Y sensitive stage and video camera connected to a computerized image analysis system. NeuN-positive cells were counted using 20x magnification and sampling boxes (250 x 250 x 40 µm) located in both superficial and deep layers of PFC and ACC cortex. Iba1-positive cells were counted using 40x magnification and sampling boxes (250 x 250 x 40 µm) located in both superficial and deep layers of PFC cortex. Cell density was calculated by averaging values obtained from at least 6-8 counting boxes per animal.

Ki67 and DCX: examination of Ki67 and DCX-positively labelled cells was confined to the hippocampal dentate gyrus (DG), specifically to the granule cell layer (GCL) and the subgranular zone of the hippocampus defined as a two-cell body-wide zone along the border between the GCL and hilus. Quantification of Ki67 or DCX-immunoreactive cells was conducted from 1-in-6 series of immunolabelled sections using 20x magnification and spanning the rostrocaudal extent of DG. All immunostained sections were analyzed using the StereoInvestigator software. The reference volume was determined as the sum of the traced areas multiplied by the distance between the sampled sections. Densities of immunopositive cells were then calculated by dividing the number of positive cells by the reference volume. Numbers of positively labelled neurons were normalized as density per unit of volume (mm3).

vGlut1 and vGAT: to quantify the density of vGlut1- and vGAT-positive puncta, the parameters of acquisition (laser intensity, gain, offset) were optimized at the beginning of the acquisition and then held constant throughout image acquisition. All sections were acquired in random order in a single session to minimize fluctuation in laser output and degradation of fluorescence. We imaged superficial and deep layers of PFC and ACC on a Zeiss laser-scanning Apotome microscope using a 63x oil immersion objective. For each section, we imaged serial optical sections at 0.33 µm intervals for a total of at least 15 optical sections (5 µm). From each animal we imaged 6 sections (3 in superficial layers and 3 in deep layers). Maximum intensity projections (MIPs) were generated from the group of 5 consecutive sections yielding the

higher mean pixel intensity. These MIPs were imported in ImageJ and quantified using Puncta analyzer plugin (Ippolito and Eroglu, 2010). The number of positive puncta was measured within the entire acquired area.

Determination of lipofuscin accumulation by autofluorescence

Coronal brain sections were mounted on microscope slides and coverslipped using Vectashield mounting medium for fluorescence (Vector Laboratories Inc.). We imaged hippocampal DG on a Zeiss laser-scanning Apotome microscope using a 40x oil immersion objective. The parameters of acquisition were optimized at the beginning of the experiment and then held constant. Lipofuscin level was measured as the presence of autofluorescence at 550 nm in the region of interest. For each section, we imaged serial optical sections at 0.5 μm intervals for a total of at least 80 optical sections (40 μm). From each animal we imaged 3 – 4 sections. MIPs were generated from the group of 5 consecutive sections yielding the higher mean pixel intensity. These MIPs were imported in ImageJ and quantified using Threshold plugin. The area of positive puncta and mean pixel intensity were measured within the entire acquired area.

Patch clamp recording

Mice (aged P30 - 40) were deeply anesthetized with isoflurane (Baxter) then quickly decapitated. The brain was rapidly removed, and coronal sections (225 μm thick) of the primary visual cortex (V1) were obtained by cutting in a solution bubbled with 99% O_2 and containing (in mM): 240 sucrose, 2.5 KCl, 1.2 $MgCl_2$, 2.4 $CaCl_2$, 1.2 NaH_2PO_4, 15 $NaHCO_3$, 10 HEPES and 5 Glucose, at pH 7.4, using a Leica VT1000S vibratome. Immediately after sectioning, slices were transferred in recording artificial cerebro-spinal fluid (aCSF) bubbled with 99% O_2, containing (in mM): 126 NaCl, 2.4 sucrose, 2.5 KCl, 2.4 $MgCl_2$, 1.2 $CaCl_2$, 1.2 NaH_2PO_4, 15 $NaHCO_3$, 10 HEPES and 5 Glucose, at pH 7.4, and maintained at 35°C for 20 – 25 min then transferred at room temperature (RT) for a further 1 h before recordings were started. Somatic whole-cell recordings were obtained from pyramidal-shaped neurons in layer 4 of V1. Intracellular solution for miniature inhibitory post-synaptic potential (mIPSCs) in current clamp recordings contained (in mM): 10 K-Gluconate, 130 KCl, 10 Hepes, 1 EGTA, 0.3 $CaCl_2$, 1 $MgCl_2$, 4 MgATP, 0.3 NaGTP, 5 Phosphocreatine, at pH 7.3. Phosphocreatine was used only for the recordings of cells from WT mice, whereas KO cells were recorded without phosphocreatine, in order to simulate better the natural condition of Cr deficiency. The osmolarity of the intracellular solution was adjusted to 280 – 290 mOsm/l. For mIPSCs, cells were voltage-clamped at -80 mV by a Multiclamp 700A computer-controlled amplifier (Molecular Devices), sampled at 10 kHz and low-pass filtered at 2 kHz. Synaptic transmission was blocked by 1 μM tetrodotoxin (TTX), glutamate AMPA receptors were blocked by 10 μM 6,7-dinitro-quinoxaline-2,3-dione (DNQX) and glutamate NMDA receptors were blocked by 50 μM (2R)-amino-5-phosphonovaleric acid (APV). Glass pipette electrodes (2 to 4 MΩ

resistance when filled with internal solutions) were pulled from borosilicate capillaries (World Precision Instruments) using a Sutter P97 Flame Brown Puller (Sutter Instruments). Data acquisition and analysis was performed by using Clampex 8.2, Clampfit 10.3 (Molecular Devices) and Mini Analysis Program (Synaptosoft Inc.). Recordings in which access resistance (Ra) was higher than 50 MΩ or in which a variation of Ra > 20% was observed between the beginning and the end of the recording were discarded.

Proteomic analysis of mitochondria

Materials used: Iodoacetamide, dithiothreitol (DTT), 3-[(3-cholamidopropyl) dimethylammonio]-1-propanesulfonate (CHAPS), urea, thiourea, glycerol, sodium dodecyl sulfate (SDS), tetramethylethylenediamine (TEMED), ammonium persulfate (APS), glycine and 30% acrylamide-N,N,N bisacrylamide were acquired from Applichem (Germany). IPGs pH 3–10 NL, IPG-buffer 3–10NL and dry stripcover fluid were purchased from GE Health Care Europe (Uppsala, Sweden). Enhanced chemiluminescence (ECL) detection system was purchased from PerkinElmer (MA, USA). Anti-cofilin-1 (CFL1), anti-peptidyl-prolyl-cis-trans isomerase A (PPIA), anti-superoxide dismutase 1 (SOD1) and anti-glyceraldehyde-3-phosphate dehydrogenase (GAPDH) antibodies were purchased from Cell Signaling Technology, Inc. (MA, USA). Anti-peroxiredoxin 6 (PRDX6) antibody and was purchased from Santa Cruz Biotechnologies (TX, USA). Anti-peroxiredoxin 5 (PRDX5) antibody was acquired from R&D Systems Biotechne (MN, USA) and anti-ubiquinol-cytochrome c reductase binding protein (UQCRB) antibody was purchased from GeneTex Inc.(CA, USA) antibodies were purchased from Thermo-Fisher Scientific Inc. (MA, USA). A donkey anti-rabbit secondary antibody horseradish peroxidase (HRP)-conjugated was purchased from Stressgen (Belgium) while a donkey anti-goat secondary antibody HRP-conjugated and a goat anti-mouse secondary antibody HRP-conjugated were acquired from Santa-Cruz Biotechnology (TX, USA). Ruthenium II tris (bathophenantroline disulfonate) tetrasodium salt stain was purchased from Cyanagen All other reagents were purchased from standard commercial sources and were of the highest grade available.

Enriched Mitochondria preparations: for proteomic studies CrT$^{+/y}$ and CrT$^{-/y}$ P30 mice whole brains were immediately removed and processed to obtain mitochondrial enriched fractions. Briefly, whole brain was weighed, dissected on ice and homogenized in 10 volumes (w/V) isolation buffer (IB) (250 mM sucrose, 10 mM HEPES, 1 mM EDTA, pH 7.5) using a Teflon-glass homogenizer (15 strokes). Sample was centrifuged at 1000 g for 10 min at 4°C and the resulting pellet, containing nuclei and unbroken cell, was further homogenized in IB and centrifuged at 1000 g for 10 min at 4°C. The resulting two supernatants were combined and centrifuged at 1000 g for 8 min at 4°C to remove any nuclei and cellular debris. Then supernatant was centrifuged at 10000 g for 10 min at 4°C to obtain enriched mitochondrial fraction. Mitochondria were resuspended in IB and washed twice. Finally, a volume of IB, depending on size

of pellet, was added to resuspend mitochondrial fraction. Protein amounts were carried out by Biorad-DC assay using BSA as a standard. Mitochondria fractions were stored at -80°C until use.

Two dimensional electrophoresis: 2DE was performed as previously described (Ciregia et al., 2013). Briefly, 250 µg of proteins were filled up to 450 _l in rehydration solution, following the protocol of Rabilloud adjusted for mitochondrial solubilitazion. Immobiline Dry-Strips, 18 cm linear gradient pH 3 - 10 were rehydrated overnight in the sample and then transferred to the Ettan IPGphor Cup Loading Manifold for isoelectrofocusing according to protocol previously described (Ciregia et al., 2013). Then Immobiline strips were equilibrated and the second dimension (SDS-PAGE) was carried out by transferring proteins to 12% polyacrylamide, running overnight at 16 mA per gel at 10°C. At the end of run, the gels were stained with Ruthenium II tris (bathophenantroline disulfonate) tetrasodium salt (RuBP). ImageQuant LAS4010 (GE Health Care) was used for the acquisition of images. The analysis of images was performed using Same Spot (v4.1, TotalLab; Newcastle Upon Tyne, UK) software. The spot volume ratios between KO and WT were calculated using the average spot normalized volume of the three biological replicates each performed in duplicate. The software included statistical analysis calculations. The protein spots of interest were cut out from the gel and identified by LC-MS analysis.

Spot Digestion and Protein Identification: the gel pieces were washed twice with the wash buffer (25 mM NH4HCO3 in 50% acetonitrile (ACN)). Afterwards, proteins were reduced with 10 mM ditiothreitol (DTT) (45 min, 56°C), and alkylated with 55 mM iodoacetamide (IAA) (30 min, RT, in the dark). After two washes with the wash buffer, spots were completely dried in a centrivap vacuum centrifuge. The dried pieces of gel were rehydrated for 30 min at 4°C in 30 µL of trypsin porcine (Promega, Madison, WI, USA) solution (3 ng/µL in 100 mM NH4HCO3) and then incubated at 37°C overnight. The reaction was stopped by adding 10% trifluoroacetic acid (TFA). Samples were analyzed by LC-MS using a shorter chromatographic gradient and in autoMS mode. Each digested spot sample was analyzed by LC-MS/MS using a Proxeon EASY-nLCII (Thermo Fisher Scientific, Milan, Italy) chromatographic system coupled to a Maxis HD UHR-TOF (Bruker Daltonics GmbH, Bremen, Germany) mass spectrometer. Peptides were loaded on the EASY-Column TM C18 trapping column (2 cm L., 100 µm I.D, 5 µm ps, Thermo Fisher Scientific), and subsequently separated on an Acclaim PepMap100 C18 (75 µm I.D., 25 cm L, 5 µm ps, Thermo Fisher Scientific) nanoscale chromatographic column. The flow rate was set to 300 nL/min and the gradient was from 2% to 20% of B in 12 min followed by 20 to 45% in 9 min and from 45% to 90% in 2 min (total run time 35 min). Mobile phase A was 0.1% formic acid in H2O and mobile phase B was 0.1% formic acid in acetonitrile. The mass spectrometer, typically providing a 60,000 full width at half maximum (FMHW) resolution throughout the mass range, was equipped with a nanoESI spray source. The mass spectrometer was operated in Data Dependent Acquisition mode (DDA), using N2 as the collision gas for collision-induced dissociation (CID) fragmentation. Precursors in the range 400 to 2200 m/z (excluding 1220.0–1224.5 m/z) with a preferred charge state +2 to +5 and absolute intensity above 4706 counts were selected for fragmentation in a fixed cycle time of 3 s. After two spectra, the precursors were actively ex-

cluded from selection for 36 s. Isolation width and collision energy for MS/MS fragmentation were set according to the mass and charge state of the precursor ions (from 2+ to 5+ and from 21 to 55 eV). In-source reference lock mass (1221.9906 m/z) was acquired online throughout runs.

The raw data were processed using PEAKS Studio v7.5 software (Bioinformatic Solutions Inc, Waterloo, ON, Canada) using the function "correct precursor only". The mass lists were searched against the nextprot database including isoforms (version as of June 2017; 42,151 entries) using 10 ppm and 0.05 Da as the highest error tolerances for parent and fragment ions, respectively. Carbamidomethylation of cysteines was selected as fixed modification and oxidation of methionines and deamidation of asparagine and glutamine as variable modifications allowing 2 missed cleavages.

Western blot analysis: proteins of all WT and KO samples were separated by 1-D gel electrophoresis and then transferred onto nitrocellulose membranes (0.2 mm) as previously described (Ciregia et al., 2013). PPIA, GAPDH and UQCRB antibodies have been used at 1:1000 dilution whereas SOD1 and PRDX6 have been used at 1:200 dilution. Finally PRDX5 has been used at concentration of 1 ⎽g/ml. HRP-goat anti-rabbit and HRP-goat anti-mouse secondary antibodies were used at 1:10000 dilution whereas HRP-anti-goat was used at 1:5000 dilution. Immunoblots were developed using the enhanced chemiluminescence detection system (ECL). The chemiluminescent images were acquired using LAS4010. The immunoreactive specific bands were quantified using Image Quant-L software. In order to normalize the optical density of immunoreactive bands the optical density of total proteins was calculated. Therefore, immediately after WB, the membranes were stained with 1 mM RuBP (Ciregia et al., 2017).

Statistical analysis

All statistical analyses were performed using SigmaStat Software. Differences between two groups were assessed with a two-tailed t test. The significance of factorial effects and differences among more than two groups were evaluated with ANOVA/RM ANOVA followed by Holm-Sidak test. Rank transformation was exploited for data not normally distributed. Mann-Whitney test was used to analyze the distribution of frequency and amplitude of mIPSCs. For proteomic analysis of 2DE, a comparison among the different treatments was performed. The significance of the differences of normalized volume for each spot was calculated by the software Same Spot including ANOVA test.

The level of significance was $p < 0.05$.

Results

Reduced body weight growth in CrT$^{-/y}$ mice

A first clue indicating that CrT deficiency elicits age-related detrimental effects emerged from the general appearance of mutant animals. Mice were weighed at different ages and compared with WT littermates (Figure 4). Even though no particular problems of breeding were observed and the face of CrT$^{-/y}$ mice was normal till P40, CrT$^{-/y}$ animals (n = 12) showed a significantly reduced body weight compared to CrT$^{+/y}$ animals at P60, P100 and P180 (n = 13; Two-Way ANOVA on rank transformed data, p < 0.001 effect of genotype, p < 0.001 interaction between genotype and age; post hoc Holm-Sidak method, p = 0.092 at P40, p < 0.001 in all other comparisons).

Age-related deterioration of cognitive functions in Cr deficiency conditions

In a previous behavioral investigation performed at P40, it was highlighted that CrT$^{-/y}$ mice exhibit a general cognitive impairment across different learning and memory tests (Baroncelli et al., 2014). To understand whether a progressive deterioration of cognitive performance is present in CrT$^{-/y}$ mice, we studied four different stages: I) during the early brain development (P28 at the beginning of testing); II) during the late brain development (P40 at the beginning of testing); III) in the adult age (P100 at the beginning of testing) and IV) in the middle age (P180 at the beginning of testing). Interestingly, a progressive worsening of cognitive symptoms was detectable in CrT$^{-/y}$ mutant mice, suggesting that age is a key feature of Cr deficiency disease.

Y maze

We first analyzed the performance of CrT$^{-/y}$ animals at P28 using the Y maze spontaneous alternation, which is an optimal task for probing memory in juveniles (Figure 5A). Animals of both groups equally explored all the three arms of the maze. Indeed, no effect of genotype was detected for either the number of entries in the single arms of the maze (designated A, B, C) or the total number of arm entries, indicating that the exploratory disposition of mutant animals (n = 9) was not altered compared to WT littermates (n = 11; Two-Way ANOVA on rank transformed data, post hoc Holm-Sidak method, p = 0.506, p = 0.941, p = 0.276, p = 0.391 respectively,

Figure 5A). However, while in young WT mice alternation rate was about 60% of total arm choices, in CrT$^{-/y}$ animals it dropped to the chance level (50%; Figure 5B), demonstrating that CrT disruption in the mouse model could reproduce the early pathological phenotype of CCDS1 patients. The same impairment was detected at P40, P100 and P180 with CrT$^{-/y}$ mice performing at chance level whereas WT age-matched controls showed significant spontaneous alternation (t-test, $p < 0.01$ for P40, $p < 0.05$ for P100 and P180, Figure 6). These data also indicated that the spontaneous alternation paradigm cannot reveal age-dependent cognitive decline in CrT mutants because of the ceiling effect in the arm alternation deficit masking the effect of the age variable.

Object recognition test (ORT)

We assessed declarative memory abilities in the ORT, a test based on the spontaneous tendency of rodents to spend more time exploring a novel object than a familiar one. No difference in short-term recognition memory between P40 CrT$^{-/y}$ mice (n = 9) and age-matched WT animals (n = 7) could be detected (t-test, $p = 0.285$). In contrast, the discrimination index at 24h was significantly lower in mutant mice, indicating that their capacity to recall the familiar object was impaired (t-test, $p < 0.05$; Figure 7A). This memory deficit became more pronounced two months later (CrT$^{-/y}$ n = 11, CrT$^{+/y}$ n = 10; P100, t-test, $p < 0.01$ at 24h; Figure 7B), eventually affecting both short- and long-term memories at P180. Indeed, at P180 CrT$^{-/y}$ mice showed a marked memory deficit both at 1- and 24-h interval between the sample and the test phase with respect to CrT$^{+/y}$ mice (CrT$^{-/y}$ n = 10, CrT$^{+/y}$ n = 9; t-test, $p < 0.05$ for both comparisons; Figure 7C), indicating that the longer the time during which neural circuits are forced to work without Cr energy buffer the worse the cognitive performance of CrT$^{-/y}$ animals.

Morris water maze (MWM)

We further assessed memory abilities in the MWM, a cognitive paradigm that allows testing spatial learning and memory. The probe test highlighted a spatial memory impairment in Cr deficient mice at all the different ages tested: WT animals, indeed, spent significantly longer time in the quadrant where the platform was located during the training days (NE*; Two-Way RM ANOVA, post hoc Holm-Sidak method, $p < 0.05$ for all comparisons), while mutant mice did not remember the location of the hidden platform and equally explored the four quadrants of the maze (Two-Way RM ANOVA, post hoc Holm-Sidak method; Figure 8).

The results obtained in the training phase of the MWM test, however, showed a clear progression of cognitive deficits in CrT$^{-/y}$ mice. Since a main effect of genotype was found on mean swimming speed recorded all along the training phase at the different ages tested (t-test, $p < 0.05$ (P40); Mann–Whitney Rank Sum test, $p < 0.05$ (P100); t-test, $p < 0.01$ (P180); Figure 9), we analyzed the length of path covered to find the submerged platform. At P40 CrT$^{-/y}$ animals (n = 12) were able to learn the

task as well as their age-matched WT controls (n = 10): although the mean distance to locate the submerged platform on the last three days of training was longer in mutant mice compared to $CrT^{+/y}$ littermates (t-test, p < 0.05), they exhibited a progressive reduction of the path length similar to WT littermates (Two-Way RM ANOVA, p = 0.084 effect of genotype) with a significant difference between the two groups only at the day 5 of training (post hoc Holm-Sidak method, p < 0.05; Figure 10). The same was true in P100 animals ($CrT^{-/y}$: n = 8, $CrT^{+/y}$: n = 7; Two-Way RM ANOVA on rank transformed data, p = 0.132 effect of genotype, post hoc Holm-Sidak method, p < 0.05 at day 5; Figure 10). In contrast, $CrT^{-/y}$ mice (n = 7) were significantly slower learners with respect to age-matched WT mice (n = 9) at P180 so much so that the distance to locate the platform was different between the two groups at days 3, 4, 5 and 6 of training (Two-Way RM ANOVA on rank transformed data, genotype, p < 0.001, interaction between genotype and day p < 0.001; post hoc Holm-Sidak method, p < 0.05 for day 3 and 6, p < 0.01 for day 4 and 5; Figure 10C).

To further corroborate the hypothesis of a premature cognitive decline in CrT null mice, we compared the performance in the MWM of P180 $CrT^{-/y}$ animals and one-year old wild-type mice (n = 4). The mean distance to locate the platform on the last three days of training (t-test, p = 0.968) and the probe test revealed a similar learning and memory impairment in these two experimental groups (Two-Way RM ANOVA, p = 0.479; Figure 11).

Emotional phenotype is not altered in CrT mutant animals

To rule out the possibility that significant differences in cognitive capacities reflect changes in the ability to cope with stress in challenging task conditions, we analyzed the general activity and anxiety-related behavior of $CrT^{-/y}$ and $CrT^{+/y}$ mice in the open field arena at the different ages used for cognitive assessment. We found that the time spent by $CrT^{-/y}$ mutant mice (n = 12 for P40 and P100, n = 11 for P180) in both the central and peripheral portion of the apparatus was not different from that recorded for WT animals (n = 13 for P40 and P100, n = 11 for P180) at any of the time point tested (Two-Way ANOVA, post hoc Holm-Sidak method, p = 0.725 at P40, p = 0.508 at P100 and p = 0.348 at P180), indicating that the vulnerability to stress and anxiety responses are not sensitive to CrT deletion and excluding the hypothesis that the progression of cognitive deficit might be related to altered emotionality (Figure 12).

$CrT^{-/y}$ mice exhibit increased repetitive and stereotyped behavior

Since the clinical picture of CCDS1 patients includes multiple traits linked to autism spectrum disorders (ASDs), we also examined social behavior in CrT null mice. Although we used two different social interaction paradigms, we detected no abnormalities in $CrT^{-/y}$ mice at P180. In the social preference test, indeed, both $CrT^{-/y}$ (n = 8) and $CrT^{+/y}$ (n = 6) animals spent significantly more time exploring the wire cup housing the conspecific subject (Mann–Whitney Rank Sum test, p = 0.662; Figure

13A). Similarly, the index measured in the social novelty task did not differ between mutant and WT mice (t-test, p = 0.784; Figure 13A).

The second core ASD symptom domain includes repetitive and stereotyped movements, routines and rituals (Etherton et al., 2009) and several mouse lines with ASD-associated mutations exhibit enhanced learning on the accelerating rotarod, a task that requires formation and consolidation of a repetitive motor routine (Rothwell et al., 2014). Thus, we tested rotarod abilities of CrT$^{-/y}$ (n = 12 for P40, n = 11 for P100 and n = 9 for P180) and CrT$^{+/y}$ (n = 13 for P40 and P100, n = 11 for P180) animals, with the speed of rotation accelerating from 4 to 40 rpm over 600 s. The performance of CrT$^{-/y}$ mutant mice diverged from that of wild-type mice, with a significant increase of fall latency from the drum at all ages tested (Two-Way ANOVA, effect of genotype p < 0.001, post hoc Holm-Sidak method, p < 0.01 at P40 and P100, p < 0.05 at P180; Figure 13B). We next examined self-grooming, another stereotyped behavior in mice (Fuccillo, 2016). While no difference was present at P40 (CrT$^{-/y}$, n = 9; CrT$^{+/y}$, n = 7; Two-Way ANOVA on rank transformed data, post hoc Holm-Sidak method, p = 0.912) CrT null mice spent about threefold as much time grooming themselves as littermate WT mice at P180 (CrT$^{-/y}$, n = 7; CrT$^{+/y}$, n = 11; p < 0.01; Figure 13C).

CrT deletion leads to a widespread Cr reduction in young and adult mice

To understand whether the progression of cognitive deficits in CrT$^{-/y}$ mice was due to a gradual reduction of brain Cr content, we measured Cr levels in various tissues in 1-month- and 6-month-old animals using GC/MS. At both ages, we observed a significant reduction of Cr in the brain (both cerebral cortex and hippocampus; Two-Way ANOVA on rank transformed data, post hoc Holm-Sidak method, p < 0.001), muscle (p < 0.001), heart (p < 0.001) and kidney (p < 0.05) of CrT$^{-/y}$ mice with respect to WT littermates (n = 4/tissue for each group; Table 1). Importantly, no difference was detected in Cr levels measured in the different tissues between P30 and P180 CrT$^{-/y}$ mice, except for the muscle: a Three-Way ANOVA on rank transformed data analysis revealed a significant interaction (p < 0.001) between genotype and age only at level of muscular tissue with a significant reduction of Cr levels in P180 CrT$^{-/y}$ mice (post hoc Holm-Sidak method, p < 0.001). A moderate change in GAA levels was observed in some tissues (Table 2) suggesting that Cr deficiency leads to a compensatory attempt by upregulating Cr biosynthesis. Also, in this case GAA content measured in P180 animals reproduced the levels reported in younger tissues: a Three-Way ANOVA on rank transformed data revealed a significant interaction (p < 0.001) between genotype and age only at level of muscular tissue, but this analysis only stressed a significant reduction of GAA levels in P180 CrT$^{-/y}$ (post hoc Holm-Sidak method, p < 0.05) and WT mice (p < 0.001). These results allow rejecting the hypothesis that higher GAA toxicity could underlie the observed age-related decline of cognitive functions in CrT$^{-/y}$ animals.

Morphological characterization of neural circuits in CrT$^{-/y}$ mice

The morpho-functional organization of neural circuits in mice carrying CrT mutations has never been studied so far. Thus, we have investigated whether the accelerated decline of learning and memory functions in CrT-deficient mice was accompanied by pathological changes in brain morphology. The cerebral cortex and the hippocampus were analyzed because they are strictly involved in the symptoms caused by CrT deficiency in mice and in humans. In the same animals subjected to behavioral characterization, we first evaluated the neuroanatomical architecture of prefrontal (PFC) and cingulate cortex (ACC) of P180 mice (n = 6 for both groups). Cortical thickness and neuronal cell density were estimated on NeuN stained sections. No difference in the cortical thickness (t-test, p = 0.785 for PFC and p = 0.880 for ACC; Figure 14) and neuronal density across cortical layers was observed in mutant animals (Two-Way ANOVA, p = 0.683 for PFC; Two-Way ANOVA on rank transformed data, p = 0.146 for ACC; Figure 14).

Loss of GABAergic synapses in the cerebral cortex of CrT$^{-/y}$ mice

Since synaptic dysfunction is a feature commonly observed in normal aging and neurodegenerative disorders likely contributing to the pathology progression (Bano et al., 2011), we analyzed the synaptic punctate expression of vGlut1 and vGAT, respectively as synaptic markers of excitatory and inhibitory neurons, in the cerebral cortex of CrT$^{-/y}$ mice. While excitatory synapses were not affected by Cr deficiency (n = 6 for both groups; Mann–Whitney Rank Sum test, p = 0.792 for PFC; t-test, p = 0.340 for ACC; Figure 15A), we detected a prominent loss of vGAT staining both in PFC and ACC, suggesting a specific contribution of GABAergic synaptic alterations to the neuropathological phenotype of CCDS1 (n = 9 for CrT$^{-/y}$ group, n = 8 CrT$^{+/y}$ group; t-test, p < 0.05 for both comparisons; Figure 15B). Importantly, the loss of vGAT-positive synapses overspread all the cortical layers.

Microglial cells dysregulation in Cr deficient brain

Since aberrant microglia activation is one of the main pathological hallmarks of brain aging (von Bernhardi, Eugenín-von Bernhardi and Eugenín, 2015; Matt and Johnson, 2016) we have also evaluated Iba-1 expression as a marker of possible morphological changes of microglia in the cerebral cortex (namely PFC) and the hippocampus (HP) of mutant mice.

During aging microglia cells undergo morphological changes towards a reactive phenotype with short, thickened and less ramified processes (Hefendehl et al., 2014). We found a strong increase of activated microglial cells in the brain of CrT null animals as compared to WT controls (n = 8 for both groups), with a parallel reduction of resting cells (Two-Way ANOVA, post hoc Holm-Sidak method, p < 0.01 for PFC and p < 0.05 for HP; Figure 16A and B), indicating that the metabolic deficit caused by

Cr deficiency leads to a dysfunction of brain-immune cells interactions and to a neu-roinflammatory state that can contribute to the cognitive decline reported in CrT$^{-/y}$ mice.

Reduced neurogenesis and enhanced lipofuscin accumulation in the hippocampus of CrT$^{-/y}$ mice

It is well known that the rate of neurogenesis declines dramatically with age, and dysregulation of hippocampal neurogenesis is an important mechanism underlying the cognitive impairment associated with normal aging (Lee, Clemenson and Gage, 2012). In order to investigate whether CrT deficiency could affect hippocampal structure and impinge on the neurogenesis process, we examined neuronal proliferation through Ki67 labelling in the dentate gyrus (DG) of wild type and CrT$^{-/y}$ mice (n = 6 for both groups). Stereological analysis first revealed that the hippocampal volume of mutant animals was markedly reduced with respect to that measured in control mice (t-test, $p < 0.05$; Figure 17A). The number of Ki67-positive cell was significantly lower in the DG of CrT$^{-/y}$ animal at P180, with approximately 30% reduction (t-test, $p < 0.01$; Figure 17B and D). We also evaluated the number of immature neurons in hippocampal DG using the neuroblast marker doublecortin (DCX). DCX-positive cells were also significantly reduced in CrT null mice DG (t-test, $p < 0.001$; Figure 17C and E), demonstrating the impairment of adult hippocampal neurogenesis and suggesting another cellular substrate of the cognitive deficit present in the CrT null model. Another characteristic neuropathological finding in CrT mice was the massive accumulation of autofluorescent material (lipofuscin).

Lipofuscin is a lipopigment consisting of aggregated products of lysosomal degradation, including oxidized and misfolded proteins, lipids, defective mitochondria and metal ions (Dunlop, Brunk and Rodgers, 2009). We observed a marked accumulation of autofluorescent lipofuscin throughout the brain, but the most prominent autofluorescent signal was seen in the DG hippocampal region. Lipofuscin deposition and accumulation within the hippocampal neurons is a marker of cellular senescence (Terman and Brunk, 2006; Assunção et al., 2011). Thus, we compared the area of lipofuscin granules in the brain cells of 6-month-old CrT$^{-/y}$ (n = 6) mice and their CrT$^{+/y}$ siblings (n = 5). The accumulation of lipofuscin was significantly exacerbated in the hippocampal DG of CrT$^{-/y}$ animals at P180 (t-test, $p < 0.05$, Figure 17F and G).

Electrophysiological characterization

We found no statistically significant difference in any of the electrical passive properties studied in neurons, between CrT$^{-/y}$ and CrT$^{+/y}$. In particular, we did not find difference in membrane resistance (t-test: $p = 0.27$; CrT$^{+/y}$ n cells/mice = 42/15; CrT$^{-/y}$: n cells/mice = 44/12; Figure 18A) and in membrane capacitance (t-test: $p = 0.37$; CrT$^{+/y}$: n cells/mice = 43/15; CrT$^{-/y}$ n cells/mice = 43/12; Figure 18B). The membrane resting potential was only slightly but not significantly altered in CrT$^{-/y}$ mice compared to CrT$^{+/y}$¬ (t- test: $p = 0.14$; CrT$^{+/y}$: n cells/mice = 42/15; CrT$^{-/y}$: n cells/mice =

33/12; Figure 18C). We then recorded mIPSCs in voltage-clamp using patch-clamp technique, finding no difference in the distribution of the amplitude of mIPSCs between $CrT^{-/y}$ and $CrT^{+/y}$ (Mann-Whitney Rank Sum test: p = 0.132; $CrT^{+/y}$: n cells/mice = 35/15; $CrT^{-/y}$: n cells/mice = 34/12, Figure 19A), whereas we found a pronounced higher interevent interval in $CrT^{-/y}$ (Mann-Whitney Rank Sum test: p < 0.001; $CrT^{+/y}$: median 132.4 ms; n cells/mice = 35/15; $CrT^{-/y}$: median: 215.9 ms; n cells/mice = 34/12, Figure 19B), indicating a reduced frequency of mIPSCs in cortical pyramidal neurons.

Nervous system-specific CrT depletion leads to significant Cr reduction in the cerebral compartment

Since $CrT^{-/y}$ mice with ubiquitous deletion of the CrT gene showed a marked Cr depletion also in peripheral tissues, we analyzed the conditional nestin-KO in which CrT is deleted in post-mitotic neurons, glial cells and BBB endothelial cells by using the Nestin promoter to drive Cre-recombinase expression: nes-CrT mice (Tronche et al., 1999).

In order to determine the validity of our approach for tissue-specific CrT gene deletion, we measured Cr levels in various tissues in 1-month- and 6-month-old animals using GC/MS. At both ages, we observed a specific reduction of Cr in the cerebral cortex and the hippocampus of mutant mice (nes-$CrT^{-/y}$) with respect to wild-type animals ($CrT^{+/y}$) and Cre-recombinase expressing littermates (nes-$CrT^{+/y}$), while no significant difference was detected between $CrT^{+/y}$ and nes-$CrT^{+/y}$ animals. Peripheral tissues including muscle, heart and kidney were not affected (n = 4/tissue for each group; Figure 20; Table 3Table 4). Only at P180, we detected a small difference of Cr content between nes-$CrT^{-/y}$ and $CrT^{+/y}$ mice, which is likely due to the scattered expression of Nestin promoter in heart cells. At both ages, we observed that CrTfl/y animals not expressing Cre recombinase did not present a hypomorph phenotype, with normal levels of Cr in all tissues (Figure 20). Importantly, no difference was detected in Cr levels measured in the different tissues between P30 and P180.

Reduced body weight growth in nes-$CRT^{-/y}$ mice

Nes-$CrT^{-/y}$ animals (n = 6) showed a slightly reduced body weight compared to WT animals (n = 13) and nes-$CrT^{+/y}$ littermates (n = 9) at P100, P180 and P365, while no difference was present at P40 and P60 (Figure 21). Despite an age-dependent progressive increase of body mass in all experimental groups, the average decrease of body weight in nes-$CrT^{-/y}$ animals was about 10%.

Age-dependent deterioration of cognitive functions in brain-specific mutant mice

We then moved to assess the cognitive functioning of our model and to compare it with the result already seen in the ubiquitous model and in patients. With this aim

and also to understand whether a progressive deterioration of learning and memory functions is present in nes-CrT$^{-/y}$ mice, we studied four different stages: I) during the brain development (P40 at the beginning of testing), II) in the adult age (P100 at the beginning of testing), III) in the middle age (P180 at the beginning of testing), and IV) in the early aging (P365 at the beginning of testing). Since mild secondary effects of Cre-recombinase transgene insertion or Cre activity on selected endophenotypes have been previously suggested (Giusti et al., 2014) we also analyzed the behavior of nes-CrT$^{+/y}$ littermates at the same time points. We report a delayed onset of cognitive decline in nervous system-specific nes-CrT$^{-/y}$ mice with respect to whole-body CrT$^{-/y}$ mutants, followed by an age-dependent increase of cognitive frailty. No alterations of learning and memory, general exploratory activity, motor function and stereotypies were detected in the Nestin-cre mouse line. These results strengthen the concept that we already drawn from our ubiquitous model, that age is a key factor of mice carrying Cr deficiency.

Y maze in nes-CrT$^{-/y}$

We first analyzed the performance of nes-CrT$^{-/y}$ animals at P40 using the Y maze spontaneous alternation. Mutant nes-CrT$^{-/y}$ (n = 6), nes-CrT$^{+/y}$ littermates (n = 9) and control wild-type animals (CrT$^{+/y}$, n = 13) equally explored the three arms of the maze with no bias towards a specific branch. Indeed, no effect of genotype was detected for the number of entries in the single arms of the maze (designated as A, B, C), despite an increased total number of entries by nes-CrT$^{-/y}$ mice (Figure 22A). At this age, the alternation rate was not different among CrT$^{+/y}$, nes-CrT$^{+/y}$ and nes-CrT$^{-/y}$ and groups (Fig. 22A). In contrast, an impairment was detected at P100 and P180, with a significantly lower performance of nes-CrT$^{-/y}$ animals with respect to CrT$^{+/y}$ age-matched mice and nes-CrT$^{+/y}$ littermates (Figure 22B,C). Also at these ages, the total number of entries by nes-CrT$^{-/y}$ mice is higher with respect to the two control groups, but no bias was present in the exploration of the three arms (Figure 22B,C).

Object recognition test (ORT) in nes-CrT$^{-/y}$

In the same animals, we assessed declarative memory abilities with the ORT, a test based on the natural tendency of rodents to spend more time exploring a novel object than a familiar one. No difference in short- (1h) and long-term (24h) recognition memory was detected at P40 in nes-CrT$^{-/y}$ mice (n = 6) with respect to CrT$^{+/y}$ (n = 10) and nes-CrT$^{+/y}$ animals (n = 8; Figure 23A).

The total time of object exploration during the test phase was also comparable among the three experimental groups. A memory deficit became apparent two months later, when the discrimination index at 24h was significantly lower in mutant mice, indicating a weakened capacity to recall a familiar object (P100, CrT$^{+/y}$: n = 10, nes-CrT$^{+/y}$: n = 9, nes-CrT$^{-/y}$: n = 6; Figure 23B). This impairment eventually affected both short and long-term memories at P180. Indeed, at this age nes-CrT$^{-/y}$ mice showed a marked memory deficit both at 1- and 24-h interval between the sample and the test

phase with respect to CrT$^{+/y}$ and nes-CrT$^{+/y}$ mice (CrT$^{+/y}$ n = 11, nes-CrT$^{+/y}$ n = 9, nes-CrT$^{-/y}$ n = 6; Fig. 23C). At both ages, total time of exploration was still comparable among groups (Figure 23B, C).

Morris water maze (MWM) in nes-CrT$^{-/y}$

We further assessed memory abilities in the MWM task, a cognitive paradigm that allows testing spatial learning and memory. No difference was observed in the MWM performance of CrT$^{+/y}$, nes-CrT$^{+/y}$ and nes-CrT$^{-/y}$ mice at P40 (CrT$^{+/y}$: n = 10, nes-CrT$^{+/y}$: n = 5, nes-CrT$^{-/y}$: n = 5), P100 (CrT$^{+/y}$: n = 7, nes-CrT$^{+/y}$: n = 5, nes-CrT$^{-/y}$: n = 5) and P180 (CrT$^{+/y}$: n = 9, nes-CrT$^{+/y}$: n = 6, nes-CrT$^{-/y}$: n = 5), with mutant animals being able to learn the task during the training phase and to remember the position of the platform in the probe trial as well as their age-matched controls (Figure 24A - C). At 1-year of age, however, nes-CrT$^{-/y}$ mice (n = 12) were significantly poorer learners with respect to age-matched CrT$^{+/y}$ (n = 12) and nes-CrT$^{-/y}$ animals (n = 14) so much so that the distance to locate the platform was different between the three groups at days 5 and 6 of training (Figure 24D, left). The probe test confirmed the presence of a spatial memory impairment in the conditional mutant mouse: animals not carrying the floxed allele, indeed, spent significantly longer time in the quadrant where the platform was located during the training days while mutant mice did not remember the location of the hidden platform and equally explored the four quadrants of the maze (Figure 24C, right). As expected, no effect of genotype was found on mean swimming speed recorded all along the training phase at the different ages tested (Figure 25), demonstrating that motor functions are largely preserved in the brain-specific CrT murine model.

Anxiety levels and motor activity are not altered in nes-CrT$^{-/y}$ mice

To exclude the possibility that differences in cognitive tasks reflect changes in anxiety levels and stress response, we evaluated general activity and anxiety-related behavior of CrT$^{+/y}$ mice, nes-CrT$^{+/y}$ and nes-CrT$^{-/y}$ in the open field arena following the same experimental schedule used for cognitive assessment (P40 and P100: CrT$^{+/y}$ n = 13, nes-CrT$^{+/y}$ n = 9, nes-CrT$^{-/y}$ n = 6; P180: CrT$^{+/y}$ n = 11, nes-CrT$^{+/y}$ n = 8, nes-CrT$^{-/y}$ n = 6). Although all animals tended to remain in the peripheral region of the arena for a significantly longer time length, the time spent by nes-CrT$^{-/y}$ mutant mice in both the central and peripheral portion of the apparatus was not different from that recorded for CrT$^{+/y}$ and nes-CrT$^{+/y}$ animals at any of the time point tested (Figure 26). No difference was detected either in motion speed or total distance moved at P40 and P180, even if a decreased activity was observed in nes-CrT$^{+/y}$ at P100 (Figure 26). These data are in line with the lack of alterations in this test previously observed in the ubiquitous CrT mutant.

To evaluate motor function in non-aversive environment, we also longitudinally investigated home-cage locomotor activity in this mouse model (P40 and P100: CrT$^{+/y}$ n = 13, nes-CrT$^{+/y}$ n = 9, nes-CrT$^{-/y}$ n = 6; P180: CrT$^{+/y}$ n = 11, nes-CrT$^{+/y}$ n = 9, nes-

CrT$^{-/y}$ n = 6). We found that nes-CrT$^{-/y}$ mice are significantly more active than the CrT$^{+/y}$ and the nes-CrT$^{+/y}$ group at P100. More specifically, nes-CrT$^{-/y}$ mice showed increased horizontal activity during the night period (Figure 27). In agreement with the data obtained with the open field test, no effect of genotype was observed at P40 and P180 Figure 27). Finally, we performed a direct measurement of muscle function using the conventional grip strength test in adult animals (P180; CrT$^{+/y}$ n = 13, nes-CrT$^{+/y}$ n = 11, nes-CrT$^{-/y}$ n = 7). Nes-CrT$^{-/y}$ mice displayed a forelimb strength totally comparable to wild-type and nes-CrT$^{+/y}$ animals (Figure 28).

Absence of pathological repetitive and stereotyped behavior in nes-CrT$^{-/y}$ mice

CCDS1 patients can show traits linked to autism spectrum disorders. Moreover, as reported above, we found that ubiquitous CrT$^{-/y}$ mutant animals exhibit increased repetitive and stereotyped behavior. Thus, we examined the performance of CrT$^{+/y}$ mice (n = 13 for P40 and P100, n = 11 for P180 and P365), nes-CrT$^{+/y}$ (n = 9 for P40, P100 and P180, n = 11 for P365) and nes-CrT$^{-/y}$ (n = 6 for P40, P100 and P180, n = 7 for P365) in the rotarod test and the amount of self-grooming at P180 (CrT$^{+/y}$: n = 11, nes-CrT$^{+/y}$: n = 11, nes-CrT$^{-/y}$: n = 7) and P365 (CrT$^{+/y}$: n = 6, nes-CrT$^{+/y}$: n = 10, nes-CrT$^{-/y}$: n = 7; (Rothwell et al., 2014; Fuccillo, 2016). Nes-CrT$^{-/y}$ mutant mice did not differ from CrT$^{+/y}$ and nes-CrT$^{+/y}$ mice in the rotarod task, with a totally comparable fall latency from the drum at all ages tested (Figure 29A). The same was true for the self-grooming: indeed, no difference was present in the time nes-CrT$^{-/y}$, CrT$^{+/y}$ and nes-CrT$^{+/y}$ spent grooming themselves (Figure 29B). These results suggest that the presence of autistic-like traits in the mouse model are related to the lack of Cr in tissues other than the CNS, that is: it seems to have a peripheral pathogenesis.

Proteomic analysis of mitochondria in ubiquitous KO

Comparative 2DE analysis

A comparative analysis between KO and WT 2DE proteomic maps was performed, at P12 and P30. Figure 30 illustrates a representative 2DE image of mitochondrial protein extracts for WT and KO P30 samples, respectively. The quality of gels was assessed by the software Same spot which includes the SpotCheck function. Overall an average of 1300 Spots was found within a nonlinear pH range from 3 to 10. Normalized spot volumes were analyzed by the ANOVA test to detect the proteins which were significantly ($p < 0.05$, q value < 0.05) differentially expressed between two classes. Fifty-five spots resulted differentially expressed in significant manner in CrT$^{-/y}$ with respect to CrT$^{+/y}$ at 30 days-old, in particular 14 spots showed fold > 2. All these spots were increased in CrT$^{-/y}$ deficiency mice. Thirty-seven spots of interest were selected and cut from the gel and identify by nano-LC-ESI-MS/MS. A list of identified proteins, with molecular weight (MW), isoelectric point (pI), score, and coverage values of MS/MS is shown in Table 5 (at the end of this section). Only four

spots resulted differentially expressed in significant manner in CrT$^{-/y}$ with respect to CrT$^{+/y}$ at 12 days-old (Table 6).

Pathway and Network Analysis

For the KO and WT comparison, proteins found differentially expressed were included in the Ingenuity Pathways Analysis (IPA) analysis to identify molecular and cellular functions and to investigate whether these proteins work together in specific networks. Therefore, the software generated a main network (score 60) (Figure 31) with associated biofunctions "Free radical scavenging, small molecules biochemistry, neurological diseases" (Figure 32) and focused on canonical pathways which showed the differentially expressed molecules to fall into functional categories such as mitochondrial dysfunction, glycolysis, sirtuin signaling, oxidative phosphorylation and Nrf2-mediated oxidative stress response (Figure 33). All the proteins found to be up- and down-regulated may concur in an upstream regulator analysis to predict if transcription factors or genes could be activated or inactivated in agreement with the z-score value (z-score > ±2 and p < 0.05). A list of activated and inhibited factors is shown in Table 5, and Figure 34 shows the interaction with the overexpressed proteins found in CrT$^{-/y}$ mice. In particular Rictor, fragile mental retardation protein 1 (FMR1) and EGLN resulted inhibited whereas mTOR, NFE2L2, ESRRD and PPARGC1A resulted activated. Furthermore, a relationship between a top regulator, APP, and a molecular function, "metabolism of reactive oxygen species", has been predicted in significant manner (Figure 35).

Western Blot Validation of proteomic results

We selected 6 proteins to perform validation by immunoblot analysis. The results confirmed the significant different expression of six proteins in CrT$^{-/y}$ with respect to WT. For each tested protein the OD of specific immunoreactive band was determined and the resulting mean values were compared (CrT$^{-/y}$ vs WT). As shown in Figure 36, it is confirmed significant the increase of expression for all proteins analyzed.

Discussion

CCDS1 is known to cause brain Cr depletion and several neurological deficits, but nothing is known about the neurobiological bases of this disease. We performed the first thorough morphological, functional, behavioral and proteomic characterization of two CCDS1 mouse models, a ubiquitous KO model and a brain-specific KO. The latter is a novel conditional model in which exons from 5 to 7 are deleted (Baroncelli et al., 2014), compared with a previous model in which a deletion of exons 2 to 4 is used (Skelton et al., 2011). However, in both models a dramatic reduction of brain Cr content is achieved, making them suitable for targeting CrT specifically in brain cells.

Cr deficiency was apparent in both the cerebral cortex and hippocampus (which are two brain regions crucially involved in the patient cognitive defects) of both $CrT^{-/y}$ and nes-$CrT^{-/y}$ mice, and the reduction observed overlapped with the levels of Cr that are found in the brain of CCDS1 patients (van de Kamp et al. 2013). Similarly, Cr levels were completely preserved in the skeletal muscle of nes-$CrT^{-/y}$ as observed in CCDS1 subjects (deGrauw et al., 2003; Pyne-Geithman et al., 2004). In contrast, $CrT^{-/y}$ mice displayed a marked reduction of Cr in extraneural tissues, that does not match what is described in human patients, where the main organ involved is the brain and the other tissues seem relatively spared (Puusepp et al., 2010; Joncquel-Chevalier Curt et al., 2015).

The longitudinal analysis revealed a progressive cognitive decline not paralleled by either a decrease of Cr levels in the brain tissue or a rise of GAA (which is a toxic metabolite), strengthening the idea that the chronic deficit of Cr energy buffer is the main event triggering cellular and molecular compensatory mechanisms that bring about the progressive deterioration of brain function. The only tissue in which we were able to detect a significant reduction of Cr levels over time was the muscle, suggesting that compensatory upregulation of Cr in the muscle declines with age. This finding raises the possibility that a muscular phenotype could also occur in patients later in life.

The phenotype associated with brain aging included progressive learning and memory deterioration, synaptic loss, microglial cell activation, neurogenesis impairment and lipofuscin deposition, and it already occurs in adult (i.e. not aged) animals. These significant differences in learning and memory performance of $CrT^{-/y}$ mice reflected changes in cognitive abilities per se: indeed, the open field test revealed that mutant mice display anxiety levels in the range of normal values, indicating that their capacity to cope with stressful conditions of behavioral tests is not altered.

The cognitive decline was similar in both the ubiquitous and the conditional model, highlighting that a local CrT loss of function is sufficient to induce a dysregulation of Cr levels in the brain. However, the cognitive impairment observed in the nes-CrT$^{-/y}$ mice was delayed compared to ubiquitous KO, and the conditional model lacks some traits usually linked to autism spectrum disorders, including repetitive and stereotyped movements, routines and rituals, all of which are present in CrT$^{-/y}$.

Nevertheless, these results clearly indicate that brain Cr depletion is a pivotal cause of the CCDS1 pathological phenotype, in particular with regard to the cognitive domain, but peripheral actors seem to play an important role. Future studies will allow elucidating the possible participation of peripheral metabolic alterations, blood biochemical milieu, immune abnormalities and intestinal microbiome in the etiology of CCDS1.

Unexpectedly, our data about the nes-CrT$^{-/y}$ are not consistent with a very recent work showing that spatial learning and memory deficits are already present in young (P60 - 90) brain-specific knockout mice (Udobi et al., 2018). We surmise that this discrepancy might be due to a lack of motivating force in the animals used in the cited paper, as suggested by the altered performance in the cued version of the MWM, in which spatial memory is not required.

The extent of the early aging that we observed is dramatically exemplified by the absence of difference in spatial learning performance when 6 months CrT$^{-/y}$ mice were compared to 12 months WT mice. We have considered the possibility that this accelerated decline in cognitive performance could be related to the documented neuroprotective (Matthews et al., 1999; Sullivan et al., 2000; Bender et al., 2008; Puusepp et al., 2010) and antiapoptotic effects of Cr (O'Gorman et al., 1997). However, when we examined the neuronal density in the cerebral cortex, we did not detect any significant reduction in the number of NeuN-positive cells either in the PFC or in the ACC. In contrast, we found a marked impairment of hippocampal neurogenesis in the brain of mature CrT$^{-/y}$ mice. This was assessed by observing significantly reduced numbers of Ki67-positive proliferating cells along with DCX-positive immature neurons in the hippocampal DG region. These results are consistent with the notion that the creation of new neurons is an energetically expensive process (Kempermann, 2015) and that the hippocampus is particularly vulnerable to metabolic alterations (Bartsch and Wulff, 2015). Since adult hippocampal neurogenesis plays a vital role in maintaining normal cognitive processing (Christian, Song and Ming, 2014) an impairment of this process could conceivably compromise hippocampal function and represent a key substrate of the cognitive defects seen in CrT$^{-/y}$ mice. Accordingly, most studies indicate a correlation between a compromised neurogenic niche and impaired performance in hippocampus-dependent cognitive tasks in aged mice (Lee, Clemenson and Gage, 2012).

In many neurodevelopmental disorders, an imbalance between excitation and inhibition is described (Bories et al., 2013; McQuail, Frazier and Bizon, 2015). In particular, inhibition seems to play a pivotal role and the dysfunction of an important class of inhibitory interneurons, namely PV-expressing (PV+) cells, could be involved in autist-like disorders (Yizhar et al., 2011). We, therefore, performed electrophysiological studies using patch clamp recording of mIPSCs from cortical principal neurons. We found a reduced frequency of events, with a normal amplitude distribution.

This could be associated with a reduction of release probability or with a decreased number of release sites. Morphological analysis revealed a reduction of presynaptic inhibitory puncta as indicated by the significant lower expression of the vesicular GABA transporter in two brain regions fundamentally involved in the processing of learning and memory tasks such as the PFC and the ACC. The whole picture, low mIPSCs frequency and less vGAT-expressing puncta, could be accounted for by a reduction of the number of inhibitory presynaptic release sites. These observations fit with the findings of a recent paper (Saunders et al., 2018) showing high expression of CrT in fast spiking PV+ inhibitory interneurons. These interneurons send axons to pyramidal neurons and to other PV+ cells as well, and because they can sustain high frequency firing, it is foreseeable that their energy requirement is very high. In turn this should require higher intracellular Cr levels and make them more vulnerable to Cr deficiency. The consequent dysfunction of inhibitory interneurons could explain the presence of epileptic phenotype in CCDS1 patients (Leuzzi et al., 2013) and some electroencephalogram (EEG) alterations (Schiaffino et al., 2005). Furthermore, the reduction of inhibition could represent another link to early aging, since many studies describe a loss of inhibitory neurons in the aged brain (Shetty and Turner, 1998; Vela et al., 2003; Shi et al., 2004).

Inflammation is increasingly being seen as a cardinal mechanism of aging (Franceschi et al., 2006), and we demonstrated that neuroinflammation plays a critical role in the progression of CrT disorder, enriching the framework of aging due to Cr deficiency. It is apparent that Cr depletion causes an aberrant activation of microglial cells in the brain of mature CrT$^{-/y}$ animals and activated microglia may release a number of cytokines and chemokines, which in turn activate many proinflammatory signal transduction pathways. It is known that coactivation of proinflammatory and cytotoxic products during neuroinflammation process is detrimental to neurons and may alter synaptic proteins (Rao et al., 2012). Recent evidence show that neuroinflammation also negatively affects hippocampal neurogenesis (Sierra et al., 2014; Ryan and Nolan, 2016). We could hypothesize that activated microglia-neuron crosstalk has detrimental effects on hippocampal neurogenesis and brain synaptic connectivity in CrT$^{-/y}$ animals. Thus, the dysregulation of microglial behavior appears to be a critical component of the negative progression of CrT deficiency pathology.

A possible trigger of neuroinflammation is the increased concentration of damaged macromolecules and protein aggregates as a result of an increase in oxidative stress as well as a result of mitochondrial dysfunction leading to excessive generation of reactive oxygen species (ROS) and oxidative damage to lipids, proteins and DNA. The Cr/PCr system is strongly implicated in the cellular bioenergetic function and several studies have revealed a correlation between Cr levels and intracellular ROS inasmuch Cr exhibits antioxidant activity either through direct interactions with oxidant species or through metabolic reactions conferring antioxidant protection (Lawler et al., 2002; Sestili et al., 2011). Accordingly, we found an enhanced accumulation of lipofuscin in the brain of CrT$^{-/y}$ mice that could be the result of increased oxidative damage (Höhn and Grune, 2013). The presence of lipofuscin can also influence important cellular processes, such as autophagy, by inhibiting the fusion between autophagosomes and lysosomes, thus further exacerbating the accumulation of degrada-

tion products and cognitive impairment (Brandenstein et al., 2016). In addition, patients with Cr deficiency syndromes have increased oxidative stress and ROS-induced apoptotic cell loss (Alcaide et al., 2011).

All these results strongly point towards a picture in which the lack of Cr sets in motion the precocious activation of detrimental cellular and molecular mechanisms typical of brain aging leading to a progressive cognitive regression. Considering that the most important function of Cr is believed to be its energy-buffering property, and that mitochondria are the sites in which most of the cell energy is produced, the missing link between Cr lack and the subsequent cognitive decline could be represented by mitochondria themselves and their role in energy metabolism. To investigate deeper this aspect, we performed a proteomic analysis of mitochondria enriched samples, which showed a marked alteration of the mitochondrial proteomic landscape in Cr deficient animals, with a total of 37 upregulated (identified) peptides in the brain of young (P30) CrT–/y mice. In contrast, pups carrying the same gene deletion at P12 did show a significant change of expression only in 4 proteins. Many of the differentially regulated peptides at P30 are enzymes and other proteins involved in the energy metabolism chain, including glucose metabolism, the tricarboxylic acid cycle, oxidative phosphorylation and fatty acid oxidation. Moreover, we observed an increased expression of multiple antioxidant enzymes.

Therefore, a general pattern emerges of enhanced energy-generating pathways attempting to compensate for the power failure caused by Cr depletion. This forced metabolic phenotype is likely to originate an overload of potentially harmful by-products of cellular metabolism, which in turn activates the antioxidant defense system. Considering the central role of Cr in energy regulation, it is not surprising that brain Cr deficit, in the attempt to compensate for loss of efficiency in the cellular network of ATP distribution, resonates in abnormal cellular metabolism, eventually resulting in a shift of the critical balance between free radical generation and antioxidant protection. Accordingly, it has been shown that the skeletal muscle of AGAT knockout animals exhibits a conspicuous increase in inorganic phosphate/ATP ratio and overall mitochondrial content, paralleled by a significant reduction of ATP levels (Nabuurs et al., 2013). Cellular metabolism and mitochondrial respiration increased in muscle fibers and brain of CrT$^{-/y}$ mice, with a higher number of mitochondria in CrT deficient cells (Perna et al., 2016). Moreover, pleomorphic and enlarged mitochondria, alterations of mitochondrial matrix and cristae appearance were observed at the electron microscope, in rats treated with an inhibitor of Cr uptake (Gori et al., 1988). Larger populations of motile mitochondria are present in cells with energy deficiency (Kuiper et al., 2008), potentially facilitating the recycling and elimination of damaged mitochondria. In agreement with this interpretation, we found an upregulation of several proteins pertaining to the lysosomal catabolic and the ubiquitin proteasome pathways.

IPA enrichment analysis unveiled further cellular processes and components, which are impaired in CrT deficiency. The expression of cofilin-1 was 2-fold increased in Cr deficient brain compared to WT animals, suggesting that energy stress condition leads to the accumulation of this protein. Cytoplasmic cofilin rods have been demonstrated to disrupt dendritic transport, cause loss of dendritic spines and corrupt synaptic function in other neurological disorders including Alzheimer disease, bipolar disorders and autism (Chen and Wang, 2015; Woo et al., 2015; Shaw and Bamburg,

2017). Moreover, a possible link between cofilin, and mitochondrial dynamics and function has been proposed (Beck et al., 2012). Thus, neuronal dysregulation of cofilin might be involved in CCDS1 pathogenesis. A possible trigger of cofilin polymerization is the increased concentration of damaged lipids, proteins and DNA as a result of oxidative stress (Bamburg and Bernstein, 2016), a phenotype indeed observed in our KO model.

The excessive generation of ROS and dysfunctional mitochondria might also be involved in the overexpression of the mitogen-activated protein kinase 1 (MAPK1/ERK2) signal transduction pathway (Zhu et al., 2002). Depending on the cellular context, MAPK cascade plays a pivotal role in diverse biological functions including cell growth, adhesion, survival, differentiation, synaptic plasticity and spine dynamics (Thomas and Huganir, 2004; Ratto and Pizzorusso, 2006), but ERK pathway may bidirectionally affect brain function and plasticity. A growing number of recent studies connect ERK kinase to autism spectrum disorders and other syndromes characterized by intellectual disability (Kalkman, 2012), providing evidence that developmental abnormalities in neurogenesis and cortical cytoarchitecture can be associated with a paradoxical increase of ERK signaling (Pucilowska et al., 2015; Grissom et al., 2018). Although we do not know whether the overexpression of ERK1 corresponds to an actual hyperactivation, it is described in literature that ERK1 activation is associated with inhibition of ERK2, and the latter seems to modulate positively long-term recognition memory (Silingardi et al., 2011); in agreement with this picture, both our KO models, the ubiquitous and the conditional one, show strong impairment in recognition memory. These data raise the possibility that normalization of ERK activity, by treatment with ERK inhibitor peptides (Papale et al., 2017; Pucilowska et al., 2018), might rescue the CNS phenotype recorded in CrT$^{-/y}$ mice.

Our data also suggest that neuroinflammation and aberrant activation of microglial cells are crucial actors in the progression of CCDS1 disorder. It is known that activated microglia can release proinflammatory cytokines, such as peptidyl-prolyl cis-trans isomerase A (PPIA), also known as Cyclophilin A (Nigro, Pompilio and Capogrossi, 2013), another protein that we found overexpressed in CrT$^{-/y}$. Research in animal models and humans provided compelling evidence supporting the critical function of PPIA in acute and chronic inflammatory diseases (Hoffmann and Schiene-Fischer, 2014). Interestingly, PPIA expression increases with aging (Nigro, Pompilio and Capogrossi, 2013).

Finally, upregulation of pyridoxal kinase (PLK) expression may be involved in alterations of network excitability recurring in Cr deficiency syndromes (Leuzzi et al., 2013). Excessive pyridoxal phosphate concentration induced by increased PLK, indeed, may result in altered GABA levels (Ebadi and Klangkalya, 1979; Gospe, Olin and Keen, 1994) and/or the modification of specific residues on the GABA-A receptor producing the degeneration of GABAergic neurotransmission (Ishioka et al., 1995). In addition, patients with inborn errors of metabolism affecting vitamin B6 concentrations in the brain present early-onset epilepsy (Wang and Kuo, 2007; di Salvo et al., 2017). Therefore, the modulation of PLK expression may regulate seizure susceptibility in CCDS1 patients.

Despite the absence of a clear overlap in the neural proteomic milieu at P12 and P30, IPA analysis indicates that antioxidative defense is precociously reinforced in

the brain of CrT$^{-/y}$ mice, suggesting early compensatory changes to preserve the balance between ROS production and their detoxifying enzymes. It is worth noting that we did not find a Cr-concentration dose-dependency for molecular changes detected in the proteomic analysis, with the progressive alteration of protein expression not being paralleled by either a decrease of Cr levels or a rise of GAA toxicity in the brain tissue. Indeed, Cr and GAA levels were totally comparable in the cortex and the hippocampus of P30 CrT$^{-/y}$ mice with respect to P12 genotype-matched animals. These results suggest that the prolonged and continued lack of Cr energy buffer might set in motion detrimental mitochondrial and molecular mechanisms leading to free radical adverse reactions that accumulate with age throughout the brain and cause the gradual shutdown of its function. This hypothesis fits our findings of progressive deterioration of cognitive functions accompanied by a massive lipofuscin deposition in brain cells.

The changes in expression levels of the specific genes that we observed require that upstream modulators (e.g. transcription factors, co-activators, etc.) must be activated or repressed. Interestingly, our model predicts that the activation of the amyloid precursor protein (APP) would account for the overexpression of a significant subset of proteins, and this whole network would converge mainly towards the metabolism of ROS. APP is well known for its role in neural development (Nicolas and Hassan, 2014) and in Alzheimer disease. These findings need to be validated with further studies, but the prediction of APP activation in a picture dominated by a process of early aging is compelling, and, moreover, many studies have found a relation between APP expression and severe autism (Ray et al., 2011; Lahiri et al., 2013)

Among other up-stream regulators, some others are particularly worth mentioning. TP53 is predicted to be activated. Its role in brain in development has been highlighted in many studies (Brynczka and Merrick, 2008; Di Giovanni and Rathore, 2012), and according to a recent gene expression analysis based on large database, the gene coding for TP53 is linked to neurodegeneration and alterations in mitochondrial DNA and energy metabolism (Diaz-Beltran, Esteban and Wall, 2016).

RICTOR is predicted to be inhibited and the inhibition of this protein has been associated to inflammatory tissue infiltration, enhanced production of ROS and regulation of proliferation (Xu et al., 2018), alterations that we described in our models.

mTOR is predicted to be activated: this protein is involved in many vital cell functions like regulation of energy metabolism and proliferation and it has been linked to autism, epilepsy and neurodegenerative disorders (Lipton and Sahin, 2014).

FMR1, fragile X mental retardation 1 protein, is predicted inhibited. The deficiency of the protein leads to severe learning deficits and intellectual disability, characteristic of the fragile X syndrome, another well-known defect of neurodevelopment (Vanderklish and Edelman, 2002). Further analysis with Western blot will be required to confirm the alterations of all these proteins as predicted by our analysis.

This is the first proteomic analysis of brain samples in a CTD mouse model exploring molecular mechanisms linking Cr deficit, energy metabolism alterations and brain dysfunction. Previously, Zervou et al., 2016 used a high-throughput approach to examine Cr-dependent changes in the myocardial proteome (Zervou et al., 2016) and RNA sequencing of CrT deficient fibroblasts revealed a possible impairment of extracellular matrix and cytoskeleton, suggesting a role for Cr in structural regulation of cells (Nota et al., 2014). Despite the great relevance of investigating the effects of

Slc6a8 mutations at the whole-body level, CrT deficiency is primarily characterized by Cr depletion in the brain and unraveling the molecular pathophysiology affecting the cerebral compartment in animal models of this disorder could be a goldmine for the discovery of novel biomarkers and druggable targets. In particular, we believe that antioxidant drugs, inflammation inhibitors, and peptides modulating cofilin activity and ERK signaling might be valid therapeutic avenues for CTD cure. Given the complexity and high dynamic range of biological samples, however, future studies will be required to confirm that cognitive and neuropsychiatric symptoms of CCDS1 disorder are amenable to targeted drug therapy. We also bring to attention that our findings corroborate the hypothesis that multiple disorders of impaired cognition and autistic-like behavioral disturbances converge onto a few fundamental cellular processes, such as spine dynamics and the ERK/MAPK signaling cascade, affecting brain structural and functional plasticity.

In contrast to what observed at P30, only few proteins are differentially expressed at P12. This observation, if confirmed, can have translational relevance allowing to identify the exact time window in which many of the changes in the normal cell transcription program happen and could theoretically permit, together with early diagnosis, treating patients with drugs able to reverse these transcriptional alterations.

All the findings described in this work indicate that a massive impairment of cell metabolism follows the lack of Cr and that a long chain of events, only the first of which involving Cr directly, is started. Each of these steps can become, after adequate studies, a putative molecular target for therapeutic strategies.

The current study presents many elements of novelty: I) identification of the earliest cognitive phenotype observed so far in CCDS1 mice; II) discovering of early aging, inflammation and progressive neurodegeneration as fundamental aspects of this disorder; III) description of molecular pathways altered in samples enriched with mitochondria; IV) first insights into alterations of inhibitory circuits.

Impact on CCDS1 patients

The present results have demonstrated that brain-specific and ubiquitous CrT mull mice undergo to an early onset of brain aging. One fundamental conclusion emerging from this work is that CCDS1 is a metabolic disorder associated with early brain aging and that age should be a key factor to deal with in the clinical evaluation of patients. It has been previously reported that, in patients, intellectual disability becomes more pronounced with age (van de Kamp, Mancini, and Salomons 2014), but longitudinal studies in human are totally lacking and little is known about the progression of the disease.

In addition, our CrT mouse model allowed us to discover alterations of cellular and molecular mechanisms that play a pivotal role in the generation of the CCDS1 neurological phenotype. Mutant mice displayed alteration of GABAergic system, reduction of hippocampal neurogenesis, marked activation of microglia, altered oxidative metabolism and disruption of relevant molecular networks related to cell metabolism, mitochondrial function and ROS, leading to a general cognitive deterioration

progressively worsening with age. Moreover, the conditional KO showed that extraneural Cr loss might participate in the pathogenesis of the whole phenotype showed by CrT mutants.

This knowledge opens the important possibility to design targeted drug intervention protocols aimed at overcoming brain alterations. If we could rescue brain alterations underlying CCDS1, indeed, both clinical and behavioral amelioration should be achieved. The use of non-invasive methods for behavioral assessment suitable for longitudinal analysis and the morphological characterization of brain alterations in CrT$^{-/y}$ and nes-CrT$^{-/y}$ mice set a firm background for translational studies using this model, providing normative data and protocols necessary to validate potential treatment strategies prior to launching costly clinical trials.

Finally, our data also suggest that these mice models may be useful for exploring the mechanisms of age-related damage in the brain. The conditional mouse model lacks the early phenotype and the autistic-like traits of CCDS1 patients, highlighting that it does not represent a comprehensive tool for preclinical evaluation of potential CCDS1 treatments. However, we showed that extraneural Cr loss might modulate the phenotype of CrT mutants, making the use of nervous system specific models like nes-CrT mice important tools to understand the pathogenic mechanisms underlying neurological deficits induced by Cr deficiency.

A large number of neurodevelopmental and neurological disorders, including Down syndrome, Batten disease, progranulin deficiency, brain iron dysregulation, have been associated with early brain aging (Kopra et al., 2004; Ahmed et al., 2010; Maccarinelli et al., 2015; Head et al., 2016). Thus, a better understanding of factors that accelerate age-related deterioration of cognitive performance is critical both for improving the likelihood for successful aging and for revealing pathological changes of translational value.

Conclusions

Our work identifies new important features of CrT defects. In particular:

I) CCDS1 is a progressive neurodegenerative disorder in which, even if Cr concentration does not significantly change during the aging, a set of maladaptive compensatory mechanisms (many of which are still to be identified) leads to a progressive damage of brain functions.

II) Cell energy metabolism and mitochondria seem strongly involved in the pathogenesis of CCDS1 and they could represent useful potential targets for therapeutic interventions.

III) Inflammation seems to play an important part in this progressive damage, and this observation can pave the way to treatment strategies, given the number of drugs already available to modulate the immune/inflammation response.

IV) Neural circuits disruption involving inhibitory systems could give a huge contribute to many of the clinical aspects observed in patients, as epilepsy and cognitive impairment, since the excitatory/inhibitory balance is fundamental for the normal function of neural circuits.

V) Factors outside the CNS are important in the pathogenesis of at least some aspects of the disorder, since the conditional KO model show difference in the timing of onset of some cognitive defects and in the presence of stereotypies. This observation is in part foreseeable, because of the great importance that the "body" has to the development of the brain, but it also carries interesting questions about how and how far periphery contributes to the normal neurodevelopment and, therefore, to the pathogenesis of CCDS1.

Abbreviations

ACC: anterior cingulate cortex.
aCSF: artificial cerebro-spinal fluid.
AGAT: L-arginine:glycine amidinotransferase.
ADP: adenosine diphosphate.
Arg: arginine.
ASD: autism spectrum disorder.
ATP: adenosine 5'-triphosphate.
BBB: blood brain barrier
CaMKII: Ca2+/calmodulin-dependent protein kinase II.
CCDS1: cerebral creatine deficiency syndrome type 1.
CK: creatine kinase.
CNS: central nervous system.
Cr: creatine.
CrT: creatine transporter.
CSF: cerebro-spinal fluid.
CTD: creatine transporter deficiency.
CycloCr: cyclocreatine.
DG: dentate gyrus.
DNA: deoxyribonucleic acid.
GAA: guanidinoacetic acid.
GAMT: guanidinoacetate methyltransferase.
GCL: granule cell layer.
GC/MS: gas chromatography/mass spectrometry.
Gly: glycine.
HP: hippocampus
1H-MRS: proton magnetic-resonance spectroscopy.
KO: knock-out.
MIP: maximum intensity projection.
mIPSC: miniature inhibitory post-synaptic potential.
MWM: Morris water maze.
ORT: object recognition test.
PBS: phosphate buffered saline.
PCr: phosphocreatine.
PCR: polymerase chain reaction.
PFC: prefrontal cortex.
Pn: post-natal day n.

PV: parvalbumin.
ROS: reactive oxygen species.
RT: room temperature.
SEM: standard error of mean.
WT: wild-type.

Figures
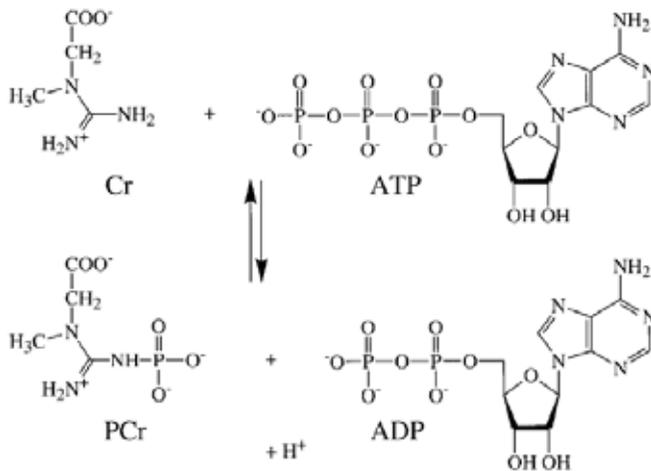
Figure 1. The creatine cycle.
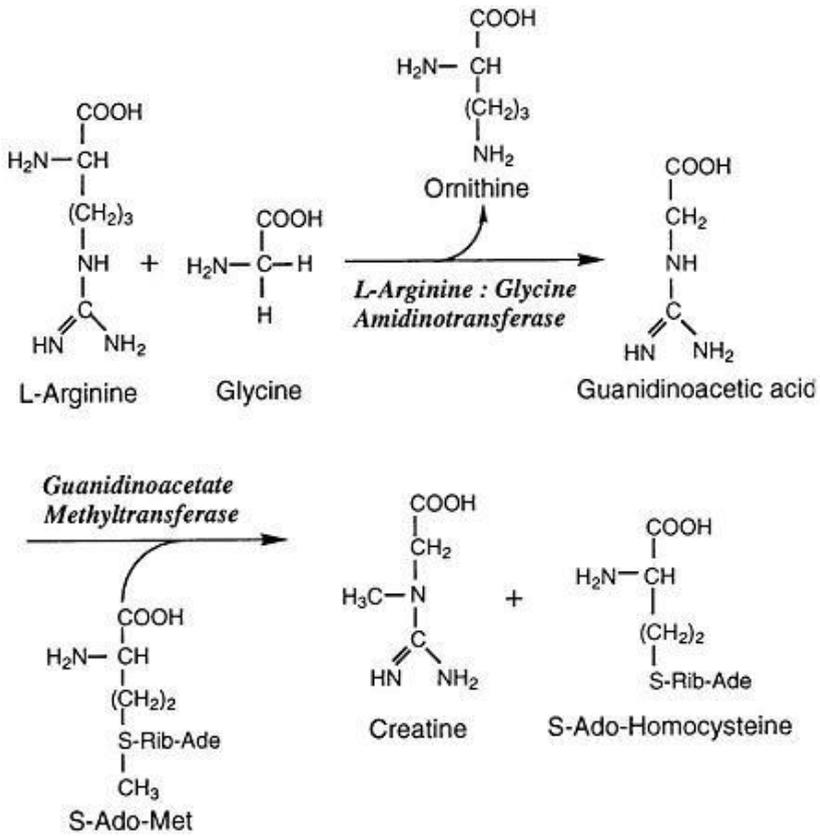
Figure 2. The synthesis of creatine.
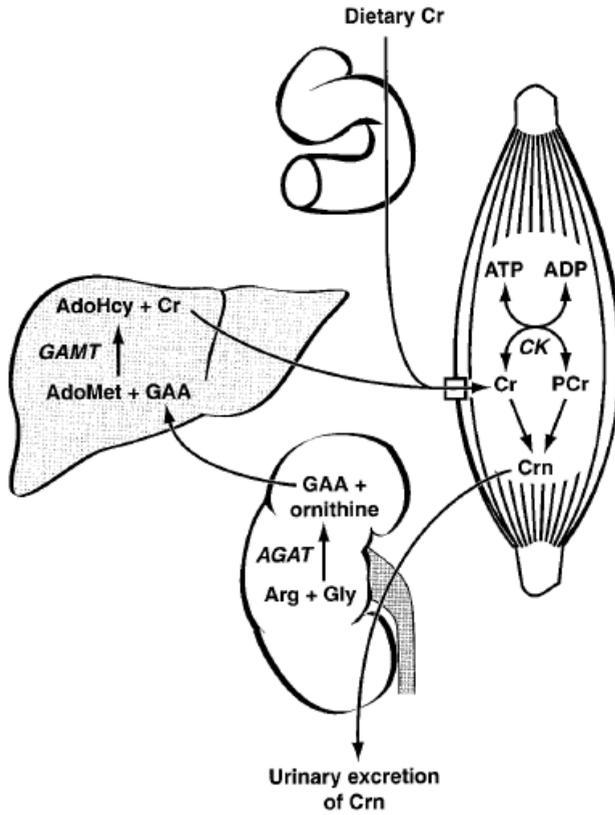
Figure 3. Hypothesized model of Cr synthesis in mammals (Wyss and Kaddurah-Daouk, 2000)
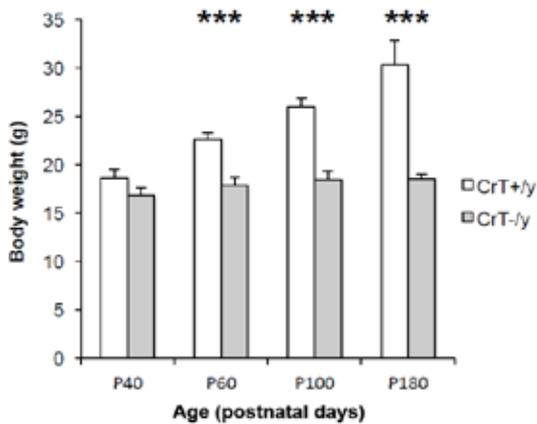
Figure 4. The weight of CrT$^{-/y}$ mice (n = 12) was significantly reduced compared to CrT$^{+/y}$ animals (n = 13) at P60, P100 and P180 (Two Way ANOVA on rank transformed data, post hoc Holm-Sidak method). *** $p < 0.001$. Error bars: SEM.
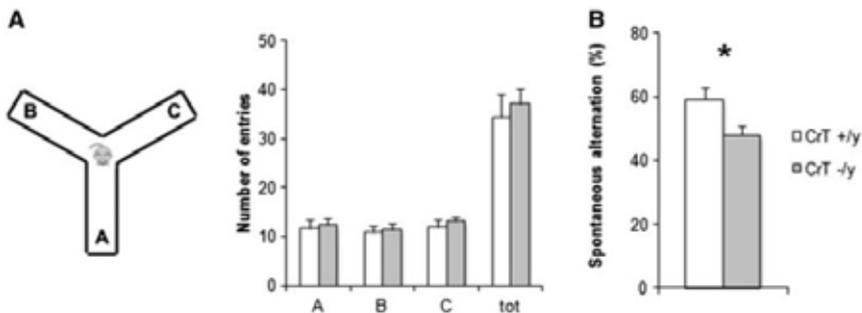
Figure 5. Early deficiency of working memory in CrT$^{-/y}$ mice. (A) Schematic diagram of the Y maze apparatus. The mean number of entries in the single arms of the maze (A, B, C) and the total number of arm entries were comparable for the different experimental groups (Two-Way ANOVA on rank transformed data, post hoc Holm-Sidak method, $p = 0.506$, $p = 0.941$, $p = 0.276$, $p = 0.391$, respectively). (B) Alternation rate in the Y maze was significantly lower in CrT$^{-/y}$ mice (n = 9) compared to that recorded for CrT$^{+/y}$ littermates (n = 11; t test, $p < 0.05$) at P28. * $p < 0.05$. Error bars: SEM.
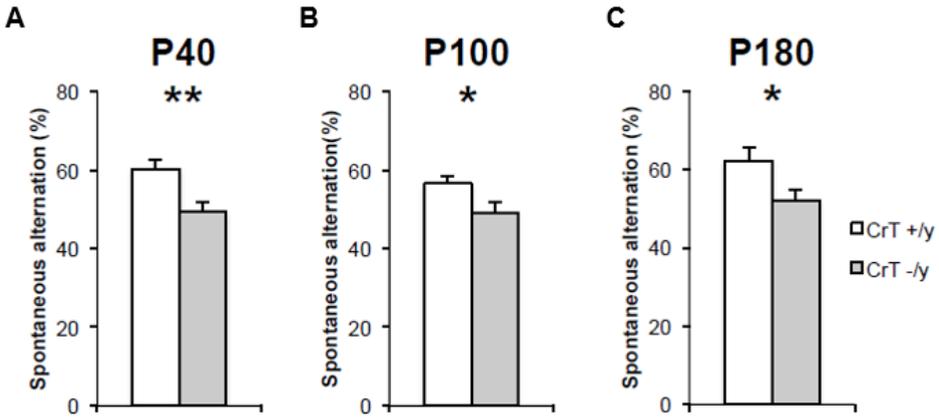
Figure 6. Impaired working memory in CrT$^{-/y}$ mice. Alternation rate in the Y maze was significantly lower in CrT$^{-/y}$ mice compared to that recorded for CrT$^{+/y}$ littermates at P40 (CrT$^{+/y}$, n = 13, CrT$^{-/y}$, n = 12; t-test, p < 0.01, panel A), P100 (CrT$^{+/y}$, n = 13, CrT$^{-/y}$, n = 12; t-test, p < 0.05, panel B) and P180 (CrT$^{+/y}$, n = 9, CrT$^{-/y}$, n = 7; t-test, p < 0.05, panel C). * p < 0.05; ** p < 0.01. Error bars: SEM.
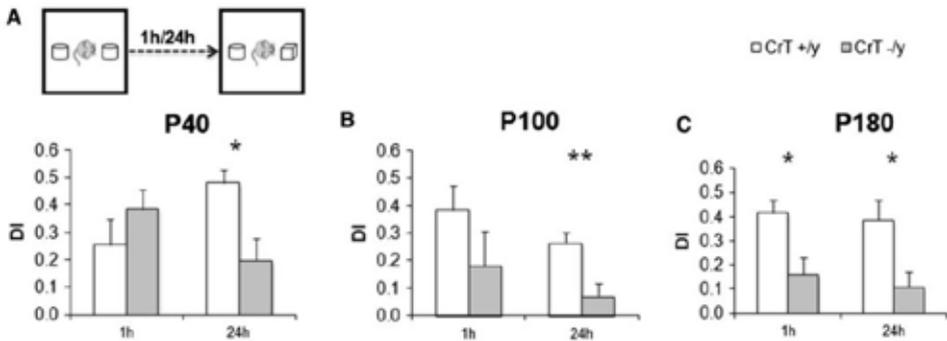
Figure 7. Progressive impairment of object recognition memory in CrT$^{-/y}$ mice. Top, a schematic representation of the object recognition task. Histograms display object discrimination indexes of CrT$^{+/y}$ and CrT$^{-/y}$ during the testing phase performed after a delay of 1 and 24h since the sample phase at different ages. (A) P40. While both experimental groups can recognize the new object in the test at 1h (t-test, p = 0.285), a significantly lower discrimination index was found in CrT$^{-/y}$ mice (n = 9) compared to CrT$^{+/y}$ animals (n = 7; t-test, p < 0.05). (B) P100. Even if still not significant, the recall capacity of CrT$^{-/y}$ animals at 1h was reduced (t-test, p = 0.242). At 24h, a t-test revealed that the performance of CrT$^{-/y}$ animals (n = 11) was strongly impaired with respect to controls (n = 10; p < 0.01). (C) P180. A significant deficit of both short (t-test, p < 0.05) and long-term (t-test, p < 0.05) memory was detected in mutant mice (n = 10) compared to controls (n = 9). * p < 0.05; ** p < 0.01. Error bars: SEM.
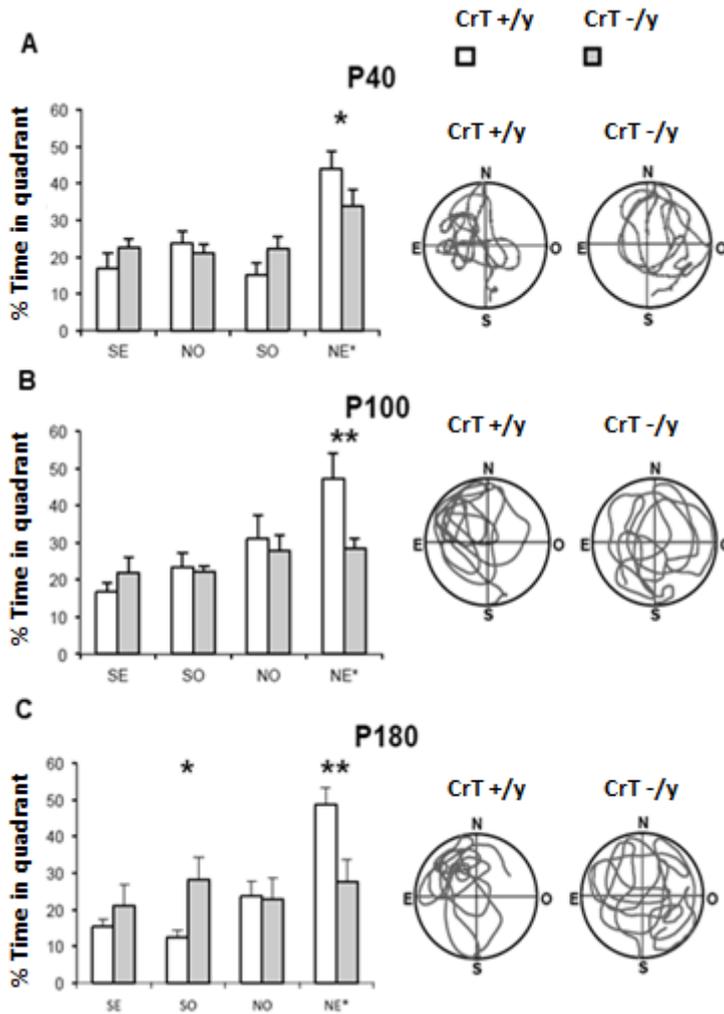
Figure 8. Spatial memory impairment in CrT$^{-/y}$ mice. A Two-Way RM ANOVA followed by Holm-Sidak multiple comparison revealed that while CrT$^{+/y}$ spent significantly more time in the NE* quadrant than in the other ones, CrT$^{-/y}$ did not show any preference for the target quadrant at P40 (CrT$^{+/y}$, n = 10, CrT$^{-/y}$, n = 12; panel A), P100 (CrT$^{+/y}$, n = 7, CrT$^{-/y}$, n = 8; panel B) and P180 (CrT$^{+/y}$, n = 9, CrT$^{-/y}$, n = 7; Two-Way RM ANOVA, post hoc Holm-Sidak method, panel C). At all ages tested, the percentage of time spent in the target quadrant was shorter in CrT$^{-/y}$ mice than in the control group (Two-Way RM ANOVA, post hoc Holm-Sidak method, $p < 0.05$ at P40 and $p < 0.01$ at P100 and P180). At P180, a significant difference was also detected in the percentage of time spent in the SO quadrant by CrT$^{+/y}$ and CrT$^{-/y}$ mice ($p < 0.05$). * $p < 0.05$; ** $p < 0.01$. Error bars: SEM.
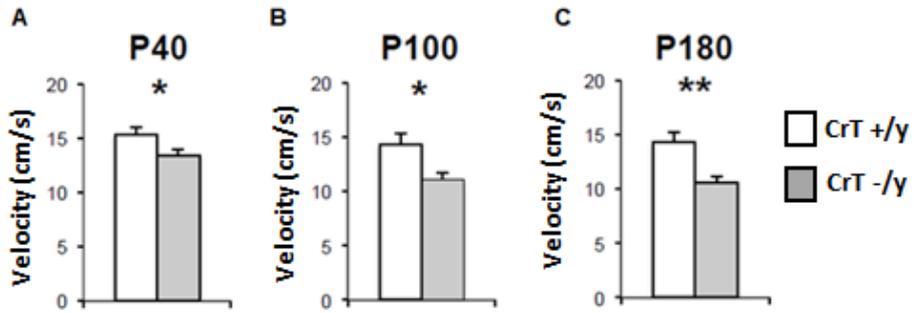
Figure 9. Slower swimming velocity in CrT$^{-/y}$ mice. Mean swimming speed measured all along the training phase of the Morris water maze for CrT$^{+/y}$ and CrT$^{-/y}$ animals at P40 (CrT$^{+/y}$, n = 10, CrT$^{-/y}$, n = 12; panel A), P100 (CrT$^{+/y}$, n = 7, CrT$^{-/y}$, n = 8; panel B) and P180 (CrT$^{+/y}$, n = 9, CrT$^{-/y}$, n = 7; panel C). At all ages tested mutant mice resulted to be slower swimmers with respect to control littermates (t-test, $p < 0.05$ at P40 and $p < 0.01$ at P180; Mann-Whitney Rank Sum test, $p < 0.05$ at P100). * $p < 0.05$; ** $p < 0.01$. Error bars: SEM.
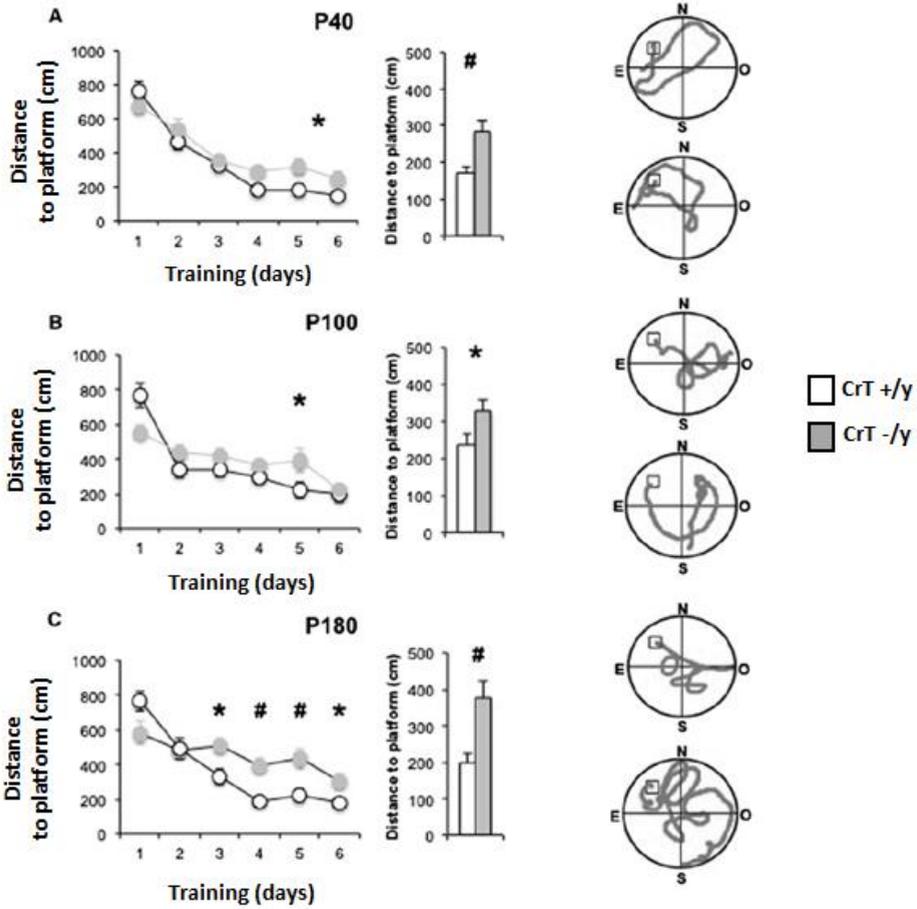
Figure 10. CrT deletion progressively deteriorates spatial learning and memory in mutant mice. (A) Left, learning curves for CrT$^{+/y}$ (n = 10, white) and CrT$^{-/y}$ mice (n = 12, grey) at P40. A significant difference was detected at day 5 (Two-Way RM ANOVA, post hoc Holm-Sidak method, p < 0.05). Right, histograms showing the mean swimming path covered to locate the submerged platform on the last three days of training for the two groups. A significant differ- ence between CrT$^{-/y}$ and CrT$^{+/y}$ animals was present (t-test, p < 0.01). Representative examples of swimming path during the day 3 of the training phase for a CrT$^{+/y}$ (top) and a CrT$^{-/y}$ mouse (bottom) are also reported. (B) Left, learning curves for CrT$^{+/y}$ (n = 7, white) and CrT$^{-/y}$ mice (n = 8, grey) at P100. A significant difference was detected at day 5 (Two-Way RM ANOVA, post hoc Holm-Sidak method, p < 0.05). Right, histograms showing the mean swimming path on the last three training days for the two groups. A significant difference between CrT$^{+/y}$ and CrT$^{-/y}$ animals was present (t-test, p < 0.05). Representative examples of swimming path during the day 3 of the training phase for a CrT$^{+/y}$ (top) and a CrT$^{-/y}$ mouse (bottom) are also reported. (C) Left, learning curves for CrT$^{+/y}$ (n = 9, white) and CrT$^{-/y}$ mice (n = 7, grey) at P180: mutant mice were poorer learners with respect to control littermates and a significant difference was detected at day 3, 4, 5 and 6 (Two-Way RM ANOVA on rank transformed data, post hoc Holm-Sidak method, p < 0.05 for day 3 and 6, p < 0.01 for day 4 and 5). Right, histograms showing the mean swimming path on the last three days of training. A t-test analysis showed a statistical

difference between $CrT^{+/y}$ and $CrT^{-/y}$ animals ($p < 0.01$). Representative examples of swimming path during the day 3 of the training phase for a $CrT^{+/y}$ (top) and a $CrT^{-/y}$ mouse (bottom) are also depicted. * $p < 0.05$; # $p < 0.01$. Error bars: SEM.
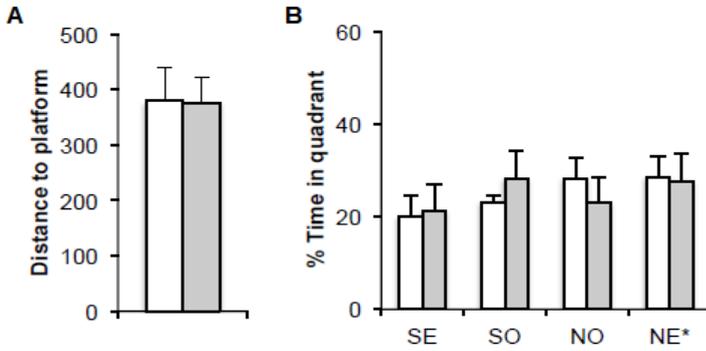
Figure 11. Premature cognitive decline in CrT null mice. (A) No difference was found in the mean swimming path on the last three days of training between P365 $CrT^{+/y}$ (n = 4) and P180 $CrT^{-/y}$ animals (n = 7; t-test, p = 0.968). (B) In the probe test, the percentage of time spent in the different two quadrants was totally comparable in P180 $CrT^{-/y}$ mice and six-month older $CrT^{+/y}$ animals (Two-Way RM ANOVA, p = 0.479). Error bars: SEM.
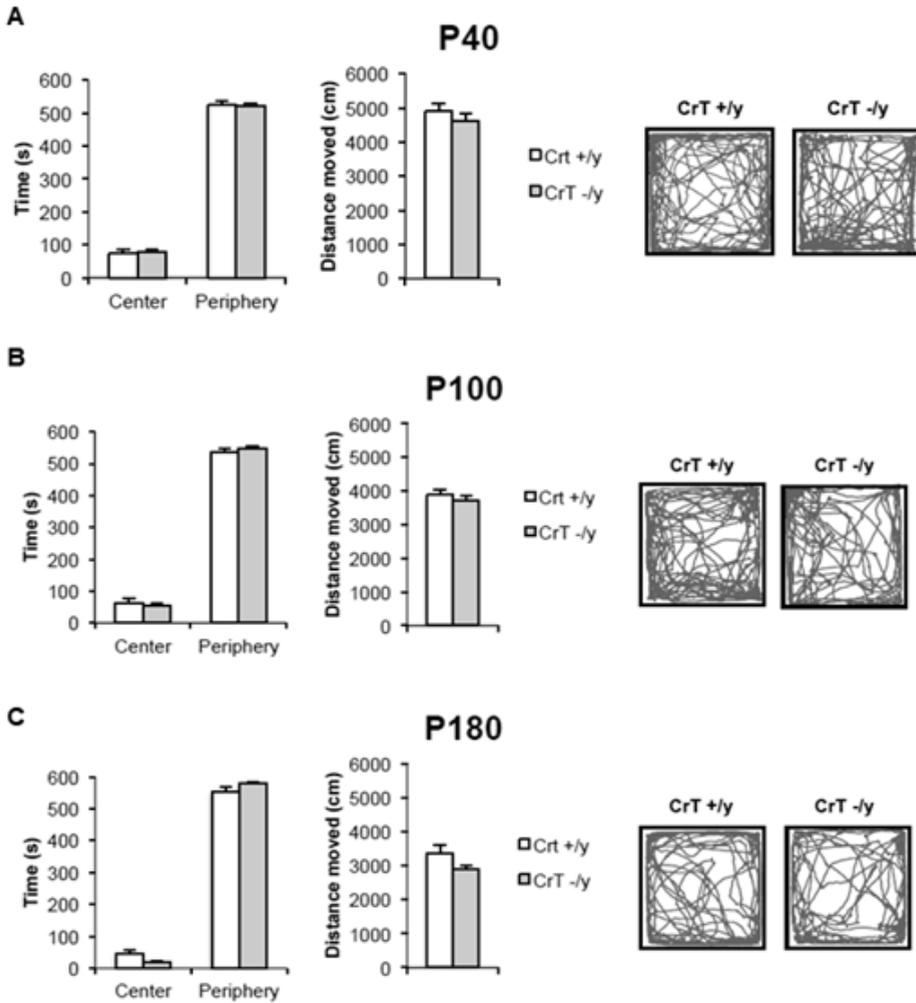
Figure 12. Normal behavior of CrT mutant mice in the open field arena. Left, CrT$^{+/y}$ and CrT$^{-/y}$ mice spent a comparable amount of time in the center and in the peripheral region of the open field arena. A Two-Way ANOVA analysis shows no significant effect of genotype at P40 (CrT$^{+/y}$ n = 13, CrT–/y n = 12; p = 0.725; panel A), P100 (CrT$^{+/y}$, n = 13, CrT$^{-/y}$, n = 12; p = 0.508; panel B) and P180 (CrT$^{+/y}$, n = 11, CrT$^{-/y}$, n = 11; panel C; p = 0.348). Right, total distance moved did not differ between CrT mutants and wild-type animals at all ages tested (t-test, p = 0.363, p = 0.452 and p = 0.101, respectively). Representative examples of movement path during the open field session for a CrT$^{+/y}$ and a CrT$^{-/y}$ mouse are also reported. Error bars: SEM.
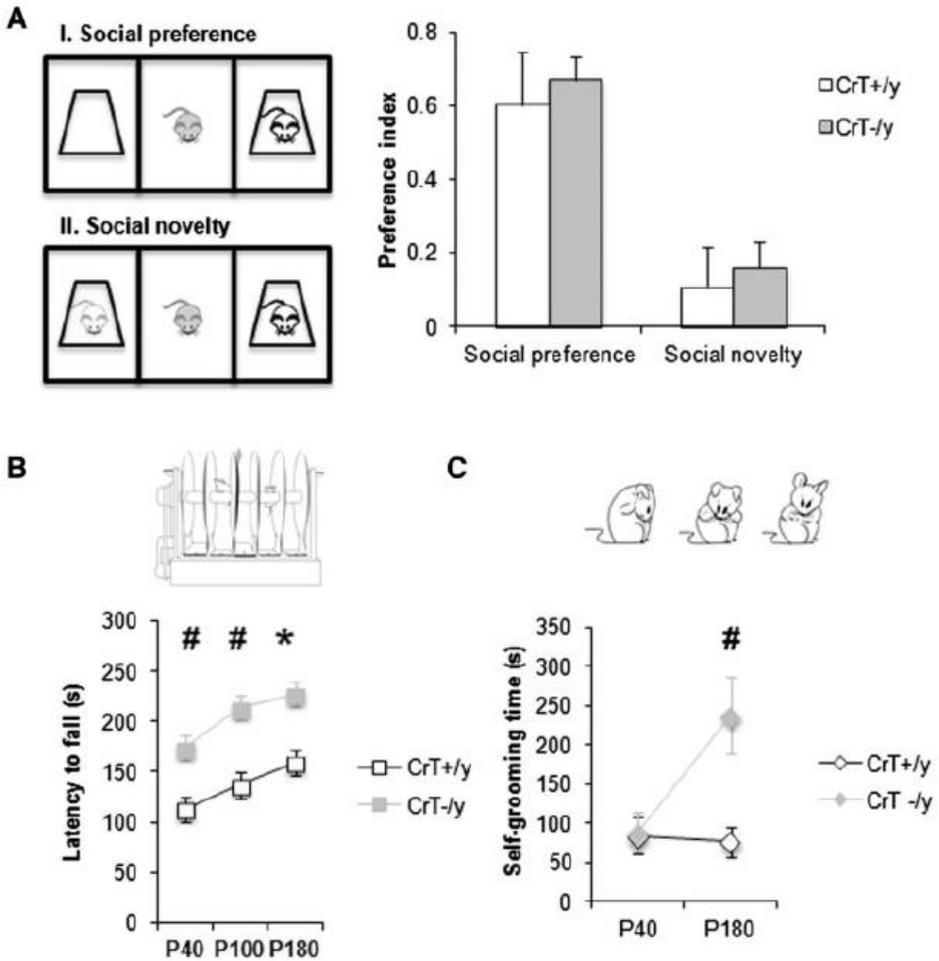
Figure 13. CrT mutation enhances repetitive and stereotyped behaviors. (A) Social interaction behaviors in CrT$^{-/y}$ mice. Histograms display discrimination indexes of CrT$^{+/y}$ (n = 6) and CrT$^{-/y}$ (n = 8) mice during the social preference (session I) and the social novelty phase (session II). No difference was detected between the two groups (Mann–Whitney Rank Sum test, p = 0.662 for session I; t-test, p = 0.784 for session II). A schematic representation of the three-chamber test is also depicted. (B) Performance of littermate WT (n = 11) and CrT$^{-/y}$ mice (n = 9) on the accelerating rotarod. Inset shows an illustration of the rotarod apparatus. A Two-Way ANOVA showed a significant effect of genotype (p < 0.001). Post hoc Holm-Sidak test revealed that the fall latency of mutant animals was significantly different from that of wild-type mice at all ages tested (p < 0.01 at P40 and P100, p < 0.05 at P180). (C) Histograms display mean time spent self-grooming in CrT$^{+/y}$ and CrT$^{-/y}$ animals at P40 and P180. While no difference was detected at P40 (CrT$^{+/y}$, n = 7; CrT$^{-/y}$, n = 9; Two Way ANOVA on rank transformed data, post hoc Holm-Sidak method, p = 0.912), CrT null mice exhibit increased grooming behavior at P180 (CrT$^{+/y}$, n = 11; CrT$^{-/y}$, n = 7; p < 0.01). A schematic representation of self-grooming behavior is reported. * p < 0.05; # p < 0.01. Error bars: SEM.
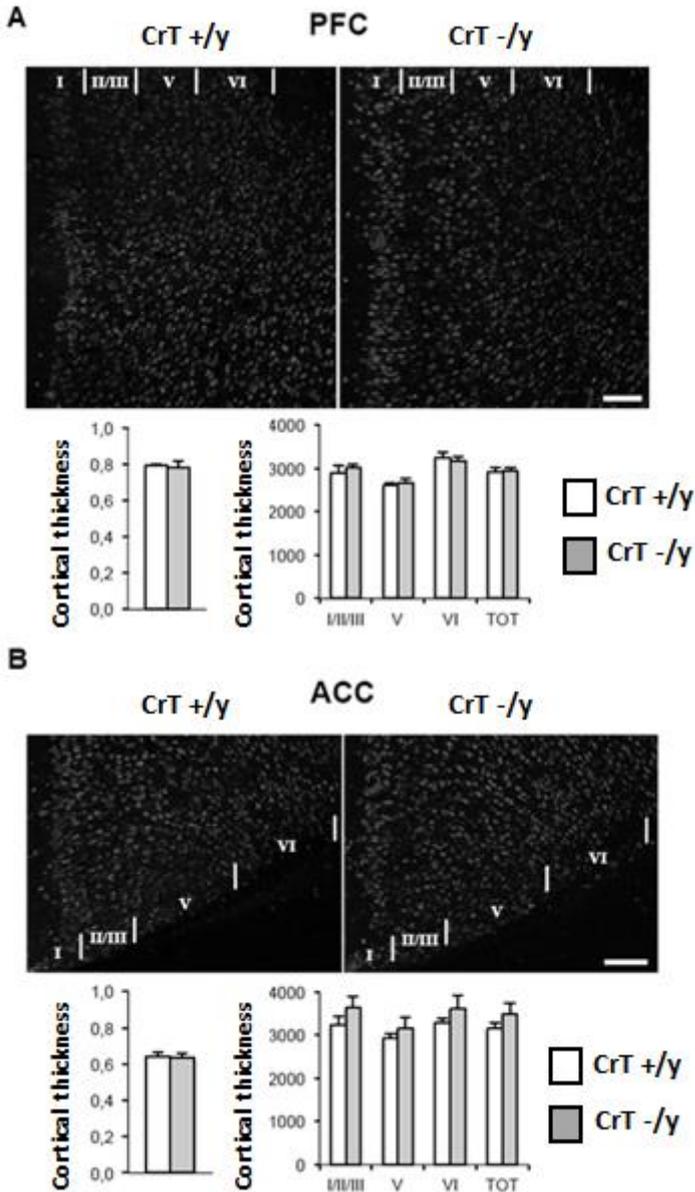
Figure 14. Morphological characterization of cerebral cortex in CrT$^{+/y}$ and CrT$^{-/y}$ animals at P180 (n = 6 for both groups). (A) Left, cortical thickness of prefrontal cortex was comparable in the two groups of animals (t-test, p = 0.838). Right, no difference in neuronal cell density measured in different layers (layer I/II/III, layer V, layer VI) and in the entire cortical thickness was detected between CrT$^{+/y}$ and CrT$^{-/y}$ mice (Two-Way ANOVA, post hoc Holm-Sidak method, p = 0.414, p = 0.670, p = 0.526 and p = 0.837, respectively). (B) Left, cortical thickness of cingulate cortex was similar in the two experimental groups (t-test, p = 0.824). Neuronal cell density measured in different layers and in the entire cortical thickness was not different in the

two groups (Two- Way ANOVA, post hoc Holm-Sidak method, p = 0.197, p = 0.454, p = 0.302 and p = 0.262, respectively). Representative immunostainings for NeuN from PFC and ACC of a CrT$^{+/y}$ and a CrT /y mouse are also reported. Calibration bars: 100 μm. Error bars: SEM.
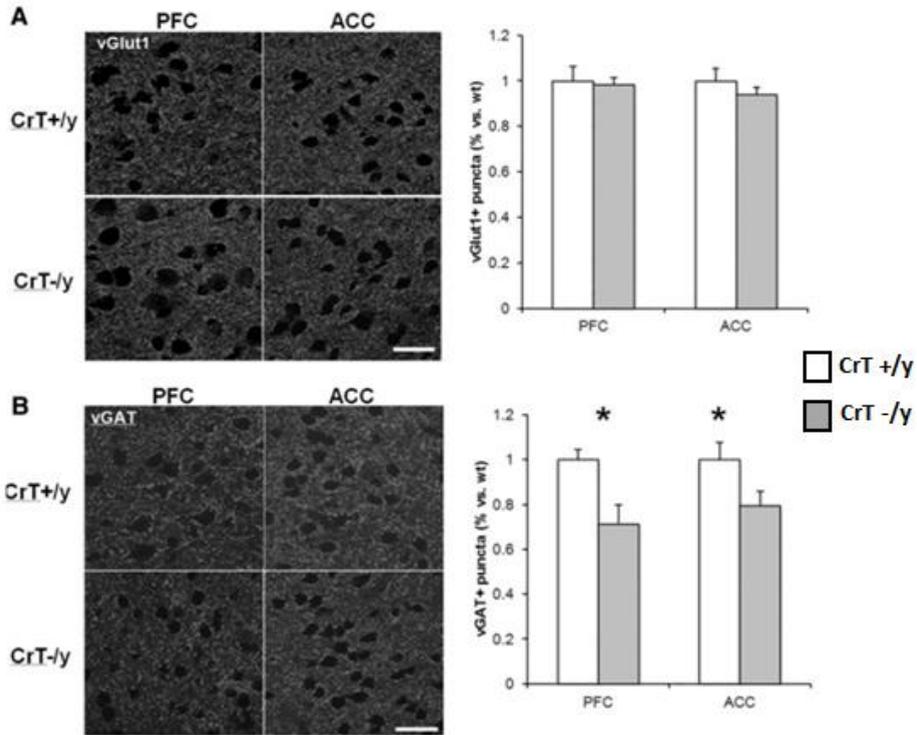
Figure 15. Synaptic neurotransmission in CrT$^{+/y}$ and CrT$^{-/y}$ animals at P180. (A) Left, representative immunostaining for vGlut1 from PFC and ACC of a CrT$^{+/y}$ and a CrT$^{-/y}$ mouse. Right, no difference in vGlut1 staining was detected between the two experimental groups (n = 6 for both groups) either in PFC (t-test, p = 0.792) or ACC (t-test, p = 0.340). (B) Left, representative immunostaining for vGAT from PFC and ACC of a CrT$^{+/y}$ and a CrT$^{-/y}$ mouse. The number of vGAT-positive puncta was significantly reduced both in the PFC and the ACC of mutant animals (n = 9) with respect to controls (n = 8; t-test, p < 0.05 for both comparisons). * p < 0.05. Calibration bars: 25 μm. Error bars: SEM.
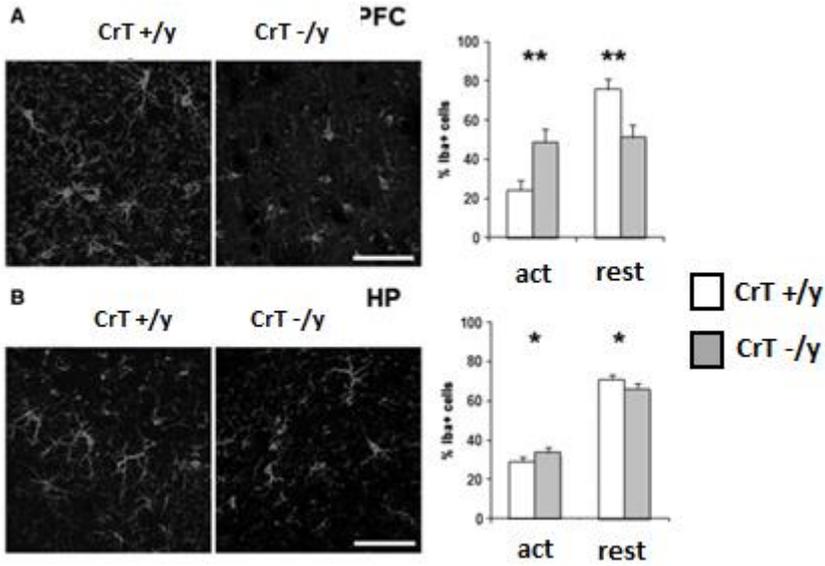
Figure 16. Pathological activation of microglial cells in CrT$^{-/y}$ animals (A) Left, representative immunostaining for Iba-1 from PFC of a CrT$^{+/y}$ and a CrT$^{-/y}$ mouse. Right, a significant increase of the percentage of activated microglial cells, with a parallel decrease of resting microglia, was detected in mutant mice with respect to wild-type animals (n = 8 for both groups; Two Way ANOVA, post hoc Holm-Sidak method, $p < 0.01$). (B) Left, representative immunostaining for Iba-1 from the hippocampus (HP) of a CrT$^{+/y}$ and a CrT$^{-/y}$ mouse. Right, the percentage of activated microglia was increased in mutant mice, whereas the relative number of resting cells was reduced compared to controls (n = 8 for both groups; Two-Way ANOVA, post hoc Holm-Sidak method, $p < 0.05$). * $p < 0.05$; ** $p < 0.01$. Calibration bar: 100 μm. Error bars: SEM.
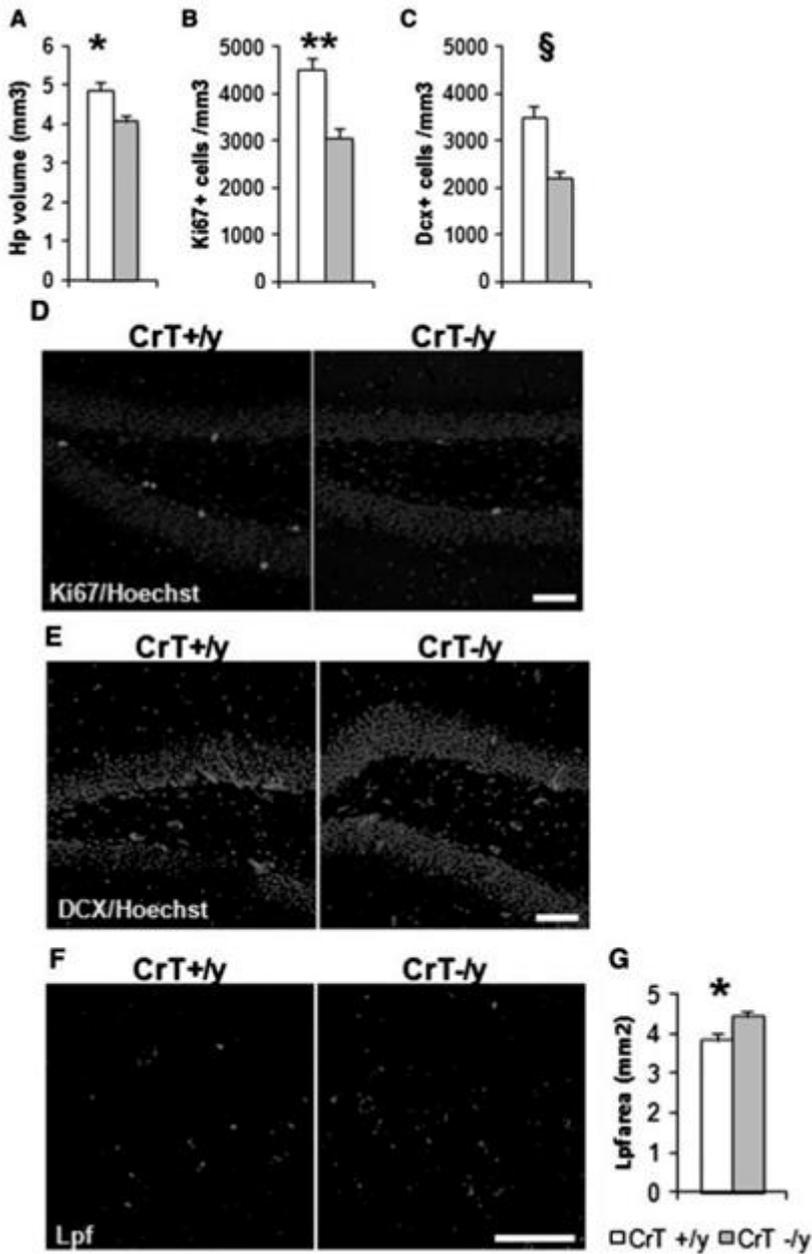
Figure 17. Neurogenesis impairment and enhanced lipofuscin accumulation in the hippocampus of CrT$^{-/y}$ animals at P180. (A) The hippocampal volume of CrT$^{-/y}$ mice was smaller compared to CrT$^{+/y}$ mice (n = 6 for both groups; t-test, p < 0.05). (B) Stereological counting revealed that the density of Ki67-positive cells was significantly reduced in the DG of CrT$^{-/y}$ mice, with approximately 30% reduction with respect to WT littermates (n = 6 for both groups; t-test, p < 0.01). (C) A significant decrease of the DCX-positive immature neurons was detected in the hippocampus of adult CrT$^{-/y}$ mice compared to controls (n = 6 for both groups; t-test, p

< 0.001). (D) Representative immunostaining for Ki-67, a nuclear protein required for cellular proliferation, from a CrT$^{+/y}$ and a CrT$^{-/y}$ mouse. (E) Representative immunostaining for DCX, a microtubule-associated phosphoprotein expressed in early neuronal differentiation, from a CrT$^{+/y}$ and a CrT$^{-/y}$ mouse. (F) Representative images for lipofuscin autofluorescence from a CrT$^{+/y}$ and a CrT$^{-/y}$ mouse. (G) Six-month-old CrT$^{-/y}$ mice (n = 6) show extensive accumulation of autofluorescent material throughout the brain when compared to the wild-type control (n = 5). A significant increase of abnormal autofluorescent storage was mainly found in DG granular and polymorph layer of CrT$^{-/y}$ mice (t-test, p < 0.05). * p < 0.05; ** p < 0.01; § p < 0.001. Calibration bars: 50 μm. Error bars: SEM.
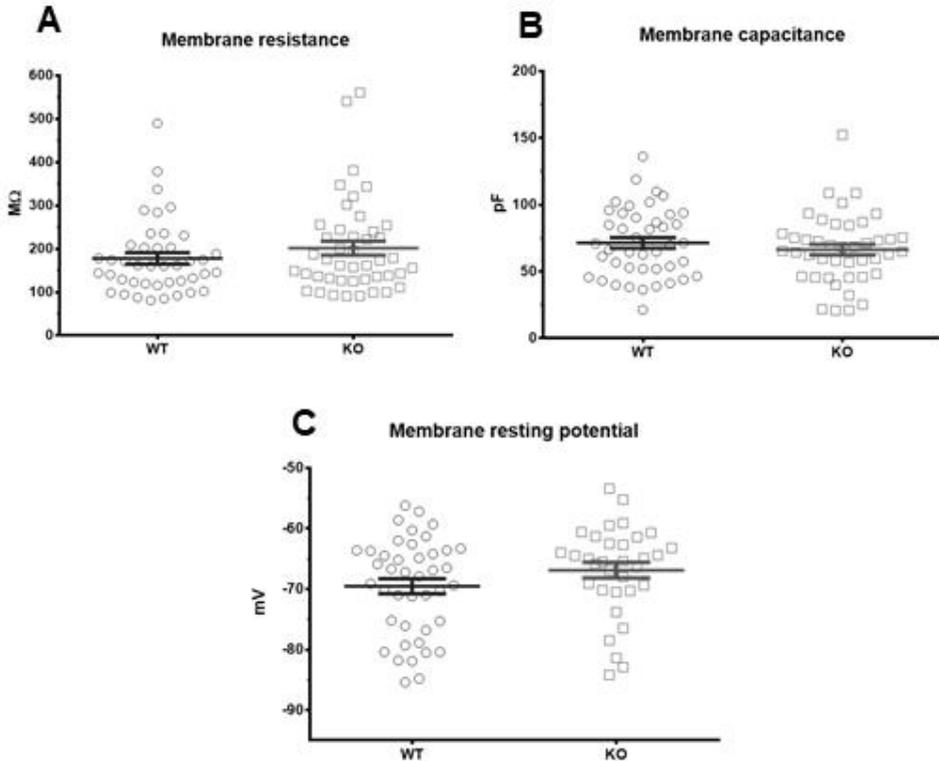
Figure 18. Passive properties of pyramidal neurons in L4 of V1 cortex. (A) No difference was observed in membrane resistance (in MΩ) between CrT$^{-/y}$ compared to control mice (t-test: p = 0.27; CrT$^{+/y}$ n (cells/mice) = 42/15; CrT$^{-/y}$: n (cells/mice) = 44/12). (B) No difference in membrane capacitance was found between CrT$^{-/y}$ and CrT$^{+/y}$ mice (t-test: p = 0.37; CrT$^{+/y}$: n (cells/mice) = 43/15; CrT$^{-/y}$ n (cells/mice) = 43/12). (C) Membrane resting potential was only slightly reduced in CrT$^{-/y}$ with respect to WT in a statistically non-significant manner (t-test: p = 0.14; CrT$^{+/y}$: n (cells/mice) = 42/15; CrT-/y: n (cells/mice) = 33/12). Mean ± SEM.
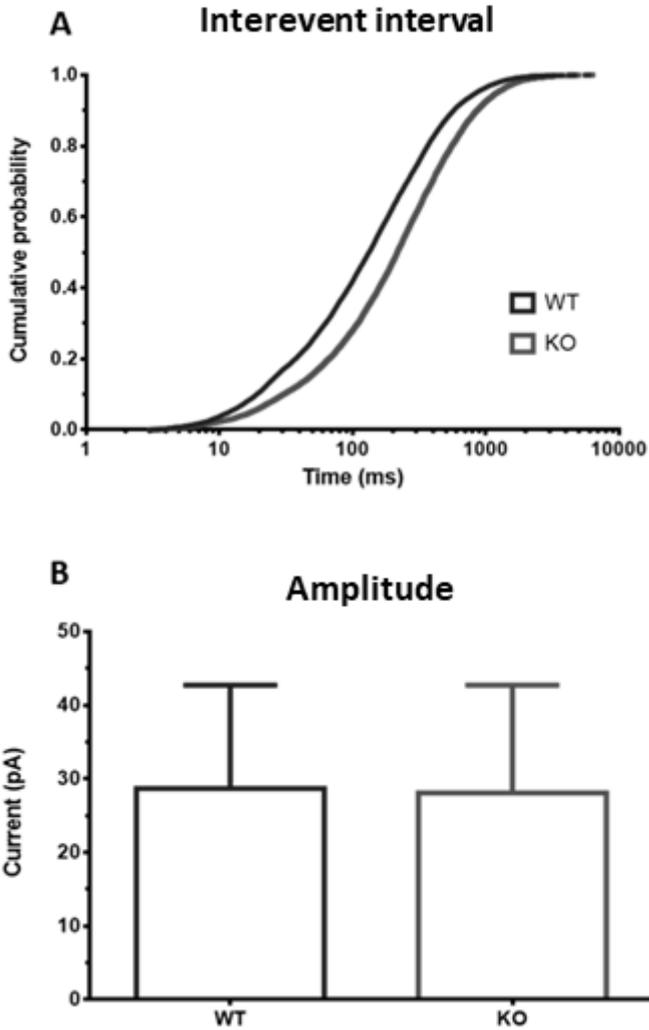
Figure 19. Properties of mIPSCs recorded in pyramidal neurons in L4 of V1 cortex. (A) The interevent interval was higher in CrT$^{-/y}$ mice compared to WT (x-axis is Log; Mann-Whitney Rank Sum test: $p < 0.001$; CrT$^{+/y}$: median 132.4 ms; n (cells/mice) = 35/15; CrT$^{-/y}$: median: 215.9 ms; n (cells/mice) = 34/12). (B) Absolute amplitude of mIPSCs was similar in CrT$^{-/y}$ mice and in CrT$^{+/y}$ (Mann-Whitney Rank Sum test: $p = 0.132$; CrT$^{+/y}$: n (cells/mice) = 35/15;

CrT$^{-/y}$:   n   (cells/mice)   =   34/12).   Median   ±   interquartile   range.
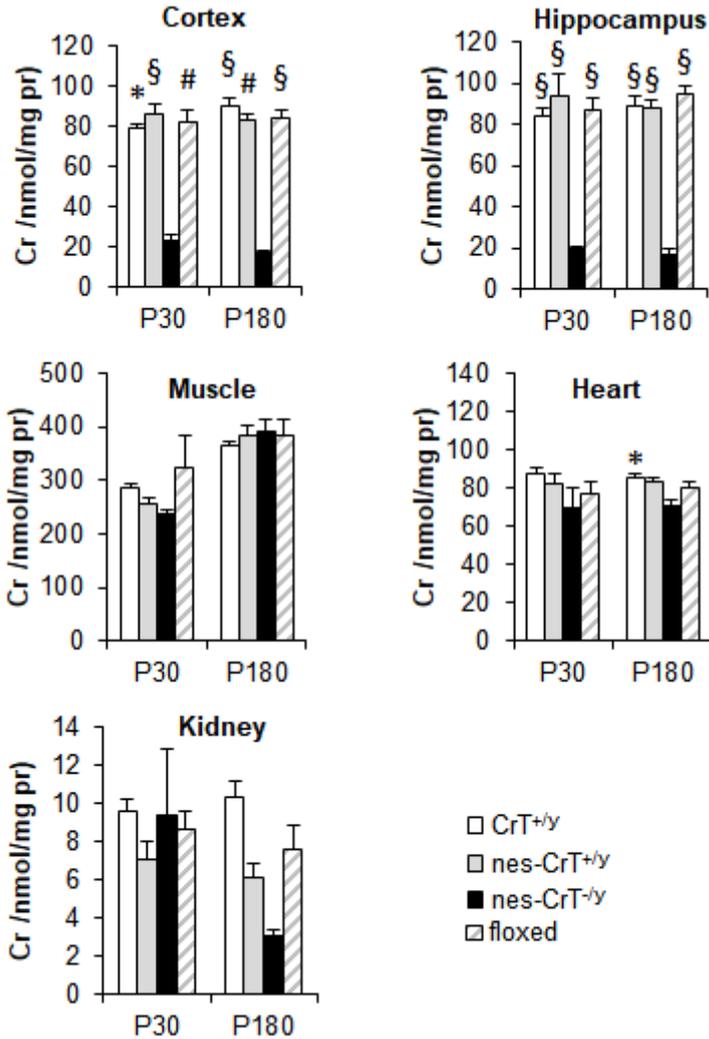
Figure 20. Histograms show Cr levels in CrT$^{+/y}$, nes-CrT$^{+/y}$, nes-CrT$^{-/y}$ and CrTfl/y animals in brain and peripheral tissues at P30 and P180 (n = 4 per tissue for both groups). Cr levels have been measured by GC/MS. At both ages tested, a reduction of Cr content was evident in the cerebral cortex (Two-Way ANOVA on rank transformed data, post hoc Holm-Sidak method; P30: p < 0.05 vs. CrT$^{+/y}$, p < 0.001 vs. nes-CrT$^{+/y}$, p < 0.01 vs. CrTfl/y; P180: p < 0.001 vs. CrT$^{+/y}$, p < 0.01 vs. nes-CrT$^{+/y}$, p < 0.001 vs. CrTfl/y) and the hippocampus of nes-CrT$^{-/y}$ mice (p < 0.001 for all comparisons at both ages). Muscle (Two-Way ANOVA on rank transformed data, post hoc Holm-Sidak method; P30: p = 0.889 vs. CrT$^{+/y}$, p = 0.965 vs. nes-CrT$^{+/y}$, p = 0.880 vs. CrTfl/y; P180: p = 0.985 vs. CrT$^{+/y}$, p = 0.964 vs. nes-CrT$^{+/y}$, p = 0.994 vs. CrTfl/y), heart (P30: p = 0.254 vs. CrT$^{+/y}$, p = 0.624 vs. nes-CrT$^{+/y}$, p = 0.969 vs. CrTfl/y; P180: p = 0.109 vs. nes-CrT$^{+/y}$, p = 0.304 vs. CrTfl/y) and kidney (P30: p = 0.991 vs. CrT$^{+/y}$, p = 0.971 vs. nes-CrT$^{+/y}$, p = 0.937 vs. CrTfl/y; P180: p = 0.213 vs. CrT$^{+/y}$, p = 0.742 vs. nes-CrT$^{+/y}$, p = 0.583 vs. CrTfl/y) of mutant animals were preserved from Cr depletion, with the exception of

the heart at P180 showing slightly decreased Cr levels with respect to CrT$^{+/y}$ mice (p < 0.05). In addition, a Three-Way ANOVA on rank transformed data analysis revealed no difference for the age factor (p = 0.301). * p < 0.05, # p < 0.01, § p < 0.001. Error bars: SEM.
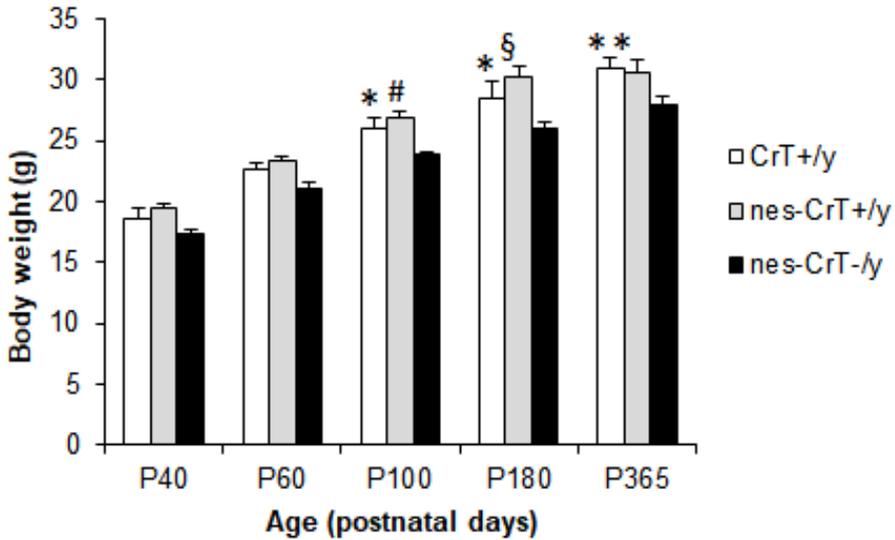

Figure 21. The weight of nes-CrT–/y mice (n = 6) was significantly reduced compared to CrT$^{+/y}$ (n = 13) and nes-CrT$^{+/y}$ animals (n = 9) at P100 (Two-Way ANOVA on rank transformed data, post hoc Holm-Sidak method, p < 0.05 vs. CrT$^{+/y}$, p < 0.01 vs. nes-CrT$^{+/y}$), P180 (p < 0.05 vs. CrT$^{+/y}$, p < 0.001 vs. nes-CrT$^{+/y}$) and P365 (p < 0.05 for both comparisons). No difference was detected among the three groups at P40 (Two-Way ANOVA on rank transformed data, post hoc Holm-Sidak method, p = 0.457 vs. CrT$^{+/y}$, p = 0.373 vs. nes-CrT$^{+/y}$) and P60 (p = 0.192 vs. CrT$^{+/y}$, p = 0.069 vs. nes-CrT$^{+/y}$), although the body weight of mutant animals is slightly lower even at these ages with respect to the other two groups. It is worth noting that age-dependent growth of body mass was not compromised in nes-CrT$^{-/y}$ animals showing a progressive increase of their weight (Two-Way ANOVA on rank transformed data, p < 0.001 effect of age, p < 0.05 for all age comparisons within CrT$^{+/y}$, nes-CrT$^{-/y}$ and nes-CrT$^{+/y}$ groups). * p < 0.05, # p < 0.01, § p < 0.001. Error bars: SEM.
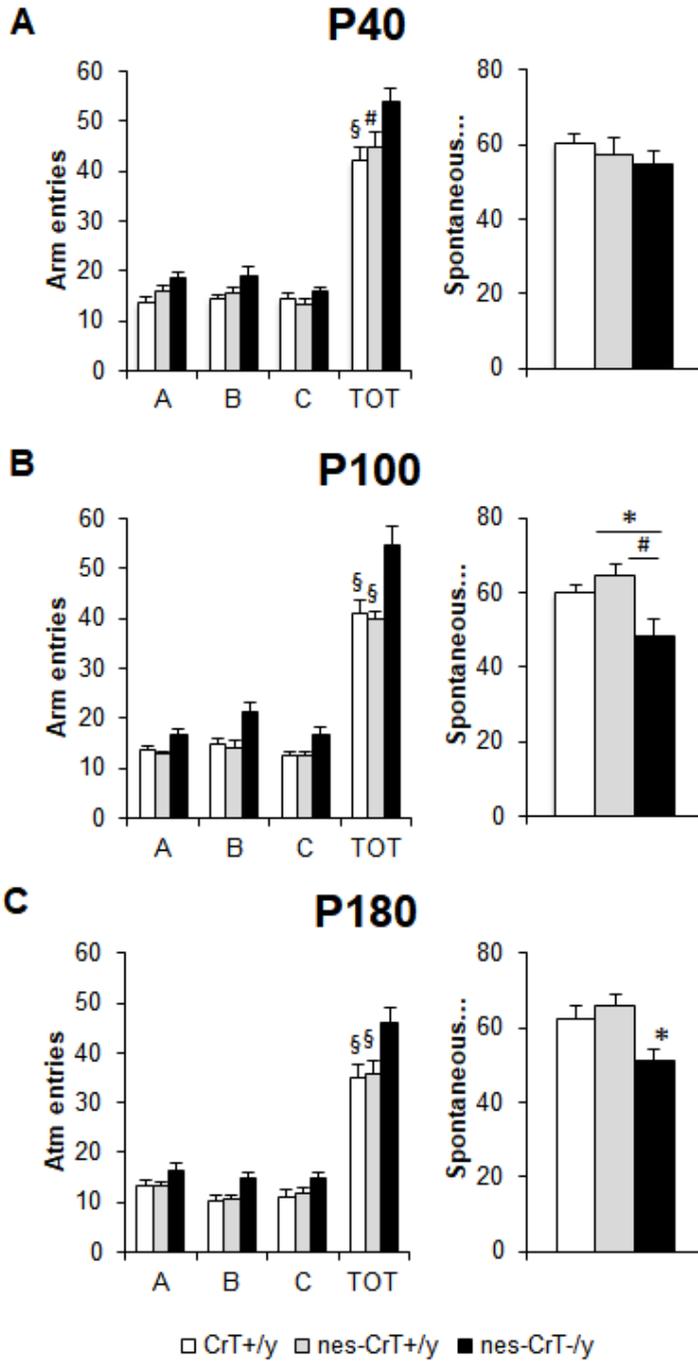
Figure 22. At all ages tested, no effect of genotype was detected for the number of entries in the single arms of the maze (A, B, C; Two-Way ANOVA, post hoc Holm-Sidak method), while

an higher total number of entries were scored for nes-CrT$^{-/y}$ mice (P40: $p < 0.001$ vs. CrT$^{+/y}$, $p < 0.01$ vs. nes-CrT$^{+/y}$; P100 and P180: $p < 0.001$ for both comparisons; A, B, C left). No difference in the Y maze performance was present among the three groups tested at P40 (CrT$^{+/y}$, n = 12, nes-CrT$^{+/y}$, n = 9, nes-CrT$^{-/y}$, n = 6; One-Way ANOVA, $p = 0.417$, panel A right). In contrast, spontaneous alternation rate was significantly lower in nes-CrT$^{-/y}$ mice compared to that recorded for CrT$^{+/y}$ animals and nes-CrT$^{+/y}$ littermates at P100 (One-Way ANOVA, post hoc Holm-Sidak method, $p < 0.05$ vs. CrT$^{+/y}$, $p < 0.01$ vs. nes-CrT$^{+/y}$; panel B right) and P180 (CrT$^{+/y}$, n = 9, nes-CrT$^{+/y}$, n = 9, nes-CrT$^{-/y}$, n = 6; One-Way ANOVA, post hoc Holm-Sidak method, $p < 0.05$ for both comparisons; panel C right). * $p < 0.05$, # $p < 0.01$. Error bars: SEM.

A **P40**

B **P100**

C **P180**

□ CrT+/y ☐ nes-CrT+/y ■ nes-CrT-/y
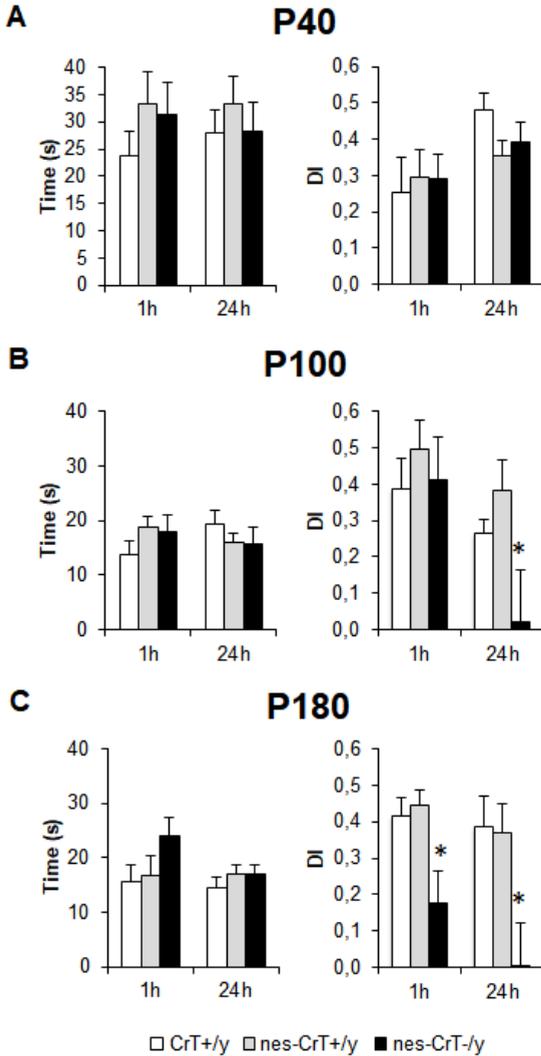
Figure 23. Left, diagrams describe total time of object exploration during the testing phase. (A, B, C) No difference was present among the different groups at all ages tested (One-Way ANOVA, P40: p = 0.372 for 1h and p = 0.686 for 24h; P100: p = 0.309 for 1h and p = 0.531 for 24h; P180: p = 0.097 for 1h and p = 0.526 for 24h). Right, histograms display object discrimination indexes of CrT$^{+/y}$, nes-CrT$^{+/y}$ and nes-CrT$^{-/y}$ during the testing phase performed after a delay of 1 and 24h at different ages. (a) P40. The experimental groups (CrT$^{+/y}$: n = 10, nes-CrT$^{+/y}$: n = 8 and nes-CrT$^{-/y}$: n = 6) can recognize the new object in the test both at 1h (One-Way ANOVA, p = 0.916) and at 24h (p < 0.183). (B) P100. While the three experimental groups can recall the memory of the familiar object in the test at 1h (One-Way ANOVA, p = 0.671), a significantly lower discrimination index was found in nes-CrT–/y mice (n = 6) compared to CrT$^{+/y}$ (n = 10) and nes-CrT$^{+/y}$ animals at 24h (n = 9; One-Way ANOVA, post hoc Holm-Sidak method p < 0.05 for both comparisons). (C) P180. A significant deficit of both short (One-Way ANOVA, post hoc Holm-Sidak method p < 0.05 for both comparisons) and

long-term memory (One-Way ANOVA, post hoc Holm-Sidak method $p < 0.05$ for both comparisons) was detected in mutant mice (n = 6) compared to controls ($CrT^{+/y}$: n = 11, nes-$CrT^{+/y}$: n = 9). * $p < 0.05$. Error bars: SEM.
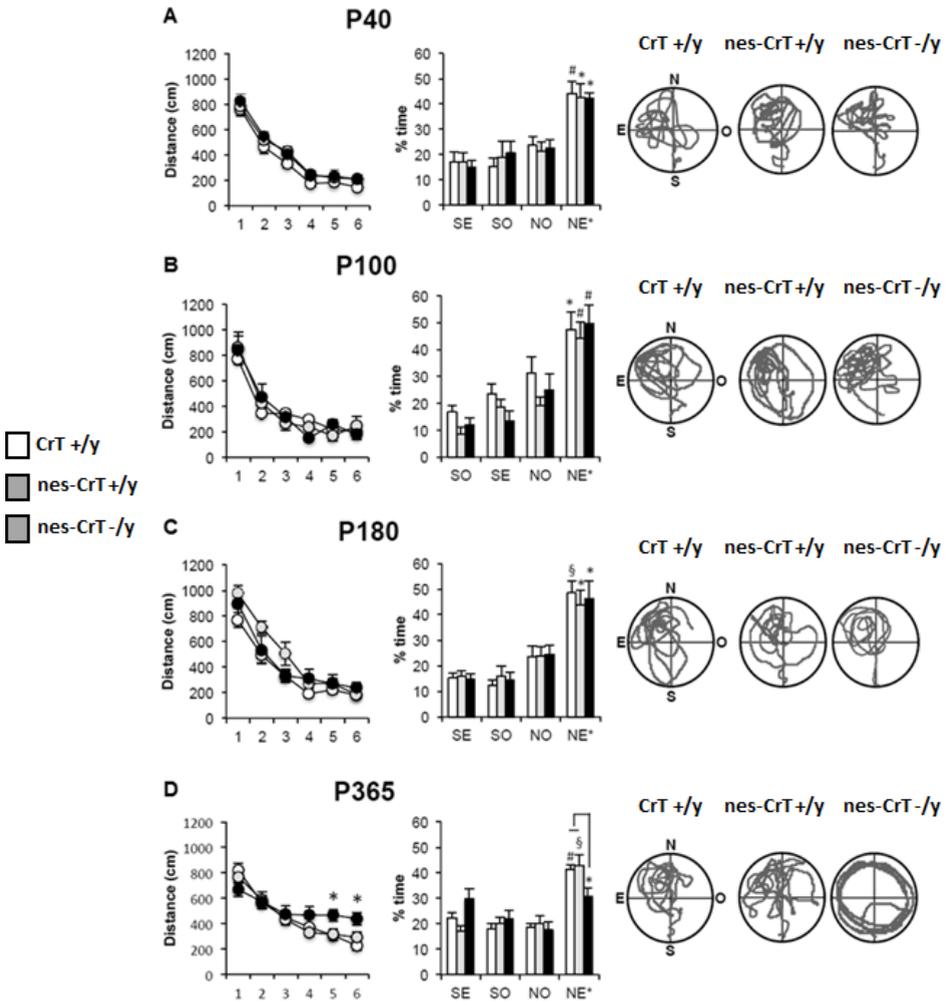

Figure 24. Left, learning curves for $CrT^{+/y}$ (white), nes-$CrT^{+/y}$ mice (grey) and nes-CrT–/y (black) at P40 (A; $CrT^{+/y}$: n = 10, nes-$CrT^{+/y}$: n = 5, nes-$CrT^{-/y}$: n = 5), P100 (B; $CrT^{+/y}$: n = 7, nes-$CrT^{+/y}$: n = 5, nes-$CrT^{-/y}$: n = 5), P180 (C; $CrT^{+/y}$: n = 9, nes-$CrT^{+/y}$: n = 6, nes-$CrT^{-/y}$: n = 5) and P365 (D; $CrT^{+/y}$: n = 12, nes-$CrT^{+/y}$: n = 14, nes-$CrT^{-/y}$: n = 12). No significant difference was detected along the training phase at P40 (Two-Way RM ANOVA, effect of genotype p = 0.114, interaction genotype x day p = 0.999), P100 (effect of genotype p = 0.976, interaction genotype x day p = 0.464) and P180 (Two-Way RM ANOVA on rank transformed data, effect of genotype p = 0.091, interaction genotype x day p = 0.748). In contrast, 1-year old nes-$CrT^{-/y}$ animals were poorer learners with respect to control groups, with a significant longer distance covered at day 5 and 6 of training (Two-Way RM ANOVA, interaction genotype x day p <

0.05, post hoc Holm-Sidak method, $p < 0.05$ for all comparisons at day 5, $p < 0.01$ vs. $CrT^{+/y}$, $p < 0.05$ vs. nes-$CrT^{+/y}$ at day 6). Right, histograms showing the mean time percentage spent in the four quadrants during the probe trial. No significant difference among the three groups was present at P40 (A; Two-Way RM ANOVA, effect of genotype $p = 0.173$, interaction genotype x quadrant $p = 0.985$), P100 (B; effect of genotype $p = 0.111$, interaction genotype x quadrant $p = 0.856$) and P180 (C; effect of genotype $p = 0.133$, interaction genotype x quadrant $p = 0.985$). At all ages, $CrT^{+/y}$, nes-$CrT^{+/y}$, nes-$CrT–/y$ spent significantly more time in the NE* target quadrant than in the other ones (Two-Way RM ANOVA, post hoc Holm-Sidak method, $p < 0.05$ for all comparisons). At P365 (D), a Two-Way RM ANOVA followed by Holm-Sidak multiple comparison revealed that nes-$CrT^{-/y}$ did not show any preference for the target quadrant ($p = 0.296$ NE* vs. SO, $p = 0.850$ NE* vs SE, $p = 0.060$ NE* vs. NO), while $CrT^{+/y}$ and nes-$CrT^{+/y}$ spent significantly more time in the NE* target quadrant ($p < 0.01$ for all comparisons in $CrT^{+/y}$, $p < 0.001$ for all comparisons in nes-$CrT^{+/y}$). The percentage of time spent in the target quadrant was shorter in nes-$CrT^{-/y}$ mice than in the other two control groups ($p < 0.05$ for both comparisons). Representative examples of the swimming path during the probe session for a $CrT^{+/y}$, a nes-$CrT^{+/y}$ and a nes-$CrT^{-/y}$ mouse are also depicted. * $p < 0.05$, # $p < 0.01$, § $p < 0.001$. Error bar: SEM.
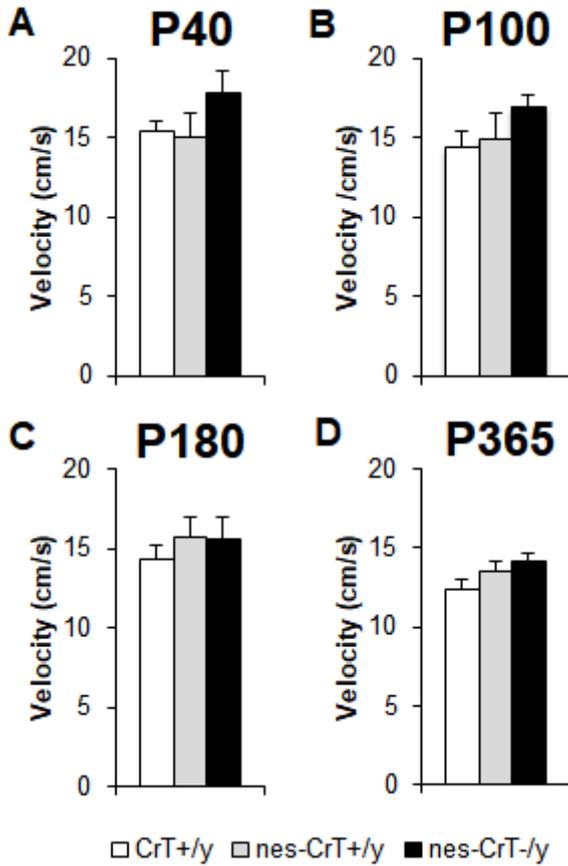
Figure 25. Mean swimming speed measured all along the training phase of the Morris water maze for CrT$^{+/y}$, nes- CrT$^{+/y}$, and nes-CrT$^{-/y}$ animals at P40 (A; CrT$^{+/y}$: n = 10, nes-CrT$^{+/y}$: n = 5, nes-CrT /y: n = 5), P100 (B; CrT$^{+/y}$: n = 7, nes-CrT$^{+/y}$: n = 5, nes-CrT$^{-/y}$: n = 5), P180 (C; CrT$^{+/y}$: n = 9, nes-CrT$^{+/y}$: n = 6, nes-CrT$^{-/y}$: n = 5) and P365 (D; CrT$^{+/y}$: n = 12, nes-CrT$^{+/y}$: n = 14, nes-CrT$^{-/y}$: n = 12). At all ages tested, mutant nes-CrT$^{-/y}$ mice resulted to be good swimmers as well as control animals (One-Way ANOVA, p = 0.191 at P40, p = 0.336 at P100, p = 0.592 at P180, p = 0.177 at P365). Error bars: SEM.
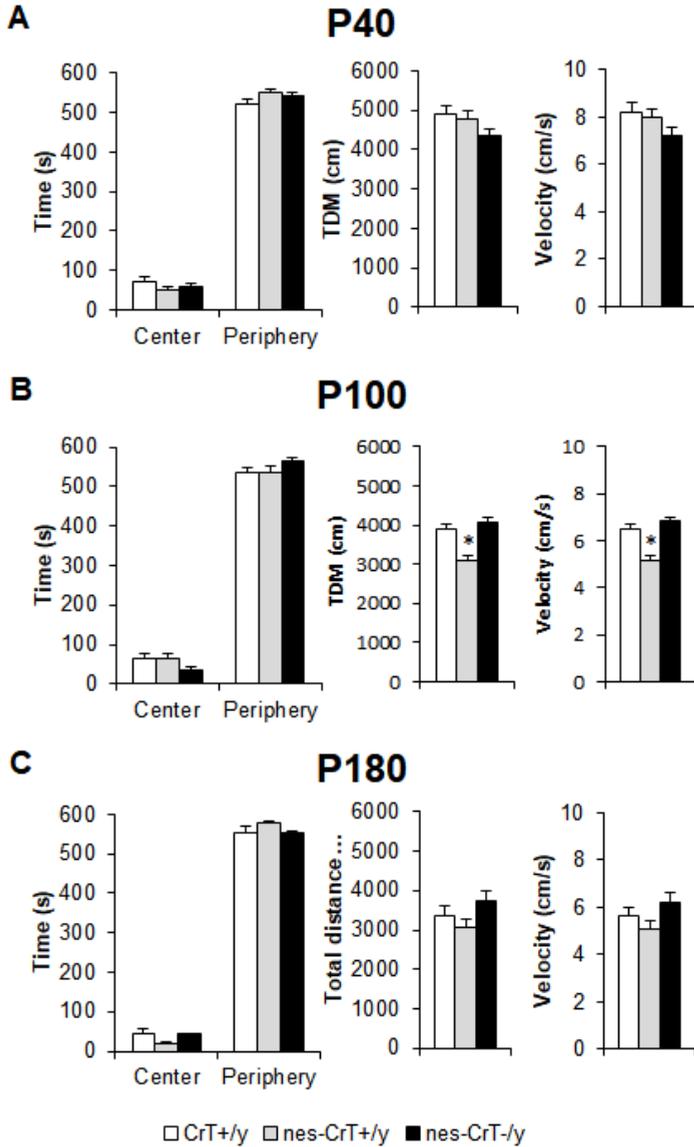
Figure 26. Left, CrT$^{+/y}$, nes-CrT$^{+/y}$ and nes-CrT$^{-/y}$ and CrT$^{+/y}$ mice spent a comparable amount of time in the center and in the peripheral region of the open field arena. A One-Way ANOVA on ranks analysis shows no significant effect of genotype at P40 (CrT$^{+/y}$ n = 13, nes-CrT$^{+/y}$ n = 9, nes-CrT$^{-/y}$ n = 6; p = 0.384; panel A), P100 (CrT$^{+/y}$ n = 13, nes-CrT$^{+/y}$ n = 9, nes-CrT$^{-/y}$ n = 6; p = 0.162; panel B) and P180 (CrT$^{+/y}$ n = 11, nes-CrT$^{+/y}$ n = 8, nes-CrT$^{-/y}$ n = 6; p = 0.588; panel C). Middle and right, total distance moved and velocity did not differ between CrT conditional mutants and control animals at P40 and P180 (One-Way ANOVA, p = 0.159, p = 0.215, respectively), while nes-CrT$^{+/y}$ mice displayed a lower speed and, consequently, a shorter path covered in the arena at P100 (One-Way ANOVA on ranks, effect of genotype p < 0.01, post hoc Dunn's method p < 0.05 for both comparisons). * p < 0.05. Error bars: SEM.
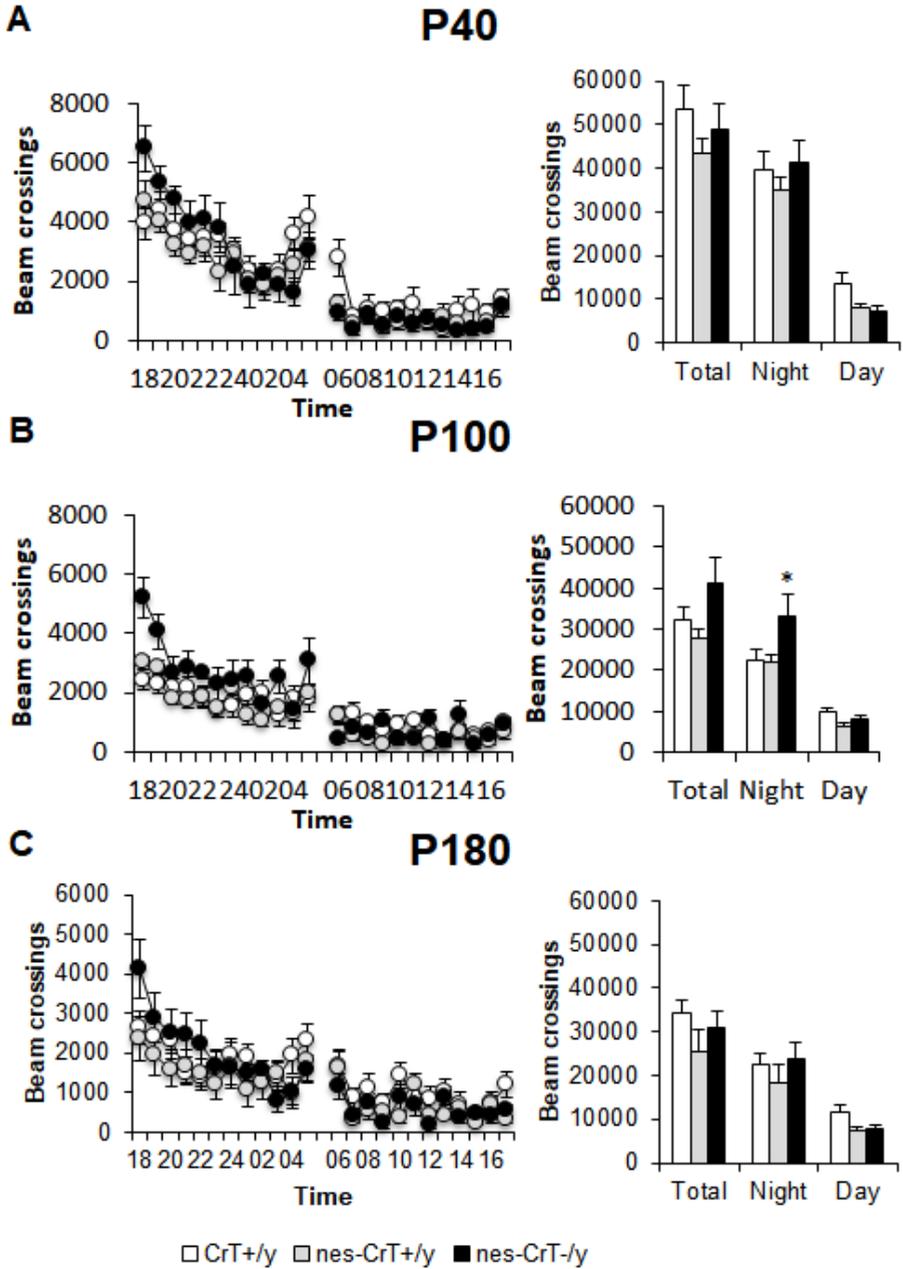
Figure 27. Left, Time course of horizontal activity of CrT[+/y] (white), nes-CrT[+/y] (grey) and nes-CrT /y (black) animals during 24h at P40 (A), P100 (B) and P180 (C). Data are plotted as total number of beam crossings ± SEM in each time block of 60 min. Right, total horizontal distance travelled throughout 24h (total), and over the dark (night) or light phase (day). No significant difference was detected among the three experimental groups at P40 and P180 (Two-Way ANOVA on rank transformed data, $p = 0.384$ and $p = 0.157$, respectively), while nes-CrT[-/y]

mice had a significant increase in motor activity at P100 in comparison to control groups during the night period (Two-Way ANOVA, post hoc Holm-Sidak method, $p < 0.05$ for both comparisons). * $p < 0.05$. Error bars: SEM.
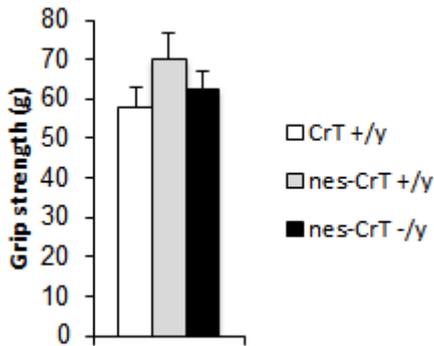
Figure 28. The performance of nes-CrT$^{-/y}$ mice (n = 7) in the grip strength displayed no significant difference with respect to CrT$^{+/y}$ (n = 13) and nes-CrT$^{+/y}$ (n = 11) animals (One-Way ANOVA, p = 0.191). Error bars: SEM.
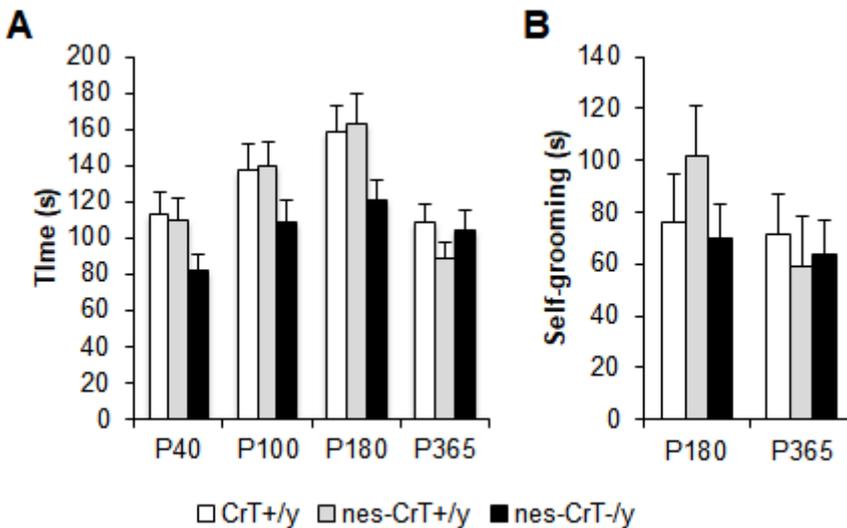

Figure 29. (A) Longitudinal performance of CrT$^{+/y}$ mice (n = 13 for P40 and P100, n = 11 for P180 and P365), nes-CrT$^{+/y}$ (n = 9 for P40, P100 and P180, n = 11 for P365) and nes-CrT$^{-/y}$ (n = 6 for P40, P100 and P180, n = 7 for P365) on the accelerating rotarod. A Two-Way ANOVA on rank transformed data showed no significant effect of genotype (p = 0.06) and the lack of a statistically significant interaction between genotype and age (p = 0.474). (B) Histograms display mean time spent self-grooming in CrT$^{+/y}$, nes-CrT$^{+/y}$ and nes-CrT$^{-/y}$ at P180 (CrT$^{+/y}$: n = 11, nes-CrT$^{+/y}$: n = 11, nes-CrT$^{-/y}$: n = 7) and P365 (CrT$^{+/y}$: n = 6, nes-CrT$^{+/y}$: n = 10, nes-CrT$^{-/y}$: n = 7). No difference was detected in grooming behavior at both ages (Two-Way ANOVA

on rank transformed data, effect of genotype p = 0.564, interaction genotype x age p = 0.131). Error bars: SEM.
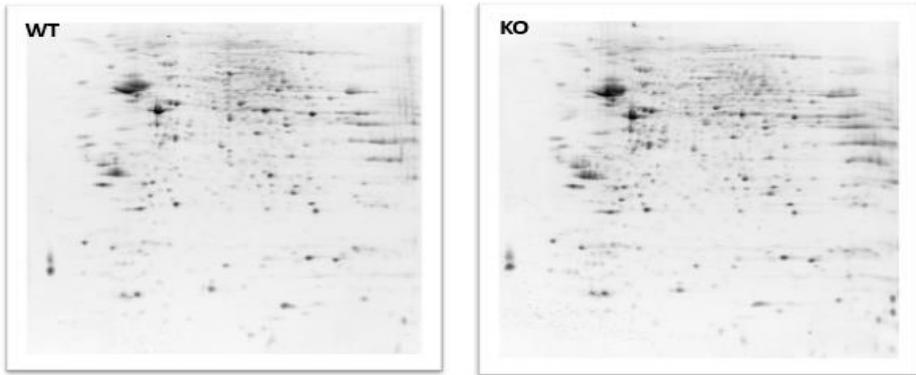

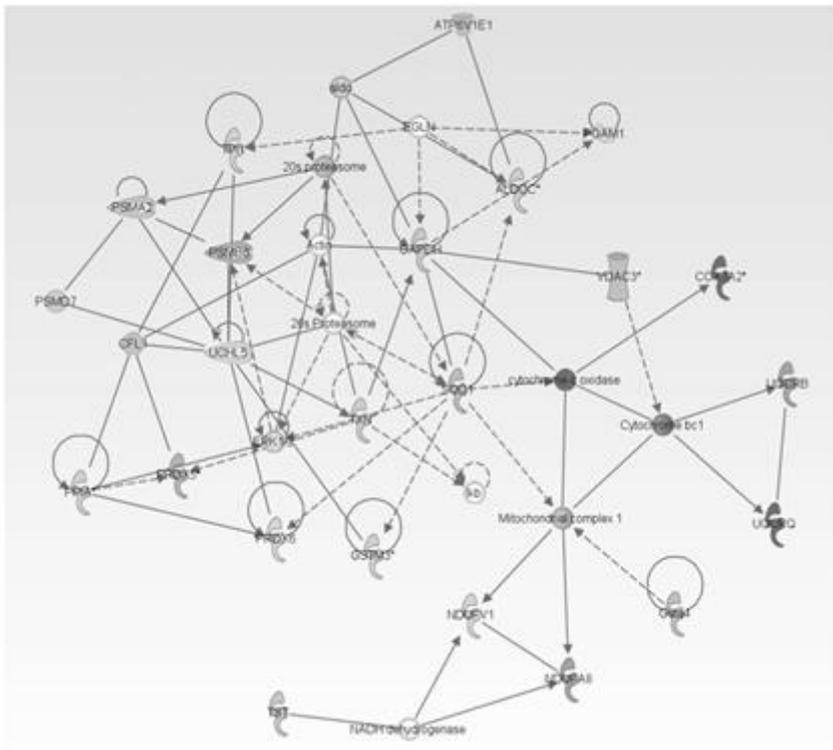Figure 30. Comparison between CrT$^{-/y}$ and WT proteomic gels.

Figure 31. Main network generated by Ingenuity Pathways Analysis (IPA) software to show the relation between the identified proteins and to recognize cellular and molecular functions in which these proteins could be involved.
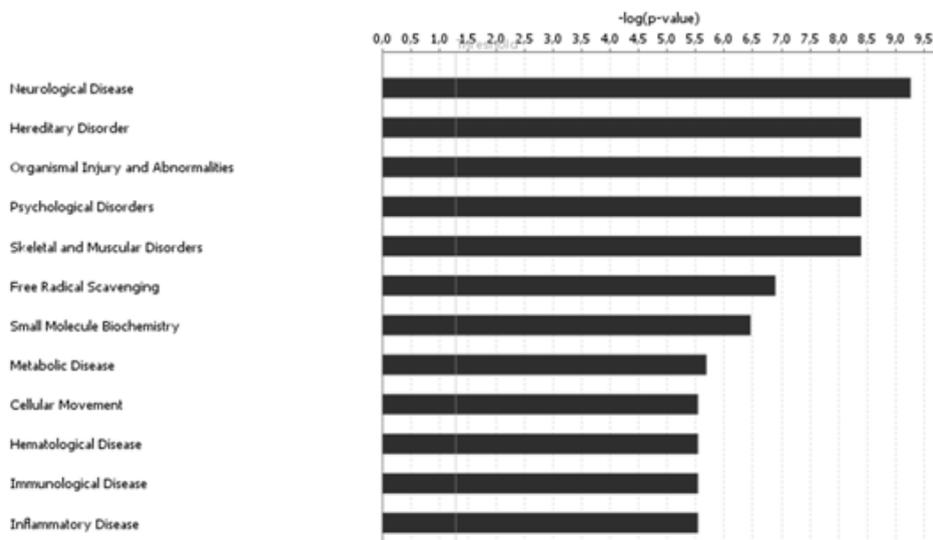
Figure 32. Group of cellular functions or diseases to which the differentially expressed proteins are associated.
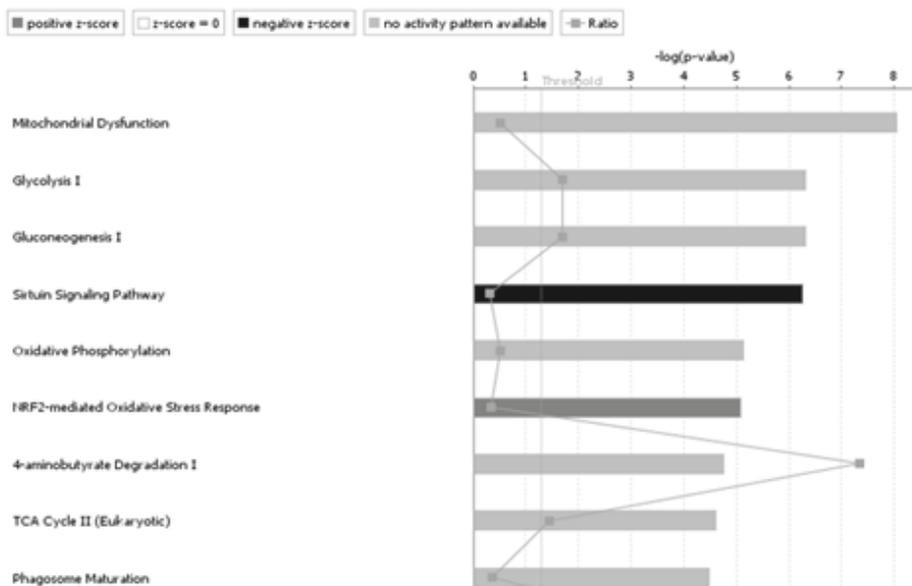

Figure 33. Main canonical pathways in which the differentially expressed proteins could be involved.
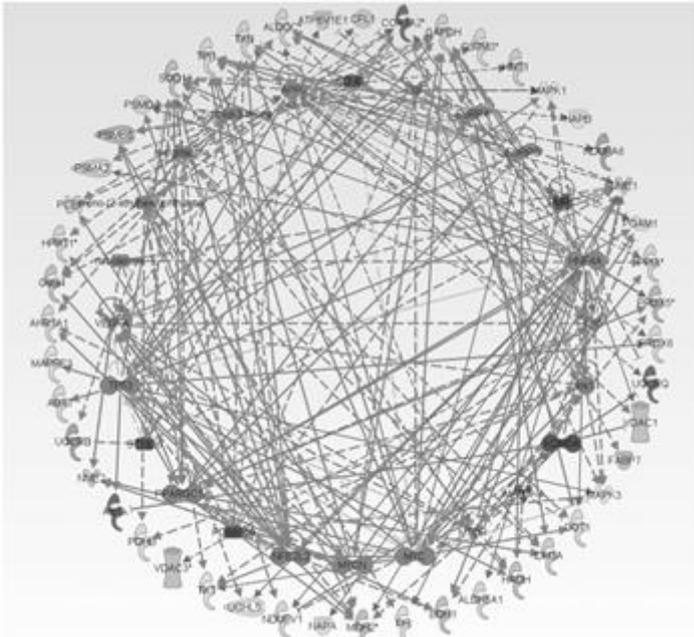
Figure 34. Interaction of the factors identified, with the proteins differently regulated.
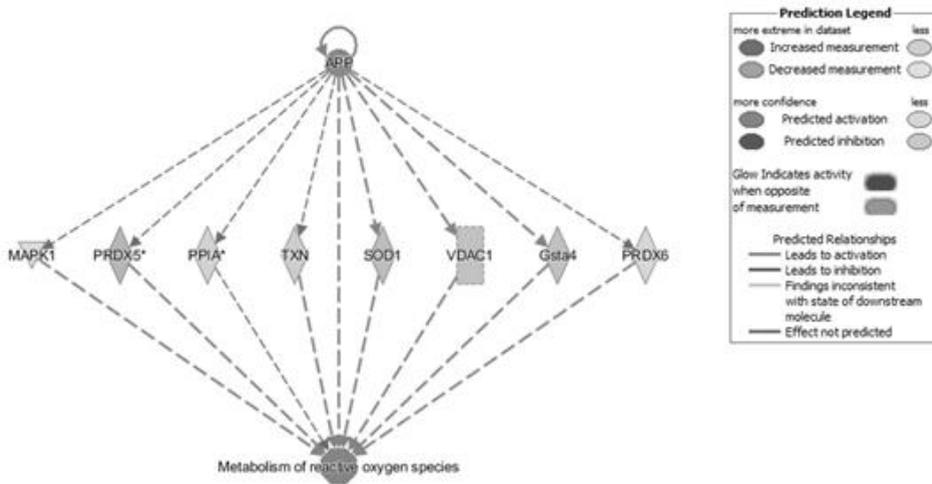

Figure 35. A main regulator, APP, interacts with many proteins identified by proteomic analysis, and a pathway emerges which converges towards the regulation of the metabolism of reactive oxygen species.
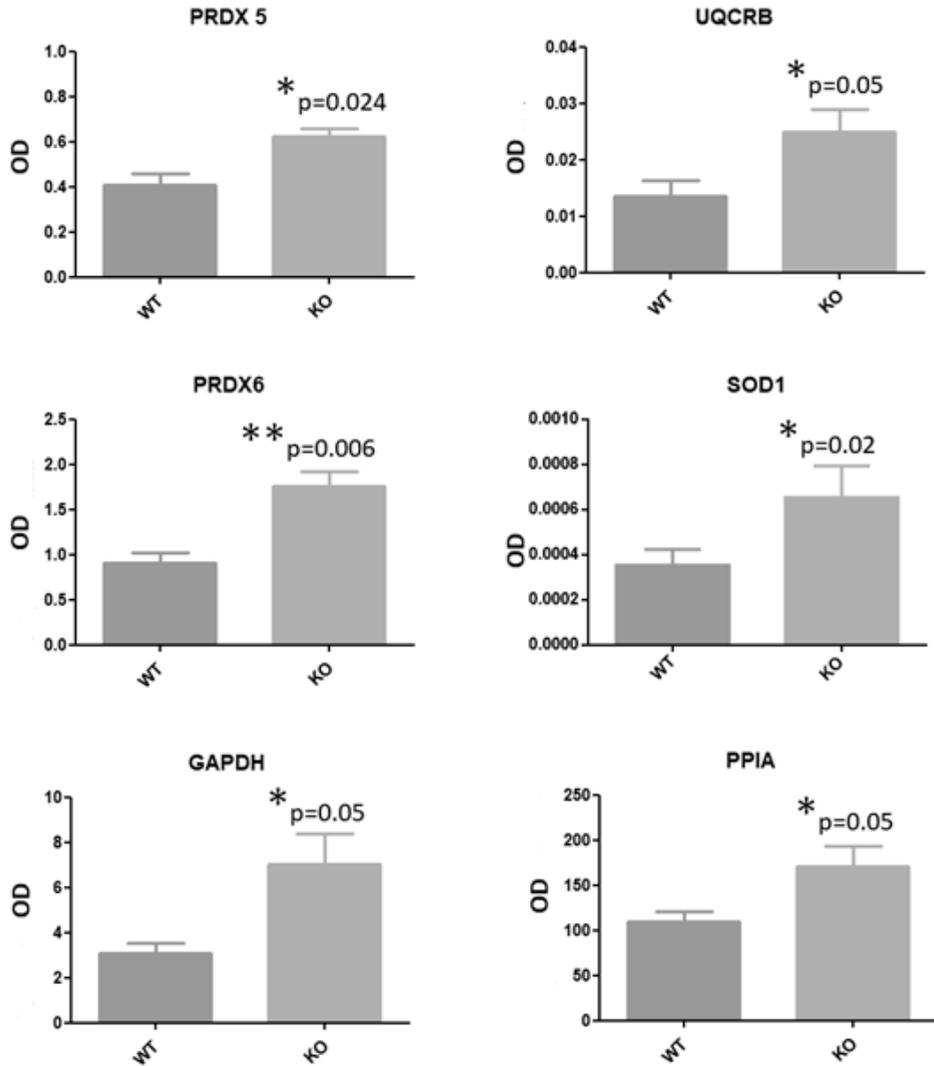
Figure 36. Western Blot Validation of proteomic results. OD: optical density (normalized volume). KO: $CrT^{-/y}$. Error bars: SEM.

Tables

Tissue (nmol/ mg protein)	P30		P180	
	CrT$^{+/y}$	CrT$^{-/y}$	CrT$^{+/y}$	CrT$^{-/y}$
Cortex	76.36 ± 3.16	13.61 ± 1.06***	92.41 ± 0.66	14.15 ± 0.66***
Hippocampus	83.69 ± 4.37	14.14 ± 1.52***	88.73 ± 4.97	14.79 ± 1.46***
Muscle	310.20 ± 31.59	111.57 ± 21.27***	365.38 ± 8.19	15.94 ± 5.55***
Heart	89.92 ± 5.15	1.19 ± 0.27***	100.91 ± 3.36	2.39 ± 0.61***
Kidney	9.60 ± 0.65	1.59 ± 0.13*	10.36 ± 0.80	1.80 ± 0.78**

Table 1. Cr levels (mean ± SEM) in CrT$^{+/y}$ and CrT$^{-/y}$ animals at P30 and P180 (n = 4 per tissue for both groups). Cr levels have been measured by GC/MS. A reduction of Cr content was evident in the brain, muscle, heart and kidney of mutant animals at both P30 and P180 (Two-Way ANOVA on rank transformed data, post hoc Holm-Sidak method). * p < 0.05; ** p < 0.01; *** p < 0.001.

Tissue (nmol/ mg protein)	P30		P180	
	CrT$^{+/y}$	CrT$^{-/y}$	CrT$^{+/y}$	CrT$^{-/y}$
Cortex	0.060 ± 0.002	0.114 ± 0.016***	0.050 ± 0.006	0.066 ± 0.005
Hippocampus	0	0.091 ± 0.007 ***	0.026 ± 0.015	0.079 ± 0.009**
Muscle	0.106 ± 0.006	0.282 ± 0.068**	0.026 ± 0.010	0.150 ± 0.050**
Heart	0.094 ± 0.010	0.060 ± 0.004***	0.052 ± 0.007	0.033 ± 0.015
Kidney	10.700 ± 0.627	9.758 ± 0.712	2.205 ± 0.259	2.411 ± 0.112

Table 2. GAA levels (mean ± SEM) in CrT$^{+/y}$ and CrT$^{-/y}$ animals at P30 and P180 (n = 4 per tissue for both groups). At P30, a moderate increase of GAA content was evident in the brain and the muscle of mutant animals (Two-Way ANOVA on rank transformed data, post hoc Holm-Sidak method, $p < 0.05$), whereas GAA was decreased in the heart of CrT$^{-/y}$ animals ($p < 0.05$) and no difference was detected in the kidney tissue ($p = 0.359$). At P180, GAA levels were higher in the hippocampus and the muscle of mutant animals (Two-Way ANOVA on rank transformed data, post hoc Holm-Sidak method, $p < 0.01$), whereas no difference was detected in cortex, heart and kidney ($p = 0.175$, $p = 0.320$ and $p = 0.920$, respectively). ** $p < 0.01$; *** $p < 0.001$.

Tissue (nmol/ mg protein)	nes-CrT$^{+/y}$	nes-CrT$^{-/y}$	CrT$^{fl/y}$
Cortex	73.29 ± 1.88	17.36 ± 0.87***	71.55 ± 4.15
Hippocampus	87.45 ± 4.17	17.13 ± 2.22***	94.62 ± 4.35
Muscle	382.97 ± 20.46	390.58 ± 22.66	385.36 ± 27.59
Heart	78.24 ± 3.72	70.35 ± 3.10	68.02 ± 1.79
Kidney	6.10 ± 0.81	3.11 ± 0.27	7.60 ± 1.22

Table 3. Cr levels (mean ± SEM) in nes-CrT$^{+/y}$, nes-CrT$^{-/y}$ and CrTfl/y animals at P180 (n = 4 per tissue for all groups). A reduction of Cr content was evident in the brain of mutant animals, while peripheral tissues were not affected (Two-Way ANOVA on rank transformed data, post hoc Holm-Sidak method). *** $p < 0.001$.

Tissue (nmol/ mg protein)	nes-CrT$^{+/y}$	nes-CrT$^{-/y}$	CrT$^{fl/y}$
Cortex	0.048 ± 0.005	0.059 ± 0.004***	0.048 ± 0.004
Hippocampus	0.068 ± 0.005	0.131 ± 0.018*	0.074 ± 0.011
Muscle	0.054 ± 0.006	0.061 ± 0.002	0.059 ± 0.003
Heart	0.045 ± 0.004	0.047 ± 0.003	0.054 ± 0.007
Kidney	1.705 ± 0.373	1.231 ± 0.099	3.051 ± 0.914

Table 4. GAA levels (mean ± SEM) in nes-CrT$^{+/y}$, nes-CrT$^{-/y}$ and CrTfl/y animals at P180 (n = 4 per tissue for all groups). An increase of GAA content was evident in the brain of mutant animals, while peripheral tissues were not affected (Two-Way ANOVA on rank transformed data, post hoc Holm-Sidak method). * $p < 0.05$; *** $p < 0.001$.

n°	ID	Description	Protein	Fold (CrT +/y / CrT +/y)	Coverage	Peptides	MW (th)	pI (th)	CrT +/y	CrT -/y	p-value
2110	Q06185	ATP synthase subunit e, mitochondrial	ATP5I	5.8	68	7	8	9.34	7,36E+05	4,28E+06	0.001
2110	Q9CQ69	Cytochrome b-c1 complex subunit	QCR8	5.8	39	4	9	10.26	7,36E+05	4,28E+06	0.001
1225	Q8K183	Pyridoxal kinase	PDXK	1.4	20	2	35	5.88	4,96E+05	6,80E+05	0.002
1616	P24472	Glutathione S-transferase A4	GSTA4	2.1	15	4	25	6.77	1,51E+05	3,15E+05	0.004
2016	P70349	Histidine triad nucleotide-binding protein 1	HINT1	1.9	30	2	13	6.36	3,63E+05	6,90E+05	0.005
1853	P18760	Cofilin-1	COF1	2	27	3	18	8.22	4,29E+05	8,57E+05	0.007
1627	Q60692	Proteasome subunit beta type-6	PSB6	2.6	30	2	25	4.97	2,00E+05	5,29E+05	0.01
2309	P08249	Malate dehydrogenase, mitochondrial	MDHM	2	69	33	36	8.93	1,22E+06	2,44E+06	0.011
2309	Q60931	Voltage-dependent anion-selective channel protein 3	VDAC3		19	4	31	8.96	1,22E+06	2,44E+06	
2049	P10639	Thioredoxin	THIO	1.8	23	2	11	4.8	2,53E+06	4,53E+06	0.012
1562	P17751	Triosephosphate isomerase	TPIS	1.7	60	7	32	5.56	1,11E+05	1,87E+05	0.013
1921	P99029	Peroxiredoxin-5, mitochondrial	PRDX5	2.2	45	4	21	9.1	2,99E+05	6,53E+05	0.014
1597	P49722	Proteasome subunit alpha type-2	PSA2	1.9	46	11	26	6.91	3,65E+05	6,86E+05	0.015
2264	P48771	Cytochrome c oxidase subunit 7A2, mitochondrial	CX7A2	2.4	15	2	9	10.28	3,90E+05	9,36E+05	0.016

n*	ID	Description	Protein	Fold (CrT -/v/ CrT +/v)	Coverage	Peptides	MW (th)	pI (th)	CrT +/v	CrT -/v	p-value
1329	Q9CY64	Biliverdin reductase A	BLEA	1.8	43	4	33	6.53	2.26E+05	3.99E+05	0.017
1329	P08228	Superoxide dismutase [Cu-Zn]	SODC	2.2	25	3	16	6.02	5.29E+05	1.14E+06	0.017
660	Q8K2B3	Succinate dehydrogenase [ubiquinone] flavoprotein subunit, mitoch	SDHA	1.4	17	2	72	7.06	8.92E+05	1.25E+06	0.021
911	Q91YT0	NADH dehydrogenase [ubiquinone] flavoprotein 1, mitochondrial	NDUV1	1.6	23	10	51	8.51	1.12E+06	1.80E+06	0.021
2233	P62984	Ubiquitin-60S ribosomal protein L40	RL40	1.9	37	4	15	9.87	8.52E+05	1.65E+06	0.023
1394	Q60932	Voltage-dependent anion-selective channel protein 1	VDAC1	2.1	63	19	32	8.55	1.47E+06	3.11E+06	0.023
1394	P50518	V-type proton ATPase subunit E 1	VATE1	2.1	50	20	26	8.44	1.47E+06	3.11E+06	0.023
2331	P99029	Peroxiredoxin-5, mitochondrial	PRDX5	2.4	41	3	21	9.1	2.32E+05	5.54E+05	0.023
2062	Q9DB65	Cytochrome b-c1 complex subunit 7	QCR7	3	37	8	13	9.1	1.72E+06	5.10E+06	0.024
1899	P17742	Peptidyl-prolyl cis-trans isomerase A	PPIA	1.6	66	12	18	7.73	3.79E+06	6.18E+06	0.024
2005	P51880	Fatty acid binding protein, brain	FABP7	2.1	78	15	15	5.46	2.54E+05	5.36E+05	0.03
1563	O08709	Peroxiredoxin-6	PRDX6	1.6	35	6	25	5.71	1.13E+06	1.81E+06	0.031
1566	P48774	Glutathione S-transferase Mu 5	GSTM5	1.7	54	13	27	6.82	1.03E+06	1.74E+06	0.034

continues…

n°	ID	Description	Protein	Fold (CrT -/y/ CrT +/y)	Coverage	Peptides	MW (th)	pI (th)	CrT +/y	CrT -/y	p-value
1823	Q9CQZ1	NADH dehydrogenase [ubiquinone] iron-sulfur protein 4, mitoch	NDUS4	3	20	2	19	10	6,00E+05	1,80E-06	0.035
1823	Q9DCI5	NADH dehydrogenase [ubiquinone] 1 alpha subcomplex subunit 8	NDUA8	3	22	3	20	8.76	6,00E+05	1,80E-06	0.035
983	P97807	Fumarate hydratase, mitochondrial	FUMH	1.5	39	15	54	9.12	6,60E+05	1,02E-06	0.035
1199	P05063	Fructose-bisphosphate aldolase C	ALDOC	1.7	79	28	39	6.67	9,70E+05	1,65E-06	0.038
1262	P16858	Glyceraldehyde-3-phosphate dehydrogenase	G3P	1.9	54	19	36	8.44	4,90E+05	9,12E-05	0.042
1888	P17742	Peptidyl-prolyl cis-trans isomerase A	PPIA	1.7	54	8	18	7.73	8,25E+05	1,39E-06	0.044
1123	P63085	Mitogen-activated protein kinase 1	MK01	1.5	52	16	41	6.50	1,73E+06	2,57E-06	0.045
1139	P26516	26S proteasome non-ATPase regulatory subunit 7	PSMD7	1.8	37	8	36	6.29	1,41E+06	2,58E-06	0.047
1483	Q9DBJ1	Phosphoglycerate mutase 1	PGAM1	1.6	29	6	29	6.67	9,30E+05	1,49E-06	0.047
1323	Q9WU77	Ubiquitin carboxyl-terminal hydrolase isozyme L5	UCHL5	1.5	13	4	37	5.24	4,63E+05	6,93E-05	0.048

Table 5. List of differentially expressed proteins at P30 identified by MS/MS spectrometry. ID: SwissProt accession number, MW (th): theorical molecular weight, pI (th): theorical isoelectric point (continuing to next pages).

Table 6. List of differentially expressed proteins at P12 identified by MS/MS spectrometry. ID: SwissProt accession number, MW (th): theorical molecular weight.

Upstream Regulator	Molecule Type	Predicted Activation State	Activation z-score	p-value of overlap	Target molecules in dataset
RICTOR	other	Inhibited	-3.162	9.88E-10	ATP6V1E1,COX7A2,NDUFA8,NDUFV1,PSMA2,PSMB6,PSMD7,Uba5,2,UQCRB,UQCRQ
FMR1	translation regulator	Inhibited	-2.236	0.000000214	ATP6V1E1,CFL1,GAPDH,PPIA,UQCRQ
KDM5A	transcription regulator	Inhibited	-2.449	0.000000872	Atp5k,COX7A2,NDUFV1,NME1,UQCRQ,VDAC1
ELN	group	Inhibited	-2	0.0000984	ALDOC,GAPDH,PGAM1,TPI1
MAP4K4	kinase	Inhibited	-2	0.000218	GOT1,HADH,NDUFV1,PGAM1
miR-7515 (miRNAs w/seed GAAGGGA)	mature microRNA	Inhibited	-2	0.00563	CFL1,PGAM1,SEPT3,TPI1
miR-3151-5p (and other miRNAs w/seed GUGGGGC)	mature microRNA	Inhibited	-2	0.00673	CFL1,GOT1,NAPA,SEPT3
APP	other	Activated	2	9.45E-16	ALDOC,ATP6V1E1,CFL1,COX7A2,GAPDH,Gsta4,GSTM3,HINT1,MAPK1,NAPB
NFE2L2	transcription regulator	Activated	3.101	7.53E-08	AKR1A1,Gsta4,HPRT1,PCBP1,PSMB6,PSMD7,SOD1,TKT,TPI1,TXN
ESRRG	ligand-dependent nuclear receptor	Activated	2	0.00000685	ALDOC,GAPDH,HADH,TPI1
HIF4A	transcription regulator	Activated	2	0.000000894	ALDH6A1,BDH1,COX7A2,FH,GAPDH,GOT1,MDH2,NAPA,NDUFV1,NME1
IL15	cytokine	Activated	2.425	0.00000113	ALDOC,GAPDH,MAPK1,MAPK3,NME1,TKT,TPI1,VDAC3
PPARGC1A	transcription regulator	Activated	2.423	0.0000347	BDH1,IDH3A,MDH2,PGAM1,PRDX5,SOD1
ESRRA	ligand-dependent nuclear receptor	Activated	2.213	0.0000918	ALDOC,GAPDH,GOT1,IDH3A,TPI1
TP53	transcription regulator	Activated	3.234	0.000119	ABAT,Atp5k,COX7A2,GAPDH,HADH,MAPK1,MAPK3,MAPRE3,MDH2,NME1
Ins1	other	Activated	2.414	0.000124	BDH1,COX7A2,GAPDH,MAPK1,MAPK3,PDHB
TGFB1	growth factor	Activated	2.053	0.000349	ALDH6A1,BDH1,CFL1,Gsta4,HADH,HINT1,MAPK1,MAPK3,NME1,NM E2
MYC	transcription regulator	Activated	2.42	0.000358	GAPDH,GOT1,MAPK3,NME1,NME2,PGAM1,PPIA,TKT,TPI1,TXN
MYCN	transcription regulator	Activated	2.207	0.000703	GAPDH,NME1,NME2,PSMB6,TPI1
CD3	complex	Activated	2.449	0.00103	GAPDH,HINT1,MAPK1,MDH2,NME1,PGAM1,VDAC3
HIF1A	transcription regulator	Activated	2.189	0.00384	ALDOC,GAPDH,PPIA,TPI1,TXN
VEGFA	growth factor	Activated	2	0.00627	MDH2,NME1,NME2,UQCRB
MTOR	kinase	Activated	2	0.00859	AKR1A1,MDH2,PRDX5,SOD1
EGF	growth factor	Activated	2.194	0.00879	FABP7,Gsta4,MAPK1,MAPK3,PSMB6

Table 7. List of the main putative upstream regulators and their interaction with the overexpressed proteins found in the CrT$^{-/y}$ mice.

References

Ahmed, Z., Sheng, H., Xu, Y., Lin, W.-L., Innes, A. E., Gass, J., Yu, X., Hou, H., Chiba, S., Yamanouchi, K., Leissring, M., Petrucelli, L., Nishihara, M., Hutton, M. L., McGowan, E., Dickson, D. W., Lewis, J. and Lewis, J. (2010) 'Accelerated Lipofuscinosis and Ubiquitination in Granulin Knockout Mice Suggest a Role for Progranulin in Successful Aging', The American Journal of Pathology, 177(1), pp. 311–324. doi: 10.2353/ajpath.2010.090915.

Alcaide, P., Merinero, B., Ruiz-Sala, P., Richard, E., Navarrete, R., Arias, Á., Ribes, A., Artuch, R., Campistol, J., Ugarte, M. and Rodríguez-Pombo, P. (2011) 'Defining the pathogenicity of creatine deficiency syndrome', Human Mutation. Wiley-Blackwell, 32(3), pp. 282–291. doi: 10.1002/humu.21421.

Alessandrì, M. G., Celati, L., Battini, R., Casarano, M. and Cioni, G. (2005) 'Gas chromatography/mass spectrometry assay for arginine: Glycine-amidinotransferase deWciency', ANALYTICAL BIOCHEMISTRY, 343, pp. 356–358. doi: 10.1016/j.ab.2005.05.003.

Almeida, L. S., Salomons, G. S., Hogenboom, F., Jakobs, C. and Schoffelmeer, A. N. M. (2006) 'Exocytotic release of creatine in rat brain.', Synapse (New York, N.Y.), 60(2), pp. 118–23. doi: 10.1002/syn.20280.

Andres, R. H., Ducray, A. D., Schlattner, U., Wallimann, T. and Widmer, H. R. (2008) 'Functions and effects of creatine in the central nervous system.', Brain research bulletin, 76(4), pp. 329–43. doi: 10.1016/j.brainresbull.2008.02.035.

Anselm, I. M., Alkuraya, F. S., Salomons, G. S., Jakobs, C., Fulton, A. B., Mazumdar, M., Rivkin, M., Frye, R., Poussaint, T. Y., Marsden, D. and Marsden, D. (2006) 'X-linked creatine transporter defect: A report on two unrelated boys with a severe clinical phenotype', Journal of Inherited Metabolic Disease, 29(1), pp. 214–219. doi: 10.1007/s10545-006-0123-4.

Assunção, M., Santos-Marques, M. J., Carvalho, F., Lukoyanov, N. V. and Andrade, J. P. (2011) 'Chronic green tea consumption prevents age-related changes in rat hippocampal formation', Neurobiology of Aging, 32(4), pp. 707–717. doi: 10.1016/j.neurobiolaging.2009.03.016.

Balsom, P. D., Söderlund, K. and Ekblom, B. (1994) 'Creatine in humans with special reference to creatine supplementation.', Sports medicine (Auckland, N.Z.), 18(4), pp. 268–80. Available at: http://www.ncbi.nlm.nih.gov/pubmed/7817065.

Bamburg, J. R. and Bernstein, B. W. (2016) 'Actin dynamics and cofilin-actin rods in alzheimer disease', Cytoskeleton, 73(9), pp. 477–497. doi: 10.1002/cm.21282.

Bano, D., Agostini, M., Melino, G. and Nicotera, P. (2011) 'Ageing, Neuronal Connectivity and Brain Disorders: An Unsolved Ripple Effect', Molecular Neurobiology, 43(2), pp. 124–130. doi: 10.1007/s12035-011-8164-6.

Baroncelli, L., Alessandrì, M. G., Tola, J., Putignano, E., Migliore, M., Amendola, E., Gross, C., Leuzzi, V., Cioni, G. and Pizzorusso, T. (2014) 'A novel mouse model of creatine

transporter deficiency.', F1000Research, 3(0), p. 228. doi: 10.12688/f1000research.5369.1.

Bartsch, T. and Wulff, P. (2015) 'The hippocampus in aging and disease: From plasticity to vulnerability', Neuroscience, 309, pp. 1–16. doi: 10.1016/j.neuroscience.2015.07.084.

Beck, H., Flynn, K., Lindenberg, K. S., Schwarz, H., Bradke, F., Di Giovanni, S. and Knoll, B. (2012) 'Serum Response Factor (SRF)-cofilin-actin signaling axis modulates mitochondrial dynamics', Proceedings of the National Academy of Sciences, 109(38), pp. E2523–E2532. doi: 10.1073/pnas.1208141109.

Bender, A., Beckers, J., Schneider, I., Hölter, S. M., Haack, T., Ruthsatz, T., Vogt-Weisenhorn, D. M., Becker, L., Genius, J., Rujescu, D., Irmler, M., Mijalski, T., Mader, M., Quintanilla-Martinez, L., Fuchs, H., Gailus-Durner, V., de Angelis, M. H., Wurst, W., Schmidt, J. and Klopstock, T. (2008) 'Creatine improves health and survival of mice', Neurobiology of Aging, 29(9), pp. 1404–1411. doi: 10.1016/j.neurobiolaging.2007.03.001.

von Bernhardi, R., Eugenín-von Bernhardi, L. and Eugenín, J. (2015) 'Microglial cell dysregulation in brain aging and neurodegeneration', Frontiers in Aging Neuroscience, 7, p. 124. doi: 10.3389/fnagi.2015.00124.

Betsalel, O. T., Pop, A., Rosenberg, E. H., Fernandez-Ojeda, M., Creatine Transporter Research, Group, C., Jakobs, C. and Salomons, G. S. (2012) 'Detection of variants in SLC6A8 and functional analysis of unclassified missense variants.', Molecular genetics and metabolism, 105(4), pp. 596–601. doi: 10.1016/j.ymgme.2011.12.022.

Bizzi, A., Bugiani, M., Salomons, G. S., Hunneman, D. H., Moroni, I., Estienne, M., Danesi, U., Jakobs, C. and Uziel, G. (2002) 'X-linked creatine deficiency syndrome: A novel mutation in creatine transporter geneSLC6A8', Annals of Neurology, 52(2), pp. 227–231. doi: 10.1002/ana.10246.

Bories, C., Husson, Z., Guitton, M. J. and De Koninck, Y. (2013) 'Differential balance of prefrontal synaptic activity in successful versus unsuccessful cognitive aging.', The Journal of neuroscience : the official journal of the Society for Neuroscience, 33(4), pp. 1344–56. doi: 10.1523/JNEUROSCI.3258-12.2013.

Braissant, O., Cagnon, L., Monnet-Tschudi, F., Speer, O., Wallimann, T., Honegger, P. and Henry, H. (2008) 'Ammonium alters creatine transport and synthesis in a 3D culture of developing brain cells, resulting in secondary cerebral creatine deficiency', European Journal of Neuroscience, 27(7), pp. 1673–1685. doi: 10.1111/j.1460-9568.2008.06126.x.

Braissant, O., Henry, H., Loup, M., Eilers, B. and Bachmann, C. (2001) 'Endogenous synthesis and transport of creatine in the rat brain: an in situ hybridization study.', Brain research. Molecular brain research, 86(1–2), pp. 193–201.

Braissant, O., Henry, H., Villard, A.-M., Speer, O., Wallimann, T. and Bachmann, C. (2005) 'Creatine synthesis and transport during rat embryogenesis: spatiotemporal expression of AGAT, GAMT and CT1.', BMC Developmental Biology, 5(1), p. 9. doi: 10.1186/1471-213X-5-9.

Brandenstein, L., Schweizer, M., Sedlacik, J., Fiehler, J. and Storch, S. (2016) 'Lysosomal dysfunction and impaired autophagy in a novel mouse model deficient for the lysosomal membrane protein Cln7', Human Molecular Genetics, 25(4), pp. 777–791. doi: 10.1093/hmg/ddv615.

Brosnan, J. T. and Brosnan, M. E. (2007) 'Creatine: Endogenous Metabolite, Dietary, and Therapeutic Supplement', Annual Review of Nutrition, 27(1), pp. 241–261. doi: 10.1146/annurev.nutr.27.061406.093621.

Brynczka, C. and Merrick, B. A. (2008) 'The p53 transcriptional target gene wnt7b contributes to NGF-inducible neurite outgrowth in neuronal PC12 cells', Differentiation, 76(7), pp. 795–808. doi: 10.1111/j.1432-0436.2007.00261.x.

Carducci, C., Carducci, C., Santagata, S., Adriano, E., Artiola, C., Thellung, S., Gatta, E., Robello, M., Florio, T., Antonozzi, I., Leuzzi, V. and Balestrino, M. (2012) 'In vitro study

of uptake and synthesis of creatine and its precursors by cerebellar granule cells and astro-cytes suggests some hypotheses on the physiopathology of the inherited disorders of cre-atine metabolism.', BMC neuroscience. BioMed Central, 13, p. 41. doi: 10.1186/1471-2202-13-41.

Chanutin, A. (1926) 'Tha fate of creatine when administered to man', The Journal of biological chemistry, (2).

Chen, B. and Wang, Y. (2015) 'Cofilin rod formation in neurons impairs neuronal structure and function.', CNS & neurological disorders drug targets, 14(4), pp. 554–60. Available at: http://www.ncbi.nlm.nih.gov/pubmed/25714964.

Chilosi, A., Casarano, M., Comparini, A., Battaglia, F., Mancardi, M., Schiaffino, C., Tosetti, M., Leuzzi, V., Battini, R. and Cioni, G. (2012) 'Neuropsychological profile and clinical effects of arginine treatment in children with creatine transport deficiency', Orphanet Journal of Rare Diseases, 7(1), p. 43. doi: 10.1186/1750-1172-7-43.

Chilosi, A., Leuzzi, V., Battini, R., Tosetti, M., Ferretti, G., Comparini, A., Casarano, M., Moretti, E., Alessandri, M. G., Bianchi, M. C. and Cioni, G. (2008) 'Treatment with L-arginine improves neuropsychological disorders in a child with creatine transporter de-fect.', Neurocase, 14(2), pp. 151–61. doi: 10.1080/13554790802060821.

Choe, C., Nabuurs, C., Stockebrand, M. C., Neu, A., Nunes, P., Morellini, F., Sauter, K., Schil-lemeit, S., Hermans-Borgmeyer, I., Marescau, B., Heerschap, A. and Isbrandt, D. (2013) 'l-arginine:glycine amidinotransferase deficiency protects from metabolic syndrome', Hu-man Molecular Genetics. Oxford University Press, 22(1), pp. 110–123. doi: 10.1093/hmg/dds407.

Christian, K. M., Song, H. and Ming, G. (2014) 'Functions and Dysfunctions of Adult Hippo-campal Neurogenesis', Annual Review of Neuroscience, 37(1), pp. 243–262. doi: 10.1146/annurev-neuro-071013-014134.

Ciregia, F., Bugliani, M., Ronci, M., Giusti, L., Boldrini, C., Mazzoni, M. R., Mossuto, S., Grano, F., Cnop, M., Marselli, L., Giannaccini, G., Urbani, A., Lucacchini, A. and Mar-chetti, P. (2017) 'Palmitate-induced lipotoxicity alters acetylation of multiple proteins in clonal β cells and human pancreatic islets.', Scientific reports, 7(1), p. 13445. doi: 10.1038/s41598-017-13908-w.

Ciregia, F., Giusti, L., Da Valle, Y., Donadio, E., Consensi, A., Giacomelli, C., Sernissi, F., Scarpellini, P., Maggi, F., Lucacchini, A. and Bazzichi, L. (2013) 'A multidisciplinary approach to study a couple of monozygotic twins discordant for the chronic fatigue syn-drome: a focus on potential salivary biomarkers', Journal of Translational Medicine, 11(1), p. 243. doi: 10.1186/1479-5876-11-243.

deGrauw, T. J., Cecil, K. M., Byars, A. W., Salomons, G. S., Ball, W. S. and Jakobs, C. (2003) 'The clinical syndrome of creatine transporter deficiency.', Molecular and cellular bio-chemistry, 244(1–2), pp. 45–8. Available at: http://www.ncbi.nlm.nih.gov/pub-med/12701808.

Depino, A. M. (2013) 'Peripheral and central inflammation in autism spectrum disorders', Mo-lecular and Cellular Neuroscience, 53, pp. 69–76. doi: 10.1016/j.mcn.2012.10.003.

Diaz-Beltran, L., Esteban, F. J. and Wall, D. P. (2016) 'A common molecular signature in ASD gene expression: following Root 66 to autism', Translational Psychiatry. Nature Publish-ing Group, 6(1), pp. e705–e705. doi: 10.1038/tp.2015.112.

Dodd, J. R., Birch, N. P., Waldvogel, H. J. and Christie, D. L. (2010) 'Functional and immuno-cytochemical characterization of the creatine transporter in rat hippocampal neurons.', Journal of neurochemistry, 115(3), pp. 684–93. doi: 10.1111/j.1471-4159.2010.06957.x.

Dunlop, R. A., Brunk, U. T. and Rodgers, K. J. (2009) 'Oxidized proteins: Mechanisms of removal and consequences of accumulation', IUBMB Life, pp. 522–527. doi: 10.1002/iub.189.

Ebadi, M. and Klangkalya, B. (1979) 'On the mechanism of pyridoxal phosphate-related convulsions as implicated in enhanced transport of GABA.', Neuropharmacology, 18(3), pp. 301–7. Available at: http://www.ncbi.nlm.nih.gov/pubmed/440539.

Edvardson, S., Korman, S. H., Livne, A., Shaag, A., Saada, A., Nalbandian, R., Allouche-Arnon, H., Gomori, J. M. and Katz-Brull, R. (2010) 'l-arginine:glycine amidinotransferase (AGAT) deficiency: Clinical presentation and response to treatment in two patients with a novel mutation', Molecular Genetics and Metabolism, 101(2–3), pp. 228–232. doi: 10.1016/j.ymgme.2010.06.021.

Enrico, A., Patrizia, G., Luisa, P., Alessandro, P., Gianluigi, L., Carlo, G. and Maurizio, B. (2013) 'Electrophysiology and biochemical analysis of cyclocreatine uptake and effect in hippocampal slices', Journal of Integrative Neuroscience, 12(02), pp. 285–297. doi: 10.1142/S0219635213500155.

Etherton, M. R., Blaiss, C. A., Powell, C. M. and Sudhof, T. C. (2009) 'Mouse neurexin-1 deletion causes correlated electrophysiological and behavioral changes consistent with cognitive impairments', Proceedings of the National Academy of Sciences, 106(42), pp. 17998–18003. doi: 10.1073/pnas.0910297106.

Evangeliou, A., Vasilaki, K., Karagianni, P. and Nikolaidis, N. (2009) 'Clinical applications of creatine supplementation on paediatrics.', Current pharmaceutical biotechnology, 10(7), pp. 683–90. Available at: http://www.ncbi.nlm.nih.gov/pubmed/19751179.

Fons, C., Arias, A., Sempere, A., Póo, P., Pineda, M., Mas, A., López-Sala, A., Garcia-Villoria, J., Vilaseca, M. A., Ozaez, L., Lluch, M., Artuch, R., Campistol, J. and Ribes, A. (2010) 'Response to creatine analogs in fibroblasts and patients with creatine transporter deficiency', Molecular Genetics and Metabolism, 99(3), pp. 296–299. doi: 10.1016/j.ymgme.2009.10.186.

Franceschi, C., Bonafè, M., Valensin, S., Olivieri, F., De Luca, M., Ottaviani, E. and De Benedictis, G. (2006) 'Inflamm-aging: An Evolutionary Perspective on Immunosenescence', Annals of the New York Academy of Sciences. Wiley/Blackwell (10.1111), 908(1), pp. 244–254. doi: 10.1111/j.1749-6632.2000.tb06651.x.

Fuccillo, M. V. (2016) 'Striatal Circuits as a Common Node for Autism Pathophysiology', Frontiers in Neuroscience, 10, p. 27. doi: 10.3389/fnins.2016.00027.

García-Delgado, M., Peral, M. J., Cano, M., Calonge, M. L. and Ilundáin, A. A. (2001) 'Creatine transport in brush-border membrane vesicles isolated from rat kidney cortex.', Journal of the American Society of Nephrology : JASN, 12(9), pp. 1819–25. Available at: http://www.ncbi.nlm.nih.gov/pubmed/11518774 (Accessed: 16 September 2018).

Di Giovanni, S. and Rathore, K. (2012) 'p53-dependent pathways in neurite outgrowth and axonal regeneration', Cell and Tissue Research, 349(1), pp. 87–95. doi: 10.1007/s00441-011-1292-5.

Giusti, S. A., Vercelli, C. A., Vogl, A. M., Kolarz, A. W., Pino, N. S., Deussing, J. M. and Refojo, D. (2014) 'Behavioral phenotyping of Nestin-Cre mice: Implications for genetic mouse models of psychiatric disorders', Journal of Psychiatric Research, 55, pp. 87–95. doi: 10.1016/j.jpsychires.2014.04.002.

Gori, Z., De Tata, V., Pollera, M. and Bergamini, E. (1988) 'Mitochondrial myopathy in rats fed with a diet containing beta-guanidine propionic acid, an inhibitor of creatine entry in muscle cells.', British journal of experimental pathology. Wiley-Blackwell, 69(5), pp. 639–50. Available at: http://www.ncbi.nlm.nih.gov/pubmed/3196657.

Gospe, S. M., Olin, K. L. and Keen, C. L. (1994) 'Reduced GABA synthesis in pyridoxine-dependent seizures.', Lancet (London, England), 343(8906), pp. 1133–4. Available at: http://www.ncbi.nlm.nih.gov/pubmed/7910233.

Grissom, N. M., McKee, S. E., Schoch, H., Bowman, N., Havekes, R., O'Brien, W. T., Mahrt, E., Siegel, S., Commons, K., Portfors, C., Nickl-Jockschat, T., Reyes, T. M. and Abel, T.

(2018) 'Male-specific deficits in natural reward learning in a mouse model of neurodevelopmental disorders', Molecular Psychiatry, 23(3), pp. 544–555. doi: 10.1038/mp.2017.184.

Guimbal, C. and Kilimann, M. W. (1993) 'A Na(+)-dependent creatine transporter in rabbit brain, muscle, heart, and kidney. cDNA cloning and functional expression.', The Journal of biological chemistry, 268(12), pp. 8418–21. Available at: http://www.ncbi.nlm.nih.gov/pubmed/8473283.

Haffernan, C. (2015) Creatine: a short history.

Hathaway, S. C., Friez, M., Limbo, K., Parker, C., Salomons, G. S., Vockley, J., Wood, T. and Abdul-Rahman, O. A. (2010) 'X-Linked Creatine Transporter Deficiency Presenting as a Mitochondrial Disorder', Journal of Child Neurology, 25(8), pp. 1009–1012. doi: 10.1177/0883073809352109.

Head, E., Lott, I. T., Wilcock, D. M. and Lemere, C. A. (2016) 'Aging in Down Syndrome and the Development of Alzheimer's Disease Neuropathology.', Current Alzheimer research, 13(1), pp. 18–29. Available at: http://www.ncbi.nlm.nih.gov/pubmed/26651341.

Hefendehl, J. K., Neher, J. J., Sühs, R. B., Kohsaka, S., Skodras, A. and Jucker, M. (2014) 'Homeostatic and injury-induced microglia behavior in the aging brain', Aging Cell. Wiley/Blackwell (10.1111), 13(1), pp. 60–69. doi: 10.1111/acel.12149.

Hoffmann, H. and Schiene-Fischer, C. (2014) 'Functional aspects of extracellular cyclophilins', Biological Chemistry, 395(7–8), pp. 721–35. doi: 10.1515/hsz-2014-0125.

Höhn, A. and Grune, T. (2013) 'Lipofuscin: formation, effects and role of macroautophagy.', Redox biology. Elsevier, 1(1), pp. 140–4. doi: 10.1016/j.redox.2013.01.006.

Ippolito, D. M. and Eroglu, C. (2010) 'Quantifying Synapses: an Immunocytochemistry-based Assay to Quantify Synapse Number', Journal of Visualized Experiments, (45). doi: 10.3791/2270.

Ishioka, N., Sato, J., Nakamura, J., Ohkubo, T., Takeda, A. and Kurioka, S. (1995) 'In vivo modification of GABAA receptor with a high dose of pyridoxal phosphate induces tonic-clonic convulsion in immature mice.', Neurochemistry international, 26(4), pp. 369–73. Available at: http://www.ncbi.nlm.nih.gov/pubmed/7633329.

Item, C. B., Stöckler-Ipsiroglu, S., Stromberger, C., Mühl, A., Alessandrì, M. G., Bianchi, M. C., Tosetti, M., Fornai, F. and Cioni, G. (2001) 'Arginine:Glycine Amidinotransferase Deficiency: The Third Inborn Error of Creatine Metabolism in Humans', The American Journal of Human Genetics, 69(5), pp. 1127–1133. doi: 10.1086/323765.

Iyer, G. S., Krahe, R., Goodwin, L. A., Doggett, N. A., Siciliano, M. J., Funanage, V. L. and Proujansky, R. (1996) 'Identification of a testis-expressed creatine transporter gene at 16p11.2 and confirmation of the X-linked locus to Xq28.', Genomics, 34(1), pp. 143–6. doi: 10.1006/geno.1996.0254.

Joncquel-Chevalier Curt, M., Voicu, P. M., Fontaine, M., Dessein, A. F., Porchet, N., Mention-Mulliez, K., Dobbelaere, D., Soto-Ares, G., Cheillan, D. and Vamecq, J. (2015) 'Creatine biosynthesis and transport in health and disease', Biochimie, 119, pp. 146–165. doi: 10.1016/j.biochi.2015.10.022.

Kaidanovich-Beilin, O., Lipina, T., Vukobradovic, I., Roder, J. and Woodgett, J. R. (2011) 'Assessment of Social Interaction Behaviors', Journal of Visualized Experiments, (48). doi: 10.3791/2473.

Kalkman, H. O. (2012) 'Potential opposite roles of the extracellular signal-regulated kinase (ERK) pathway in autism spectrum and bipolar disorders', Neuroscience & Biobehavioral Reviews, 36(10), pp. 2206–2213. doi: 10.1016/j.neubiorev.2012.07.008.

van de Kamp, J. M., Jakobs, C., Gibson, K. M. and Salomons, G. S. (2013) 'New insights into creatine transporter deficiency: the importance of recycling creatine in the brain', Journal of Inherited Metabolic Disease, 36(1), pp. 155–156. doi: 10.1007/s10545-012-9537-3.

van de Kamp, J. M., Mancini, G. M. and Salomons, G. S. (2014) 'X-linked creatine transporter deficiency: clinical aspects and pathophysiology', Journal of Inherited Metabolic Disease, 37(5), pp. 715–733. doi: 10.1007/s10545-014-9713-8.

van de Kamp, J., Betsalel, O. T., Mercimek-Mahmutoglu, S., Abulhoul, L., Grünewald, S., Anselm, I., Azzouz, H., Bratkovic, D., de Brouwer, A., Hamel, B., Kleefstra, T., Yntema, H., Campistol, J., Vilaseca, M. A., Cheillan, D., D'Hooghe, M., Diogo, L., Garcia, P., Valongo, C., Fonseca, M., Frints, S., Wilcken, B., von der Haar, S., Meijers-Heijboer, H. E., Hofstede, F., Johnson, D., Kant, S. G., Lion-Francois, L., Pitelet, G., Longo, N., Maat-Kievit, J. A., Monteiro, J. P., Munnich, A., Muntau, A. C., Nassogne, M. C., Osaka, H., Ounap, K., Pinard, J. M., Quijano-Roy, S., Poggenburg, I., Poplawski, N., Abdul-Rahman, O., Ribes, A., Arias, A., Yaplito-Lee, J., Schulze, A., Schwartz, C. E., Schwenger, S., Soares, G., Sznajer, Y., Valayannopoulos, V., Van Esch, H., Waltz, S., Wamelink, M. M. C., Pouwels, P. J. W., Errami, A., van der Knaap, M. S., Jakobs, C., Mancini, G. M. and Salomons, G. S. (2013) 'Phenotype and genotype in 101 males with X-linked creatine transporter deficiency', Journal of Medical Genetics, 50(7), pp. 463–472. doi: 10.1136/jmedgenet-2013-101658.

van de Kamp, J., Errami, A., Howidi, M., Anselm, I., Winter, S., Phalin-Roque, J., Osaka, H., van Dooren, S. J. M., Mancini, G. M., Steinberg, S. J. and Salomons, G. S. (2015) 'Genotype-phenotype correlation of contiguous gene deletions of SLC6A8, BCAP31 and ABCD1', Clinical Genetics, 87(2), pp. 141–147. doi: 10.1111/cge.12355.

van de Kamp, J., Mancini, G., Pouwels, P., Betsalel, O., van Dooren, S., de Koning, I., Steenweg, M., Jakobs, C., van der Knaap, M. and Salomons, G. (2011) 'Clinical features and X-inactivation in females heterozygous for creatine transporter defect', Clinical Genetics. Wiley/Blackwell (10.1111), 79(3), pp. 264–272. doi: 10.1111/j.1399-0004.2010.01460.x.

van de Kap, J. M., Pouwels, P. J. W., Aarsen, F. K., ten Hoopen, L. W., Knol, D. L., de Klerk, J. B., de Coo, I. F., Huijmans, J. G. M., Jakobs, C., van der Knaap, M. S., Salomons, G. S. and Mancini, G. M. S. (2012) 'Long-term follow-up and treatment in nine boys with X-linked creatine transporter defect.', Journal of inherited metabolic disease. Springer, 35(1), pp. 141–9. doi: 10.1007/s10545-011-9345-1.

Kempermann, G. (2015) 'Activity Dependency and Aging in the Regulation of Adult Neurogenesis', Cold Spring Harbor Perspectives in Biology, 7(11), p. a018929. doi: 10.1101/cshperspect.a018929.

Kopra, O., Vesa, J., von Schantz, C., Manninen, T., Minye, H., Fabritius, A.-L., Rapola, J., Diggelen, O. P. van, Saarela, J., Jalanko, A. and Peltonen, L. (2004) 'A mouse model for Finnish variant late infantile neuronal ceroid lipofuscinosis, CLN5, reveals neuropathology associated with early aging', Human Molecular Genetics, 13(23), pp. 2893–2906. doi: 10.1093/hmg/ddh312.

Kristensen, A. S., Andersen, J., Jørgensen, T. N., Sørensen, L., Eriksen, J., Loland, C. J., Strømgaard, K. and Gether, U. (2011) 'SLC6 neurotransmitter transporters: structure, function, and regulation.', Pharmacological reviews, 63(3), pp. 585–640. doi: 10.1124/pr.108.000869.

Kuiper, J. W., Oerlemans, F. T., Fransen, J. A. and Wieringa, B. (2008) 'Creatine kinase B deficient neurons exhibit an increased fraction of motile mitochondria', BMC Neuroscience, 9(1), p. 73. doi: 10.1186/1471-2202-9-73.

Kurosawa, Y., DeGrauw, T. J., Lindquist, D. M., Blanco, V. M., Pyne-Geithman, G. J., Daikoku, T., Chambers, J. B., Benoit, S. C. and Clark, J. F. (2012) 'Cyclocreatine treatment improves cognition in mice with creatine transporter deficiency', Journal of Clinical Investigation, 122(8), pp. 2837–2846. doi: 10.1172/JCI59373.

Lahiri, D. K., Sokol, D. K., Erickson, C., Ray, B., Ho, C. Y. and Maloney, B. (2013) 'Autism as early neurodevelopmental disorder: evidence for an sAPPα-mediated anabolic pathway', Frontiers in Cellular Neuroscience, 7. doi: 10.3389/fncel.2013.00094.

Lawler, J. M., Barnes, W. S., Wu, G., Song, W. and Demaree, S. (2002) 'Direct Antioxidant Properties of Creatine', Biochemical and Biophysical Research Communications, 290(1), pp. 47–52. doi: 10.1006/bbrc.2001.6164.

Lee, S. W., Clemenson, G. D. and Gage, F. H. (2012) 'New neurons in an aged brain', Behavioural Brain Research, 227(2), pp. 497–507. doi: 10.1016/j.bbr.2011.10.009.

Leuzzi, V., Alessandrì, M. G., Casarano, M., Battini, R. and Cioni, G. (2008) 'Arginine and glycine stimulate creatine synthesis in creatine transporter 1-deficient lymphoblasts', Analytical Biochemistry, 375(1), pp. 153–155. doi: 10.1016/j.ab.2008.01.018.

Leuzzi, V., Bianchi, M. C., Tosetti, M., Carducci, C., Cerquiglini, C. A., Cioni, G. and Antonozzi, I. (2000) 'Brain creatine depletion: guanidinoacetate methyltransferase deficiency (improving with creatine supplementation).', Neurology, 55(9), pp. 1407–9. Available at: http://www.ncbi.nlm.nih.gov/pubmed/11087795.

Leuzzi, V., Mastrangelo, M., Battini, R. and Cioni, G. (2013) 'Inborn errors of creatine metabolism and epilepsy', Epilepsia, 54(2), pp. 217–227. doi: 10.1111/epi.12020.

Levillain, O., Marescau, B. and Deyn, P. P. de (1995) 'Guanidino compound metabolism in rats subjected to 20% to 90% nephrectomy', Kidney International. Elsevier, 47(2), pp. 464–472. doi: 10.1038/KI.1995.59.

Li, H., Thali, R. F., Smolak, C., Gong, F., Alzamora, R., Wallimann, T., Scholz, R., Pastor-Soler, N. M., Neumann, D. and Hallows, K. R. (2010) 'Regulation of the creatine transporter by AMP-activated protein kinase in kidney epithelial cells.', American journal of physiology. Renal physiology. American Physiological Society, 299(1), pp. F167-77. doi: 10.1152/ajprenal.00162.2010.

Lipton, J. O. and Sahin, M. (2014) 'The Neurology of mTOR', Neuron. Elsevier Inc., 84(2), pp. 275–291. doi: 10.1016/j.neuron.2014.09.034.

Loike, J. D., Zalutsky, D. L., Kaback, E., Miranda, A. F. and Silverstein, S. C. (1988) 'Extracellular creatine regulates creatine transport in rat and human muscle cells.', Proceedings of the National Academy of Sciences of the United States of America, 85(3), pp. 807–11. Available at: http://www.ncbi.nlm.nih.gov/pubmed/3422462.

Lonetti, G., Angelucci, A., Morando, L., Boggio, E. M., Giustetto, M. and Pizzorusso, T. (2010) 'Early Environmental Enrichment Moderates the Behavioral and Synaptic Phenotype of MeCP2 Null Mice', Biological Psychiatry, 67(7), pp. 657–665. doi: 10.1016/j.biopsych.2009.12.022.

Lunardi, G., Parodi, A., Perasso, L., Pohvozcheva, A. V., Scarrone, S., Adriano, E., Florio, T., Gandolfo, C., Cupello, A., Burov, S. V. and Balestrino, M. (2006) 'The creatine transporter mediates the uptake of creatine by brain tissue, but not the uptake of two creatine-derived compounds', Neuroscience, 142(4), pp. 991–997. doi: 10.1016/j.neuroscience.2006.06.058.

Maccarinelli, F., Pagani, A., Cozzi, A., Codazzi, F., Di Giacomo, G., Capoccia, S., Rapino, S., Finazzi, D., Politi, L. S., Cirulli, F., Giorgio, M., Cremona, O., Grohovaz, F. and Levi, S. (2015) 'A novel neuroferritinopathy mouse model (FTL 498InsTC) shows progressive brain iron dysregulation, morphological signs of early neurodegeneration and motor coordination deficits', Neurobiology of Disease, 81, pp. 119–133. doi: 10.1016/j.nbd.2014.10.023.

Matt, S. M. and Johnson, R. W. (2016) 'Neuro-immune dysfunction during brain aging: new insights in microglial cell regulation', Current Opinion in Pharmacology, 26, pp. 96–101. doi: 10.1016/j.coph.2015.10.009.

Matthews, R. T., Ferrante, R. J., Klivenyi, P., Yang, L., Klein, A. M., Mueller, G., Kaddurah-Daouk, R. and Beal, M. F. (1999) 'Creatine and Cyclocreatine Attenuate MPTP Neurotoxicity', Experimental Neurology, 157(1), pp. 142–149. doi: 10.1006/exnr.1999.7049.

McFarlane, H. G., Kusek, G. K., Yang, M., Phoenix, J. L., Bolivar, V. J. and Crawley, J. N. (2008) 'Autism-like behavioral phenotypes in BTBR T+tf/J mice', Genes, Brain and Behavior, 7(2), pp. 152–163. doi: 10.1111/j.1601-183X.2007.00330.x.

McQuail, J. A., Frazier, C. J. and Bizon, J. L. (2015) 'Molecular aspects of age-related cognitive decline: the role of GABA signaling', Trends in Molecular Medicine, 21(7), pp. 450–460. doi: 10.1016/j.molmed.2015.05.002.

Mercimek-Mahmutoglu, S., Connolly, M. B., Poskitt, K. J., Horvath, G. A., Lowry, N., Salomons, G. S., Casey, B., Sinclair, G., Davis, C., Jakobs, C. and Stockler-Ipsiroglu, S. (2010) 'Treatment of intractable epilepsy in a female with SLC6A8 deficiency', Molecular Genetics and Metabolism, 101(4), pp. 409–412. doi: 10.1016/j.ymgme.2010.08.016.

Mercimek-Mahmutoglu, S., Stoeckler-Ipsiroglu, S., Adami, A., Appleton, R., Araujo, H. C., Duran, M., Ensenauer, R., Fernandez-Alvarez, E., Garcia, P., Grolik, C., Item, C. B., Leuzzi, V., Marquardt, I., Muhl, A., Saelke-Kellermann, R. A., Salomons, G. S., Schulze, A., Surtees, R., van der Knaap, M. S., Vasconcelos, R., Verhoeven, N. M., Vilarinho, L., Wilichowski, E. and Jakobs, C. (2006) 'GAMT deficiency: Features, treatment, and outcome in an inborn error of creatine synthesis', Neurology, 67(3), pp. 480–484. doi: 10.1212/01.wnl.0000234852.43688.bf.

Moy, S. S., Nadler, J. J., Perez, A., Barbaro, R. P., Johns, J. M., Magnuson, T. R., Piven, J. and Crawley, J. N. (2004) 'Sociability and preference for social novelty in five inbred strains: an approach to assess autistic-like behavior in mice', Genes, Brain and Behavior, 3(5), pp. 287–302. doi: 10.1111/j.1601-1848.2004.00076.x.

Nabuurs, C. I., Choe, C. U., Veltien, A., Kan, H. E., van Loon, L. J. C., Rodenburg, R. J. T., Matschke, J., Wieringa, B., Kemp, G. J., Isbrandt, D. and Heerschap, A. (2013) 'Disturbed energy metabolism and muscular dystrophy caused by pure creatine deficiency are reversible by creatine intake', The Journal of Physiology, 591(2), pp. 571–592. doi: 10.1113/jphysiol.2012.241760.

Nash, S. R., Giros, B., Kingsmore, S. F., Rochelle, J. M., Suter, S. T., Gregor, P., Seldin, M. F. and Caron, M. G. (1994) 'Cloning, pharmacological characterization, and genomic localization of the human creatine transporter.', Receptors & channels, 2(2), pp. 165–74. Available at: http://www.ncbi.nlm.nih.gov/pubmed/7953292.

Ndika, J. D. T., Johnston, K., Barkovich, J. A., Wirt, M. D., O'Neill, P., Betsalel, O. T., Jakobs, C. and Salomons, G. S. (2012) 'Developmental progress and creatine restoration upon long-term creatine supplementation of a patient with arginine:glycine amidinotransferase deficiency', Molecular Genetics and Metabolism, 106(1), pp. 48–54. doi: 10.1016/j.ymgme.2012.01.017.

Nicolas, M. and Hassan, B. A. (2014) 'Amyloid precursor protein and neural development', Development, 141(13), pp. 2543–2548. doi: 10.1242/dev.108712.

Nigro, P., Pompilio, G. and Capogrossi, M. C. (2013) 'Cyclophilin A: a key player for human disease', Cell Death & Disease, 4(10), pp. e888–e888. doi: 10.1038/cddis.2013.410.

Nota, B., Ndika, J. D. T., van de Kamp, J. M., Kanhai, W. A., van Dooren, S. J. M., van de Wiel, M. A., Pals, G. and Salomons, G. S. (2014) 'RNA Sequencing of Creatine Transporter (SLC6A8) Deficient Fibroblasts Reveals Impairment of the Extracellular Matrix', Human Mutation, 35(9), pp. 1128–1135. doi: 10.1002/humu.22609.

Nouioua, S., Cheillan, D., Zaouidi, S., Salomons, G. S., Amedjout, N., Kessaci, F., Boulahdour, N., Hamadouche, T. and Tazir, M. (2013) 'Creatine deficiency syndrome. A treatable myopathy due to arginine–glycine amidinotransferase (AGAT) deficiency', Neuromuscular Disorders, 23(8), pp. 670–674. doi: 10.1016/j.nmd.2013.04.011.

O'Gorman, E., Beutner, G., Dolder, M., Koretsky, A. P., Brdiczka, D. and Wallimann, T. (1997) 'The role of creatine kinase in inhibition of mitochondrial permeability transition', FEBS Letters. No longer published by Elsevier, 414(2), pp. 253–257. doi: 10.1016/S0014-5793(97)01045-4.

Papale, A., d'Isa, R., Menna, E., Cerovic, M., Solari, N., Hardingham, N., Cambiaghi, M., Cursi, M., Barbacid, M., Leocani, L., Fasano, S., Matteoli, M. and Brambilla, R. (2017) 'Severe Intellectual Disability and Enhanced Gamma-Aminobutyric Acidergic Synaptogenesis in a Novel Model of Rare RASopathies', Biological Psychiatry, 81(3), pp. 179–192. doi: 10.1016/j.biopsych.2016.06.016.

Peral, M. J., Vázquez-Carretero, M. D. and Ilundain, A. A. (2010) 'Na+/Cl−/creatine transporter activity and expression in rat brain synaptosomes', Neuroscience, 165(1), pp. 53–60. doi: 10.1016/j.neuroscience.2009.10.001.

Perasso, L., Adriano, E., Ruggeri, P., Burov, S. V., Gandolfo, C. and Balestrino, M. (2009) 'In vivo neuroprotection by a creatine-derived compound: Phosphocreatine–Mg-complex acetate', Brain Research, 1285, pp. 158–163. doi: 10.1016/j.brainres.2009.06.009.

Perasso, L., Cupello, A., Lunardi, G. L., Principato, C., Gandolfo, C. and Balestrino, M. (2003) 'Kinetics of creatine in blood and brain after intraperitoneal injection in the rat.', Brain research, 974(1–2), pp. 37–42. Available at: http://www.ncbi.nlm.nih.gov/pubmed/12742622.

Perna, M. K., Kokenge, A. N., Miles, K. N., Udobi, K. C., Clark, J. F., Pyne-Geithman, G. J., Khuchua, Z. and Skelton, M. R. (2016) 'Creatine transporter deficiency leads to increased whole body and cellular metabolism', Amino Acids. Springer Vienna. doi: 10.1007/s00726-016-2291-3.

Póo-Argüelles, P., Arias, A., Vilaseca, M. A., Ribes, A., Artuch, R., Sans-Fito, A., Moreno, A., Jakobs, C. and Salomons, G. (2006) 'X-Linked creatine transporter deficiency in two patients with severe mental retardation and autism', Journal of Inherited Metabolic Disease, 29(1), pp. 220–223. doi: 10.1007/s10545-006-0212-4.

Pucilowska, J., Vithayathil, J., Pagani, M., Kelly, C., Karlo, J. C., Robol, C., Morella, I., Gozzi, A., Brambilla, R. and Landreth, G. E. (2018) 'Pharmacological Inhibition of ERK Signaling Rescues Pathophysiology and Behavioral Phenotype Associated with 16p11.2 Chromosomal Deletion in Mice', The Journal of Neuroscience, 38(30), pp. 6640–6652. doi: 10.1523/JNEUROSCI.0515-17.2018.

Pucilowska, J., Vithayathil, J., Tavares, E. J., Kelly, C., Karlo, J. C. and Landreth, G. E. (2015) 'The 16p11.2 Deletion Mouse Model of Autism Exhibits Altered Cortical Progenitor Proliferation and Brain Cytoarchitecture Linked to the ERK MAPK Pathway', Journal of Neuroscience, 35(7), pp. 3190–3200. doi: 10.1523/JNEUROSCI.4864-13.2015.

Puusepp, H., Kall, K., Salomons, G. S., Talvik, I., Männamaa, M., Rein, R., Jakobs, C. and Õunap, K. (2010) 'The screening of SLC6A8 deficiency among Estonian families with X-linked mental retardation.', Journal of inherited metabolic disease, 33 Suppl 3, pp. S5-11. Available at: http://www.ncbi.nlm.nih.gov/pubmed/24137762.

Pyne-Geithman, G. J., deGrauw, T. J., Cecil, K. M., Chuck, G., Lyons, M. A., Ishida, Y. and Clark, J. F. (2004) 'Presence of normal creatine in the muscle of a patient with a mutation in the creatine transporter: a case study.', Molecular and cellular biochemistry, 262(1–2), pp. 35–9. Available at: http://www.ncbi.nlm.nih.gov/pubmed/15532707.

Rao, J. S., Kellom, M., Kim, H.-W., Rapoport, S. I. and Reese, E. A. (2012) 'Neuroinflammation and Synaptic Loss', Neurochemical Research, 37(5), pp. 903–910. doi: 10.1007/s11064-012-0708-2.

Ratto, G. M. and Pizzorusso, T. (2006) 'A Kinase with a Vision', in Brain Repair. Boston, MA: Springer US, pp. 122–132. doi: 10.1007/0-387-30128-3_7.

Ray, B., Long, J. M., Sokol, D. K. and Lahiri, D. K. (2011) 'Increased Secreted Amyloid Precursor Protein-α (sAPPα) in Severe Autism: Proposal of a Specific, Anabolic Pathway and Putative Biomarker', PLoS ONE. Edited by A. I. Bush, 6(6), p. e20405. doi: 10.1371/journal.pone.0020405.

Rothwell, P. E., Fuccillo, M. V., Maxeiner, S., Hayton, S. J., Gokce, O., Lim, B. K., Fowler, S. C., Malenka, R. C. and Südhof, T. C. (2014) 'Autism-Associated Neuroligin-3 Mutations Commonly Impair Striatal Circuits to Boost Repetitive Behaviors', Cell, 158(1), pp. 198–212. doi: 10.1016/j.cell.2014.04.045.

Russell, A. P., Ghobrial, L., Wright, C. R., Lamon, S., Brown, E. L., Kon, M., Skelton, M. R. and Snow, R. J. (2014) 'Creatine transporter (SLC6A8) knockout mice display an increased capacity for in vitro creatine biosynthesis in skeletal muscle', Frontiers in Physiology. Frontiers, 5, p. 314. doi: 10.3389/fphys.2014.00314.

Ryan, S. M. and Nolan, Y. M. (2016) 'Neuroinflammation negatively affects adult hippocampal neurogenesis and cognition: can exercise compensate?', Neuroscience & Biobehavioral Reviews, 61, pp. 121–131. doi: 10.1016/j.neubiorev.2015.12.004.

Salomons, G. S., van Dooren, S. J. M., Verhoeven, N. M., Cecil, K. M., Ball, W. S., Degrauw, T. J. and Jakobs, C. (2001) 'X-Linked Creatine-Transporter Gene (SLC6A8) Defect: A New Creatine-Deficiency Syndrome', The American Journal of Human Genetics, 68(6), pp. 1497–1500. doi: 10.1086/320595.

di Salvo, M. L., Mastrangelo, M., Nogués, I., Tolve, M., Paiardini, A., Carducci, C., Mei, D., Montomoli, M., Tramonti, A., Guerrini, R., Contestabile, R. and Leuzzi, V. (2017) 'Pyridoxine-5'-phosphate oxidase (Pnpo) deficiency: Clinical and biochemical alterations associated with the C.347g>A (P.·Arg116gln) mutation.', Molecular genetics and metabolism. Elsevier, 122(1–2), pp. 135–142. doi: 10.1016/j.ymgme.2017.08.003.

Saunders, A., Macosko, E., Wysoker, A., Goldman, M., Krienen, F., Bien, E., Baum, M., Wang, S., Goeva, A., Nemesh, J., Kamitaki, N., Brumbaugh, S., Kulp, D. and McCarroll, S. A. (2018) 'A Single-Cell Atlas of Cell Types, States, and Other Transcriptional Patterns from Nine Regions of the Adult Mouse Brain', bioRxiv. Cold Spring Harbor Laboratory, p. 299081. doi: 10.1101/299081.

Schiaffino, M. C., Bellini, C., Costabello, L., Caruso, U., Jakobs, C., Salomons, G. S. and Bonioli, E. (2005) 'X-linked creatine transporter deficiency', Neurogenetics, 6(3), pp. 165–168. doi: 10.1007/s10048-005-0002-4.

Sestili, P., Martinelli, C., Colombo, E., Barbieri, E., Potenza, L., Sartini, S. and Fimognari, C. (2011) 'Creatine as an antioxidant', Amino Acids, 40(5), pp. 1385–1396. doi: 10.1007/s00726-011-0875-5.

Shaw, A. E. and Bamburg, J. R. (2017) 'Peptide regulation of cofilin activity in the CNS: A novel therapeutic approach for treatment of multiple neurological disorders', Pharmacology & Therapeutics, 175, pp. 17–27. doi: 10.1016/j.pharmthera.2017.02.031.

Sherwin, E., Dinan, T. G. and Cryan, J. F. (2018) 'Recent developments in understanding the role of the gut microbiota in brain health and disease', Annals of the New York Academy of Sciences, 1420(1), pp. 5–25. doi: 10.1111/nyas.13416.

Shetty, A. K. and Turner, D. A. (1998) 'Hippocampal interneurons expressing glutamic acid decarboxylase and calcium-binding proteins decrease with aging in Fischer 344 rats.', The Journal of comparative neurology, 394(2), pp. 252–69. Available at: http://www.ncbi.nlm.nih.gov/pubmed/9552130.

Shi, L., Argenta, A. E., Winseck, A. K. and Brunso-Bechtold, J. K. (2004) 'Stereological quantification of GAD-67-immunoreactive neurons and boutons in the hippocampus of middle-aged and old Fischer 344 × Brown Norway rats', Journal of Comparative Neurology, 478(3), pp. 282–291. doi: 10.1002/cne.20303.

Sierra, A., Beccari, S., Diaz-Aparicio, I., Encinas, J. M., Comeau, S. and Tremblay, M.-È. (2014) 'Surveillance, Phagocytosis, and Inflammation: How Never-Resting Microglia Influence Adult Hippocampal Neurogenesis', Neural Plasticity, 2014, pp. 1–15. doi: 10.1155/2014/610343.

Silingardi, D., Angelucci, A., De Pasquale, R., Borsotti, M., Squitieri, G., Brambilla, R., Putignano, E., Pizzorusso, T. and Berardi, N. (2011) 'ERK pathway activation bidirectionally affects visual recognition memory and synaptic plasticity in the perirhinal cortex.', Frontiers in behavioral neuroscience. Frontiers Media SA, 5, p. 84. doi: 10.3389/fnbeh.2011.00084.

Skelton, M. R., Schaefer, T. L., Graham, D. L., deGrauw, T. J., Clark, J. F., Williams, M. T. and Vorhees, C. V. (2011) 'Creatine Transporter (CrT; Slc6a8) Knockout Mice as a Model of Human CrT Deficiency', PLoS ONE. Edited by E. M. C. Skoulakis. Public Library of Science, 6(1), p. e16187. doi: 10.1371/journal.pone.0016187.

Stöckler, S., Hanefeld, F. and Frahm, J. (1996) 'Creatine replacement therapy in guanidinoacetate methyltransferase deficiency, a novel inborn error of metabolism.', Lancet (London, England), 348(9030), pp. 789–90. Available at: http://www.ncbi.nlm.nih.gov/pubmed/8813986.

Stöckler, S., Holzbach, U., Hanefeld, F., Marquardt, I., Helms, G., Requart, M., Hänicke, W. and Frahm, J. (1994) 'Creatine deficiency in the brain: a new, treatable inborn error of metabolism.', Pediatric research, 36(3), pp. 409–413. doi: 10.1203/00006450-199409000-00023.

Sullivan, P. G., Geiger, J. D., Mattson, M. P. and Scheff, S. W. (2000) 'Dietary supplement creatine protects against traumatic brain injury.', Annals of neurology, 48(5), pp. 723–9. Available at: http://www.ncbi.nlm.nih.gov/pubmed/11079535.

Tachikawa, M., Fukaya, M., Terasaki, T., Ohtsuki, S. and Watanabe, M. (2004) 'Distinct cellular expressions of creatine synthetic enzyme GAMT and creatine kinases uCK-Mi and CK-B suggest a novel neuron-glial relationship for brain energy homeostasis', European Journal of Neuroscience, 20(1), pp. 144–160. doi: 10.1111/j.1460-9568.2004.03478.x.

Terman, A. and Brunk, U. T. (2006) 'Oxidative Stress, Accumulation of Biological "Garbage", and Aging', Antioxidants & Redox Signaling, 8(1–2), pp. 197–204. doi: 10.1089/ars.2006.8.197.

Thomas, G. M. and Huganir, R. L. (2004) 'MAPK cascade signalling and synaptic plasticity', Nature Reviews Neuroscience, 5(3), pp. 173–183. doi: 10.1038/nrn1346.

Torremans, A., Marescau, B., Possemiers, I., Van Dam, D., D'Hooge, R., Isbrandt, D. and De Deyn, P. P. (2005) 'Biochemical and behavioural phenotyping of a mouse model for GAMT deficiency', Journal of the Neurological Sciences, 231(1–2), pp. 49–55. doi: 10.1016/j.jns.2004.12.014.

Tronche, F., Kellendonk, C., Kretz, O., Gass, P., Anlag, K., Orban, P. C., Bock, R., Klein, R. and Schütz, G. (1999) 'Disruption of the glucocorticoid receptor gene in the nervous system results in reduced anxiety', Nature Genetics, 23(1), pp. 99–103. doi: 10.1038/12703.

Udobi, K. C., Kokenge, A. N., Hautman, E. R., Ullio, G., Coene, J., Williams, M. T., Vorhees, C. V., Mabondzo, A. and Skelton, M. R. (2018) 'Cognitive deficits and increases in creatine precursors in a brain-specific knockout of the creatine transporter gene Slc6a8', Genes, Brain and Behavior, 17(6), p. e12461. doi: 10.1111/gbb.12461.

Vanderklish, P. W. and Edelman, G. M. (2002) 'Dendritic spines elongate after stimulation of group 1 metabotropic glutamate receptors in cultured hippocampal neurons.', Proceedings of the National Academy of Sciences of the United States of America. National Academy of Sciences, 99(3), pp. 1639–44. doi: 10.1073/pnas.032681099.

Vela, J., Gutierrez, A., Vitorica, J. and Ruano, D. (2003) 'Rat hippocampal GABAergic molecular markers are differentially affected by ageing.', Journal of neurochemistry, 85(2), pp. 368–77. Available at: http://www.ncbi.nlm.nih.gov/pubmed/12675913.

Walker, J. B. (1979) 'Creatine: biosynthesis, regulation, and function.', Advances in enzymology and related areas of molecular biology, 50, pp. 177–242. Available at: http://www.ncbi.nlm.nih.gov/pubmed/386719.

Wang, H.-S. and Kuo, M.-F. (2007) 'Vitamin B6 related epilepsy during childhood.', Chang Gung medical journal, 30(5), pp. 396–401. Available at: http://www.ncbi.nlm.nih.gov/pubmed/18062169.

Woo, J. A., Zhao, X., Khan, H., Penn, C., Wang, X., Joly-Amado, A., Weeber, E., Morgan, D. and Kang, D. E. (2015) 'Slingshot-Cofilin activation mediates mitochondrial and synaptic dysfunction via Aβ ligation to β1-integrin conformers', Cell Death & Differentiation, 22(6), pp. 921–934. doi: 10.1038/cdd.2015.5.

Wyss, M. and Kaddurah-Daouk, R. (2000) 'Creatine and Creatinine Metabolism', Physiological reviews, 80(3), pp. 1107–1213. doi: 10.1016/S1286-0115(06)74505-2.

Xu, D., Zhu, J., Jeong, S., Li, D., Hua, X., Huang, L., Zhang, J., Luo, Y. and Xia, Q. (2018) 'Rictor Deficiency Aggravates Hepatic Ischemia/Reperfusion Injury in Mice by Suppressing Autophagy and Regulating MAPK Signaling', Cellular Physiology and Biochemistry, 45(6), pp. 2199–2212. doi: 10.1159/000488165.

Yizhar, O., Fenno, L. E., Prigge, M., Schneider, F., Davidson, T. J., O'Shea, D. J., Sohal, V. S., Goshen, I., Finkelstein, J., Paz, J. T., Stehfest, K., Fudim, R., Ramakrishnan, C., Huguenard, J. R., Hegemann, P. and Deisseroth, K. (2011) 'Neocortical excitation/inhibition balance in information processing and social dysfunction', Nature. Nature Publishing Group, 477(7363), pp. 171–178. doi: 10.1038/nature10360.

Zervou, S., Whittington, H. J., Russell, A. J. and Lygate, C. A. (2016) 'Augmentation of Creatine in the Heart.', Mini reviews in medicinal chemistry, 16(1), pp. 19–28. Available at: http://www.ncbi.nlm.nih.gov/pubmed/26202199.

Zhu, X., Lee, H., Raina, A. K., Perry, G. and Smith, M. A. (2002) 'The Role of Mitogen-Activated Protein Kinase Pathways in Alzheimer's Disease', Neurosignals, 11(5), pp. 270–281. doi: 10.1159/000067426.

Ringraziamenti

Ringrazio il Prof. Tommaso Pizzorusso, la Dr.ssa Laura Baroncelli, il Prof. Giovanni Cioni, la Dr.ssa Elena Putignano, la Dr.ssa Laura Giusti, il Prof. Antonio Lucacchini, la Prof.ssa Maria Concetta Morrone, e tutti i colleghi e amici dell'Istituto di Neuroscienze del CNR di Pisa che mi hanno accompagnato in questa bellissima esperienza.

PREMIO TESI DI DOTTORATO

ANNO 2007

Bracardi M., *La Materia e lo Spirito. Mario Ridolfi nel paesaggio umbro*

Coppi E., *Purines as Transmitter Molecules. Electrophysiological Studies on Purinergic Signalling in Different Cell Systems*

Mannini M., *Molecular Magnetic Materials on Solid Surfaces*

Natali I., *The Ur-Portrait.* Stephen Hero *ed il processo di creazione artistica in* A Portrait of the Artist as a Young Man

Petretto L., *Imprenditore ed Università nello start-up di impresa. Ruoli e relazioni critiche*

ANNO 2008

Bemporad F., *Folding and Aggregation Studies in the Acylphosphatase-Like Family*

Buono A., *Esercito, istituzioni, territorio. Alloggiamenti militari e «case Herme» nello Stato di Milano (secoli XVI e XVII)*

Castenasi S., *La finanza di progetto tra interesse pubblico e interessi privati*

Colica G., *Use of Microorganisms in the Removal of Pollutants from the Wastewater*

Gabbiani C., *Proteins as Possible Targets for Antitumor Metal Complexes: Biophysical Studies of their Interactions*

ANNO 2009

Decorosi F., *Studio di ceppi batterici per il biorisanamento di suoli contaminati da Cr(VI)*

Di Carlo P., *I Kalasha del Hindu Kush: ricerche linguistiche e antropologiche*

Di Patti F., *Finite-Size Effects in Stochastic Models of Population Dynamics: Applications to Biomedicine and Biology*

Inzitari M., *Determinants of Mobility Disability in Older Adults: Evidence from Population-Based Epidemiologic Studies*

Macrì F., *Verso un nuovo diritto penale sessuale. Diritto vivente, diritto comparato e prospettive di riforma della disciplina dei reati sessuali in Italia*

Pace R., *Identità e diritti delle donne. Per una cittadinanza di genere nella formazione*

Vignolini S., *Sub-Wavelength Probing and Modification of Complex Photonic Structures*

ANNO 2010

Fedi M., *«Tuo lumine». L'accademia dei Risvegliati e lo spettacolo a Pistoia tra Sei e Settecento*

Fondi M., *Bioinformatics of genome evolution: from ancestral to modern metabolism. Phylogenomics and comparative genomics to understand microbial evolution*

Marino E., *An Integrated Nonlinear Wind-Waves Model for Offshore Wind Turbines*

Orsi V., *Crisi e Rigenerazione nella valle dell'Alto Khabur (Siria). La produzione ceramica nel passaggio dal Bronzo Antico al Bronzo Medio*

Polito C., *Molecular imaging in Parkinson's disease*

Romano R., *Smart Skin Envelope. Integrazione architettonica di tecnologie dinamiche e innovative per il risparmio energetico*

ANNO 2011

Acciaioli S., *Il* trompe-l'œil *letterario, ovvero il sorriso ironico nell'opera di Wilhelm Hauff*

Bernacchioni C., *Sfingolipidi bioattivi e loro ruolo nell'azione biologica di fattori di crescita e citochine*

Fabbri N., *Bragg spectroscopy of quantum gases: Exploring physics in one dimension*

Gordillo Hervás R., *La construcción religiosa de la Hélade imperial: El Panhelenion*

Mugelli C., *Indipendenza e professionalità del giudice in Cina*

Pollastri S., *Il ruolo di TAF12B e UVR3 nel ciclo circadiano dei vegetali*

Salizzoni E., *Paesaggi Protetti. Laboratori di sperimentazione per il paesaggio costiero euro-mediterraneo*

Evangelisti E., *Structural and functional aspects of membranes: the involvement of lipid rafts in Alzheimer's disease pathogenesis. The interplay between protein oligomers and plasma membrane physicochemical features in determining cytotoxicity*

Bondì D., *Filosofia e storiografia nel dibattito anglo-americano sulla svolta linguistica*

Petrucci F., *Petri Candidi Decembrii Epistularum iuvenilium libri octo. A cura di Federico Petrucci*

Alberti M., *La 'scoperta' dei disoccupati. Alle origini dell'indagine statistica sulla disoccupazione nell'Italia liberale (1893-1915)*

Gualdani R., *Using the Patch-Clamp technique to shed light on ion channels structure, function and pharmacology*

Adessi A., *Hydrogen production using Purple Non-Sulfur Bacteria (PNSB) cultivated under natural or artificial light conditions with synthetic or fermentation derived substrates*

Ramalli A., *Development of novel ultrasound techniques for imaging and elastography. From simulation to real-time implementation*

Lunghi C., *Early cross-modal interactions and adult human visual cortical plasticity revealed by binocular rivalry*

Brancasi I., *Architettura e illuminismo: filosofia e progetti di città nel tardo Settecento francese*

Cucinotta E., *Produzione poetica e storia nella prassi e nella teoria greca di età classica*

Pellegrini L., *Circostanze del reato: trasformazioni in atto e prospettive di riforma*

Locatelli M., *Mid infrared digital holography and terahertz imaging*

Muniz Miranda F., *Modelling of spectroscipic and structural properties using molecular dynamics*

Bacci M., *Dinamica molecolare e modelli al continuo per il trasporto di molecole proteiche - Coarse-grained molecular dynamics and continuum models for the transport of protein molecole*

Martelli R., *Characteristics of raw and cooked fillets in species of actual and potential interest for italian aquaculture: rainbow trout (oncorhynchus mykiss) and meagre (argyrosomus regius)*

Lana D., *A study on cholinergic signal transduction pathways involved in short term and long term memory formation in the rat hippocampus. Molecular and cellular alterations underlying memory impairments in animal models of neurodegeneration*

Lopez Garcia A., *Los* Auditoria *de Roma y el* Athenaeum *de Adriano*

Pastorelli G., *L'immagine del cane in Franz Kafka*

Bussoletti A., *L'età berlusconiana. Il centro-destra dai poli alla Casa della Libertà 1994-2001*

Malavolti L., *Single molecule magnets sublimated on conducting and magnetic substrates*

Belingardi C., *Comunanze urbane. Autogestione e cura dei luoghi*

Guzzo E., *Il tempio nel tempio. Il tombeau di Rousseau al Panthéon di Parigi*

Lombardi N., *MEREAFaPS: uno Studio di Farmacovigilanza Attiva e Farmacoepidemiologia in Pronto Soccorso*

Baratta L., *«A Marvellous and Strange Event». Racconti di nascite mostruose nell'Inghilterra della prima età moderna*

Richichi I.A., *La teocrazia: crisi e trasformazione di un modello politico nell'Europa del XVIII secolo*

Palandri L., *I giudici e l'arte. Stati Uniti ed Europa a confronto*

Caselli N., *Imaging and engineering optical localized modes at the nano scale*

Calabrese G., *Study and design of topologies and components for high power density dc-dc converters*

Porzilli S., *Rilevare l'architettura in legno. Protocolli metodologici per la documentazione delle architetture tradizionali lignee: i casi studio dei villaggi careliani in Russia*

New insights into creatine transporter deficiency

Creatine (Cr) transporter deficiency (CCDS1) is a very rare and severe condition due to impaired energetic metabolism. In this work we showed for the first time the following facts: this diseases is a progressive neurodegenerative disorder in which a set of maladaptive compensatory mechanisms leads to a progressive damage of brain functions; cell energy metabolism and mitochondria seem strongly involved in the pathogenesis and they could represent useful potential targets for therapeutic interventions; inflammation seems to play an important part in this progressive damage, and this observation can pave the way to treatment strategies; neural circuits disruption involving inhibitory systems could give a huge contribute to many of the clinical aspects observed in patients, as epilepsy and cognitive impairment, since the excitatory/inhibitory balance is fundamental for the normal function of neural circuits. Factors outside the CNS are important in the pathogenesis of at least some aspects of the disorder, since the conditional KO model show difference in the timing of onset of some cognitive defects and in the presence of stereotypies.

Angelo Molinaro earned an MD at University of Pisa in 2009 (cum laude) and subsequently the title of Specialist in Endocrinology and Metabolic disorders (cum laude, at University of Pisa). He was Research Fellow at Harvard Medical School and Massachusetts General Hospital, with Prof. Jüppner studying the molecular genetics of rare endocrine diseases. He worked at the Free University of Bruxelles in the lab of the Prof. Sabine Costagliola studying the cellular and molecular embryology of early thyroid development. Subsequently, earned a PhD in Neuroscience (with distinction) at the University of Florence in the lab of Prof. Tommaso Pizzorusso (Institute of Neuroscience, CNR in Pisa) and in Paris at the Institute for Brain and Spinal Cord affiliated to Sorbonne Université with Prof. Alberto Bacci and Prof. Laurence Cathala.